

Bio-Functionalized PEG Hydrogels to Study and Direct
Mesenchymal Stem Cell Migration and Differentiation

By

Kyle Anthony Kyburz

B.S., Purdue University, 2009

A thesis submitted to the
Faculty of the Graduate School of the
University of Colorado in partial fulfillment
of the requirement for the degree of
Doctor of Philosophy
Department of Chemical and Biological Engineering

2015

This thesis entitled
Bio-Functionalized PEG Hydrogels to Study and Direct
Mesenchymal Stem Cell Migration and Differentiation

written by Kyle Anthony Kyburz

has been approved for the Department of Chemical and Biological Engineering

Kristi S. Anseth, Ph.D.

Stephanie J. Bryant, Ph.D.

Date _____

The final copy of this thesis has been examined by
the signatories, and we find that both the content and the format
meet acceptable presentation standards of scholarly work
in the above mentioned discipline

Abstract

Kyburz, Kyle A. (Ph.D., Chemical Engineering)
Department of Chemical and Biological Engineering, University of Colorado

Bio-Functionalized PEG Hydrogels to Study and Direct Mesenchymal Stem Cell Migration and Differentiation

Thesis directed by Professor Kristi S. Anseth

The *in vivo* microenvironment niche is a dynamic structure that locally presents a multitude of biophysical and biochemical signals that regulate cell behavior. Reciprocally, cells remodel this local microenvironment through altering the physical structure and biochemical composition of this heterogeneous milieu. These cell-matrix interactions play an integral role in directing mesenchymal stem cell (MSC) behavior (e.g., migration, proliferation, differentiation) during bone regeneration. The focus of this thesis is to exploit synthetic PEG-based hydrogels and bio-click conjugation reactions to functionalize relevant bio-molecules (e.g., mimetic peptide, proteins) to recapitulate important facets of the native extracellular matrix (ECM) to study their role in regulating MSC behavior (e.g., migration, differentiation, proliferation) and elucidate aspects of how MSCs interact and remodel their local niche.

First, peptide-functionalized thiol-ene hydrogels are utilized to tune the biophysical (e.g., crosslinking density) and biochemical (e.g., adhesive ligand density) nature of the MSC microenvironment and observe their effect on 3D MSC spreading and migration. Next, microrheological techniques are exploited to elucidate the dynamic cell-mediated remodeling of the local hydrogel structure during 3D MSC migration. Both of these studies provide insight and characterization of cell-matrix interactions within enzymatically degradable hydrogels. Thiol-ene photoconjugation is then employed to functionalize PEG hydrogel scaffolds with full-length

proteins (e.g., stromal derived factor 1 α , bone morphogenetic protein 2) to manipulate MSC behavior *in vitro*. Subsequently, this platform is introduced into a critical-sized bone defect model to study the effect of immobilized protein signals on cellular invasion and mineralized tissue formation during bone regeneration *in vivo*. Finally, to probe the singular and synergistic effects of multiple protein signals on MSC migration, differentiation or proliferation a series of bio-click reactions (e.g., thiol-ene, thiol-yne, strain-promoted azide alkyne cycloaddition, inverse electron demand Diels-Alder) are exploited to spatiotemporally conjugate proteins to hydrogel scaffolds in biologically complex serum solutions. The knowledge garnered from these studies will contribute to better engineering of synthetic hydrogels as *in vitro* cell culture substrates, drug delivery vehicles, and cell carrier or recruitment platforms for tissue engineering applications.

**To Emily
and my family.**

Acknowledgements

This work would not have been possible without the guidance, mentorship, and support from many people. First, I would like to thank my thesis advisor, Prof. Kristi Anseth, for her passionate scientific curiosity, warmth she has for her students and colleagues, and keen intellect which has shaped who I am as a scientist. Your guidance has taught me how to investigate the world and tell the story of what I find. I would also like to thank my thesis committee members who provided thoughtful insight throughout the development of this thesis: Profs. Chris Bowman, Stephanie Bryant, Jeff Stansbury, and Xuedong Liu. I would like to thank my funding sources that financially supported me throughout my graduate work, including the Howard Hughes Medical Institute, the National Science Foundation (CBET 1236662), and the National Institutes of Health (RO1DE016523).

I had the great opportunity to work with so many passionate, intelligent and kind people in the Anseth lab. I would like to thank Dr. Sarah Anderson for her initial guidance in the lab in techniques and experimental design. Dr. Mark Tibbitt and Dr. Daniel Alge played an instrumental role in honing my research skills and providing great friendships that made lab more enjoyable. Throughout my graduate school, I was able to collaborate with many great people: Dr. Eric Dailing, Dr. Dan McKinnon, Dr. Kelly Schultz, Dr. Malar Azagarsamy, and Dr. Chun Yang. Additionally, I want to thank the hard working undergrads that I was able to closely interact with throughout these projects: Jared Young, Emi Kiyotake, Bruce Han, and Dylan

Donohue. I would like to thank all of my fellow Anseth lab members that I overlapped with that made it an enjoyable and motivating place to work.

To my family and close friends, who supported me through all of the ups-and-downs of graduate school, words fail to express my deepest gratitude. Thank you to my parents who have shown me unconditional love and support and who provided me with so many opportunities. I would like to thank my siblings, Kip and Kelsey, two of my best friends who make my life richer by knowing them. Thank you to my close friends who have provided laughter and advice and made these last years so incredible. Most importantly my deepest thanks to my amazing wife Emily, who has been my closest friend and number one supporter through all of the rough spots and bright spots of graduate school and life. We have been on so many amazing adventures, and I cannot wait to go on so many more by your side.

TABLE OF CONTENTS

LIST OF FIGURES.....	xiii
CHAPTER I – INTRODUCTION AND BACKGROUND.....	1
1.0 Overview	1
1.1 Setting the context.....	2
1.2 The ECM has a complex composition.....	5
1.3 Synthetic hydrogels as ECM mimics.....	6
1.4 The active role of biophysical cues.....	9
1.5 The ECM as a reservoir of biochemical signals.....	13
1.6 Cell-directed and user-directed microenvironmental ECM remodeling.....	18
1.7 Approach of this thesis.....	22
1.8 References.....	25
CHAPTER II – THESIS OBJECTIVES.....	30
2.1 Overview.....	30
2.2 References.....	38
CHAPTER III - THREE-DIMENSIONAL HMSC MOTILITY WITHIN PEPTIDE-FUNCTIONALIZED PEG-BASED HYDROGEL OF VARYING ADHESIVITY AND CROSSLINKING DENSITY.....	39
3.1 Abstract.....	39
3.2 Introduction.....	40
3.3 Materials and Methods.....	44
3.3.1 Macromer Synthesis.....	44
3.3.2 Cell Culture.....	45

3.3.3 Gel Formulation and Characterization.....	45
3.3.4 Real-time Cell Motility Studies.....	46
3.3.5 Immunostaining.....	47
3.3.6 Statistical Analysis.....	48
3.4 Results and Discussion.....	48
3.4.1 Peptide-Functionalized PEG Hydrogels: Controlling physical and chemical properties.....	48
3.4.2 Effect of Crosslinking Density on Cell Spreading and Morphology.....	51
3.4.3 Effect of Crosslinking Density on hMSC Motility.....	54
3.4.4 Actin Cytoskeleton and $\beta 1$ Integrin Organization and Structure.....	57
3.4.5 Effect of RGD Density on Cell Morphology.....	59
3.4.6 Actin Cytoskeleton and $\beta 1$ Integrin Organization and Structure.....	61
3.4.7 Effect of RGD on hMSC Motility.....	63
3.5 Conclusions.....	67
3.6 Supplemental Information.....	68
3.6 References.....	68
CHAPTER IV – MEASURING DYNAMIC CELL-MATERIAL INTERACTIONS AND REMODELING DURING 3D HMSC MIGRATION IN HYDROGELS.....	73
4.1 Abstract.....	73
4.2 Introduction.....	74
4.3 Results and Discussion.....	77
4.3.1 Microrheological characterization of hydrogel degradation and remodeling during hMSC migration.....	77
4.3.2 Cell-mediated degradation during early stages of motility.....	81

4.3.3 Local hydrogel remodeling by hMSCs during migration.....	87
4.3.4 Visualization of cellularly degraded pathways after migration in 3D hydrogels	88
4.4 Conclusions.....	90
4.5 Materials and Methods.....	91
4.5.1 Hydrogel scaffold.....	91
4.5.2 Device fabrication and three-dimensional cell encapsulation.....	92
4.5.3 Human mesenchymal stem cell culture.....	93
4.5.4 Multiple particle tracking microrheology and particle image velocimetry measurements.....	93
4.5.5 Visualizing cell tracks in hydrogel.....	94
4.6 Supplemental Information.....	96
4.7 References.....	98
CHAPTER V – OSTEOINDUCTIVE THIOL-ENE HYDROGELS THROUGH LOCALIZED PRESENTATION OF SDF-1 AND BMP-2.....	101
5.1 Introduction.....	101
5.2 Materials and Methods.....	105
5.2.1 Monomer Synthesis and Gel Formulation.....	105
5.2.2 Thiolation of SDF-1 and BMP-2.....	106
5.2.3 Cell Isolation and Culture.....	106
5.2.4 ELISA and Modified Section ELISA.....	107
5.2.5 Alkaline Phosphatase Assay.....	108
5.2.6 Phospho-CXCR4 Western Blot.....	109
5.2.7 Rat Calvarial Bone Defect Model.....	110

5.2.8 Statistical Analysis.....	111
5.3 Results and Discussion.....	111
5.3.1 MSC attach and migrate within peptide-functionalized hydrogels.....	111
5.3.2 Functionalization of SDF-1.....	112
5.3.3 Bioactivity and Immobilization of SH-SDF-1.....	114
5.3.4 Assessing SDF-1 functionalized hydrogels and the ability to promote cell infiltration <i>in vivo</i>	115
5.3.5 BMP-2 Thiolation and conjugation into thiol-ene hydrogel.....	119
5.3.6 BMP-2 bioactivity and cell signalling in thiol-ene hydrogels.....	120
5.3.7 Multifunctional thiol-ene hydrogels and the effect of combined protein presentation on bone regeneration.....	122
5.4 Conclusions.....	125
5.5 Supplemental Information.....	126
5.5.1 Supplemental Materials and Methods.....	126
5.5.1.1 C2C12 Culture and BMP-2 Bioactivity Assay.....	126
5.6 References.....	128
CHAPTER VI – BIOORTHOGONAL CLICK CHEMISTRIES ENABLE THREE DIMENSIONAL SIMULTANEOUS SPATIAL PATTERNING OF MULTIPLE PROTEINS TO DIRECT MSC FUNCTION.....	133
6.1 Introduction.....	133
6.2 Materials and Methods.....	136
6.2.1 Gel Formulation and Synthesis.....	136
6.2.2 DLP patterning and quantification.....	137
6.2.3 BMP-2 bioactivity assay.....	138

6.3 Results and Discussion.....	139
6.3.1 Bioorthogonal Reaction Scheme.	139
6.3.2 User-tunable spatial and concentration patterning of proteins.....	142
6.3.3 Patterning of protein molecules within complex serum solutions.....	143
6.3.4 Bioactivity of immobilized proteins.....	145
6.4 Current and Future Work.....	146
6.5 Conclusions.....	147
6.6 References.....	148
CHAPTER VII – CONCLUSIONS AND RECOMMENDATIONS.....	151
7.1 References.....	158
CHAPTER VIII – BIBLIOGRAPHY.....	160

LIST OF FIGURES

Figure 1.1 A) The extracellular matrix is composed of many different proteins, including collagen, fibronectin, and laminin, which were carefully preserved in decellularized heart tissue in a study by Ott *et al.* [5] B) The cellular microenvironment is a complex biophysical and biochemical environment where cells reside. This microenvironment includes degradable structural fibers, adhesive binding domains, and proteoglycans for biomolecule sequestration....4

Figure 1.2 Examples of prominent reactions used for bioconjugation and/or hydrogel crosslinking: A) base catalyzed thiol-vinyl sulfone Michael addition, B) radical mediated thiol-ene, C) strain-promoted azide-alkyne cycloaddition (SPAAC).....7

Figure 1.3 A) The ECM provides important biophysical cues, such as matrix elasticity, illustrated here with a stiff, dense matrix (Left) and a soft, loose matrix (Right). Synthetic hydrogels can recapitulate these properties by tuning their mechanical properties. B) Hydrogels with phototunable elasticity provide a versatile platform to study the role of biophysical cues in directing cell function. Yang *et al.* [25] cultured MSC on stiff substrates for 1 or 10 days and then softened the hydrogels *in situ* using a pre-determined dose of light. RUNX2 and YAP nuclear localization was then observed for up to 10 days, and they both followed similar trends. Shown here, the percent of hMSC with nuclear RUNX2 localization returned to basal levels after being cultured for only 1 day on stiff substrates (DSt1) and different durations on soft substrates. The stiff and soft controls correspond to the average RUNX2 localization for cells only cultured on stiff substrates (i.e., not softened with light) or only on soft substrates (i.e., softened with light) and represent full and basal levels of activation, respectively. C) When hMSC were cultured on stiff substrates for 10 days (DSt10), RUNX2 localization persisted at active levels even after culture on soft substrates, indicating that 10 days on stiff substrates induced irreversible activation of RUNX2. The data are plotted as the mean \pm s.e.m. NS, not significant; *, $p < 0.05$; **, $p < 0.01$; ***, $p < 0.001$ 12

Figure 1.4 A) Techniques based on covalent and physical immobilization are being developed for spatial biomolecule patterning to recapitulate aspects of biomolecule sequestration. Further, peptide mimics have been shown to be effective for recapitulating cell adhesion in otherwise non-adhesive hydrogels. B) Using barstar-barnase and biotin-streptavidin binding pairs, Wylie *et al.* [18] spatially tethered fluorescently labeled sonic hedgehog and ciliary neurotrophic factor into a hydrogel through physical immobilization. C) Mosewicz *et al.* [39] spatially patterned PDGF-BB to direct the invasion of encapsulated MSC. A confocal micrograph shows that MSC, labeled with DAPI (blue), more efficiently invaded the patterned region of a hydrogel with covalently immobilized PDGF-BB (purple).....17

Figure 1.5 A) Cellular remodeling and degradation play an important role in regulating the dynamic nature of the ECM. The introduction of hydrogels that degrade in response to cell-secreted enzymes begins to recapitulate this natural process. B) Patterson *et al.* [43] synthesized PEG hydrogels that were crosslinked with two different peptide sequences that vary in degradation rates. Cells from the aortic chick ring invaded the MMP-degradable network at different rates based on the cleavage rate of the peptide sequence, GPQGIWG (slower) and VPMSMRGG (faster).20

Figure 3.1 Thiol-ene photopolymerization of a tetra-functionalized PEG-norbornene, MMP cleavable peptide (KCGPQG↓IWGQCK), and adhesive ligands (CRGDS, CRDGS) occurs through a radically mediated step growth reaction to encapsulate hMSC within a 3D tunable microenvironment. The table presents mass swelling ratio (q), % water, shear modulus (G'), and crosslinking density (ρ_{xl} , calculated from Rubber Elasticity Theory) while the thiol:ene ratio was varied to produce Low, Medium, and High gels. As thiol:ene ratio increases, mass swelling decreases, % water slightly decreases, and shear modulus and crosslinking density increase.....50

Figure 3.2 Morphology of encapsulated hMSCs cultured for 30 hours in gel systems with varying crosslinking density. A) Brightfield image (10x magnification) of hMSCs in a Low (65%) gel. Cells were found to be well spread and linear. B) Brightfield image (10x magnification) of hMSCs in a Medium (72.5%) gel. Cells were found spread with many protrusions. C) Brightfield image (10x magnification) of hMSCs in a High (85%) gel. Cells were rounded with little or no protrusions. D) An elliptical form factor was calculated by dividing the length and perpendicular width of each cell. There is a significant (* $p < 0.05$) decreasing trend found from a one-way ANOVA and Tukey's Test. Scale bar represents 100 μm53

Figure 3.3 hMSC migration was followed over 7 hours using live cell videomicroscopy. Effect of varying crosslinking density on hMSC mean square displacement and sustained cell polarity was calculated from the cell tracks measured using Metamorph. (A) Mean-square displacement was similar for low and medium gels, but differed for cells in high crosslinked gels. All three gels had slopes that fell between 1 (random migration) and 2 (ballistic migration) (B) Sustained cell polarity showed a similar bias for all three systems, and a similar percentage of sustained steps.....55

Figure 3.4 Cell tracks from hMSC migration in 3D are modeled using a Persistent Random Walk model (PRW). Effect of varying crosslinking density on hMSC migration. (A) Cell speed shows a decreasing trend with increasing crosslink density. (*Significance $P < 0.05$) (B) Persistence shows no statistical difference over the varying crosslink densities. (C) Percent migration shows a decreasing although not statistically significant difference. (D) Mean free path was not affected by varying the crosslinking density.....57

Figure 3.5 Encapsulated hMSCs were cultured in gels at the three different crosslinking densities for 48 hours and immunostained for actin (red), $\beta 1$ integrin (green) and DAPI (blue). A) Low Crosslinking B) Medium Crosslinking C) High Crosslinking. Spread hMSC in all three gels systems show actin fiber formation and punctate $\beta 1$ integrin at the ends of these fibers over this range of crosslinking densities. Scale bars represent 50 μm58

Figure 3.6 Morphology of encapsulated hMSCs cultured for 30 hours in gel systems with varying CRGDS. A) Brightfield image (10x magnification) of hMSCs in 0 mM CRGDS gel. Cells were rounded. B) Brightfield image (10x magnification) of hMSCs in 0.001 mM CRGDS gel. Cells were rounded. C) Brightfield image (10x magnification) of hMSCs in 0.01 mM gels. Cells were rounded with little or no protrusions. D) Brightfield image (10x magnification) of hMSCs in 0.1 mM CRGDS gel. Cells were spread and linear. E) Brightfield image (10x magnification) of hMSCs in 1.0 mM CRGDS gel. Cells were more spread and linear. F) An

elliptical form factor was calculated by dividing the length and perpendicular width of each cell. There is a significant (* $p < 0.05$) increasing trend found from a one-way ANOVA and Tukey's Test between the first three systems with the 0.1 mM and 1.0 mM systems. Scale bar represents 100 μm60

Figure 3.7 Encapsulated hMSCs were cultured in gels with varying CRGDS concentration for 48 hours and immunostained for actin (red), $\beta 1$ integrin (green) and DAPI (blue). A) For 0.001 mM gels, cells remain rounded and show little if any $\beta 1$ integrin even on the rounded edges of the cell B) For 0.01 mM gels, actin protrusions are present although limited with few $\beta 1$ integrin staining on actin fibers C) For 0.1 mM gels, cells are spread with large, protrusive actin fiber formation with $\beta 1$ integrin staining on protrusions. D) For 1.0 mM gels, cells are similar to the 0.1 mM cells with protrusive actin fibers however, the $\beta 1$ integrin staining seems more localized to the ends of actin fibers. Scale bar represents 50 μm62

Figure 3.8 hMSC migration was followed over 7 hours using live cell videomicroscopy. The effect of varying CRGDS concentration on hMSC mean square displacement and sustained cell polarity was calculated from the cell tracks measured using Metamorph. (A) Mean-square displacement was similar for 1.0 mM and 0.1 mM gels, and 0 mM and 0.001 mM gels were also similar. All five gels had slopes that fell between 1 (random migration) and 2 (ballistic migration) (B) Sustained cell polarity showed a similar bias for all three systems, and a similar percentage of sustained steps.....63

Figure 3.9 Cell tracks from hMSC migration in 3D are modeled using a Persistent Random Walk model (PRW). Effect of varying CRGDS concentration on hMSC migration was studied. (A) Cell speed shows an increasing trend with increasing CRGDS concentration. (*Significance $P < 0.05$) (B) Persistence shows no statistical difference over the varying CRGDS (C) Percent migration shows an increasing trend with increasing CRGDS concentration that plateaus for 0.1 mM and 1.0 mM gels. (*Significance $P < 0.05$) (D) Mean free path was not affected by varying the CRGDS concentration.....65

Figure 3.S1 hNMR spectra of PEG-Norbornene. Functionalization was calculated by dividing the norbornene alkene peaks by the PEG alkyl peaks.....68

Figure 4.1 Human mesenchymal stem cells (hMSCs) migrate and form focal adhesions within the MMP-degradable thiol-ene hydrogel. (a) Schematic of network formation for the MMP-degradable PEG-norbornene hydrogel scaffold (0.65 thiol:ene, 3 mM 4-arm PEG-norbornene M_n 20,000 g mol^{-1} $f = 4$, 3.9 mM KCGPQG \downarrow IWGQCK M_n 1,305 g mol^{-1} , $f = 2$, 1mM CRGDS). (b) hMSCs were encapsulated at a density of 2×10^5 cells/mL, and the motility of individual cells was followed in real time for a period of 6 hours, scale bar: 100 μm , phase contrast image. (c) Representative image of an encapsulated hMSC immunostained for actin (red), $\beta 1$ integrin (green), and DAPI (blue). 48 hours after encapsulation, hMSCs spread within the gel and form actin stress fibers and punctate $\beta 1$ integrin staining as observed at the end of these fibers, scalebar: 20 μm . (d) The migratory speed of hMSCs decreased when cells were treated with either an MMP inhibitor (InSolutionTM GM 6001, 10 μM , immediately after encapsulation) or blebbistatin (50 μM , 2 hours post encapsulation). * $p < 0.05$80

Figure 4.2 hMSC remodeling and degradation of peptide cross-linked PEG hydrogels. Schematic image of changes that occur in cell-laden hydrogels, where the changes in the gel properties are captured by MPT probe particle trajectories. (a) Initial state, before hMSCs have caused any substantial changes in the local material properties and the cells experience a solid gel environment (b) during cell spreading, the local environment degrades in response to cellular activity and the material begins to transition from a gel to a sol in a local region and (c) at longer time scales, the pericellular region is extensively degraded, becoming a sol, and cell motility is observed. (d) Logarithmic slope of the mean-squared displacement $\langle \alpha |_{0.1 < \tau < 1 s} = \frac{d \log \langle \Delta r^2(\tau) \rangle}{d \log \tau} |_{0.1 < \tau < 1 s}$ of probe particles in the pericellular region during hMSC migration. The gel-sol transition occurs at the critical relaxation exponent, $n = 0.2$. Values of $\alpha > 0.2$ represent materials that are a sol and $\alpha < 0.2$ are gelled materials. Data are highlighted for two stages of cell motility that will be described in detail in Figure 3 and 4. 3a-c shows a cell that is spreading and starting to degrade the pericellular region and 4a-c is a cell that is very motile in a sol.....82

Figure 4.3 Dynamic rheological changes in the pericellular region during migration of an encapsulated hMSC overtime. Data are taken at (a) 0, (b) 9 and (c) 27 minutes after the cell is identified. Particle image velocimetry (PIV) measurements quantify the long time movement of probe particles between (d) 0 – 4, (e) 9 – 14 and (f) 23 – 27 minutes. Every other particle trajectory is displayed on PIV plots for clarity. Brightfield images are set in the background of MPT measurements with mean-squared displacement values calculated spatially as the distance away from the cell. The z axis, indicated by color, is the logarithmic slope of the mean-squared displacement, α , where a slope of 0, red, indicates no particle movement, a slope of 1, light blue, indicates Brownian motion and a slope of 1.6, purple, indicates ballistic motion. PIV measurements show the displacements using color and size of arrows. Warm colors and small arrows indicate small particle displacement, while cool colors and large arrows show large particle displacement. Both of these measurements confirm that through time as the cell is spreading the largest extent of degradation occurs furthest from the cell.....85

Figure 4.4 Dynamic spatial rheological data of the pericellular region during cell migration. Data are taken through time at (a) 0, (b) 24 and (c) 43 minutes after the cell is identified. This rapidly moving cell is causing the particles to move with the cell (outlined in black) as it migrates through the acquisition window. These measurements indicate that once the cell is spread and begins to move that the scaffold is a viscoelastic fluid.....88

Figure 4.5 Fluorescently labeled hydrogels allow for the visualization of cell-mediated remodeling of the hydrogel during migration. (a) A minimum intensity projection of a compressed z-stack of a fluorescently labeled (AF-546) hydrogel permits visualization of the black (void) regions present in the gel from cellular degradation and remodeling. Over 48 hours, the cell migrated $\sim 175 \mu m$ from its original location, α , to its final location, β . Void tracks from cell spreading and migration can be seen developing off of this spherical void. (b) The bright field image depicts the initial cell location after polymerization circled with a dashed line, α , and the cell is located at its final position, β , after 48 hours of migration. Scale bar = $50 \mu m$90

Figure 4.S1 Dynamic rheological data of the material during cell migration of a hMSC treated with a MMP inhibitor. The left panels are brightfield images of the cell encapsulated in

3D. The right panels are measurements of probe particle movement in the same field of view. The z axis, indicated by color of the marker and the rings that are averages of the particles within them, is the logarithmic slope of the mean-squared displacement, dark gray rings indicate that no particles fall within their area. Data are taken through time at (a) 0, (b) 21 and (c) 38 minutes after cell is identified.....96

Figure 4.S2 Dynamic rheological data of the material during cell migration of a hMSC treated with blebbistatin, which inhibits myosin II. The left panels are brightfield images of the cell encapsulated in 3D. The right panels are measurements of probe particle movement in the same field of view. The z axis, indicated by color of the marker and the rings that are averages of the particles within them, is the logarithmic slope of the mean-squared displacement. Data are taken through time at (a) 12, (b) 20 and (c) 35 minutes after cell is identified.....97

Figure 5.1 MSC attach, migrate three-dimensionally, and remain viable within peptide-functionalized thiol-ene hydrogels. A) Four-arm PEG Norbornene (M_n 20,000, 3 mM) is photopolymerized with a di-thiol MMP-degradable peptide (thiol:ene = 0.65:1) and mono-thiol adhesion peptide (1 mM) with 1.7 mM LAP and 3 minutes of 10 mW cm⁻². B) MSC were encapsulated within the hydrogel and cultured for 24 hours. Live-cell videomicroscopy was performed and cell movement was tracked over a 6-hour period. Mean-squared displacements for individual cells were then modeled with a persistent random walk to elucidate important migration metrics. The mean cell speed for 3D MSC migration was 18 ± 1 , the persistence was found to be 156 ± 24 , and a mean free path of 48 ± 9 . Mean \pm S.E.112

Figure 5.2 SDF-1 Thiolation and antibody recognition. A) The concentration of thiols per SDF-1 and SH-SDF-1 was measured using the commercially available Measure-IT™ Thiol Assay Kit (Life Technologies). SDF-1 had no free thiols present before modification, but SH-SDF-1 was found to have 2.7 ± 0.2 thiols/molecule. B) An ELISA was performed to determine recognition of SH-SDF-1 by a primary antibody. Absorbance values were normalized to the native protein, SDF-1. The SH-SDF-1 protein was 0.65 ± 0.02 relative to the unmodified SDF-1, indicating that the modified SH-SDF-1 is recognized by the primary antibody, but at a reduced level. Mean \pm S.D. * $p < 0.05$113

Figure 5.3 SH-SDF-1 retains bioactivity post-modification. To detect SH-SDF-1 bioactivity, a western blot was performed to measure the elevated levels of phospho-CXCR4 on MSC after dosing with SDF-1 and SH-SDF-1. Phospho-CXCR4 was normalized to total levels of CXCR4 and a fold-increase of 1.22 was found for SH-SDF-1, and a fold-increase of 1.45 was found after dosing with SDF-1.....114

Figure 5.4 Covalently immobilized SH-SDF increases cellular invasion in rat calvarial defects. Two 5 mm critical sized defects were created on the top of a rat cranium and thiol-ene hydrogels with either 10 ng/mL of soluble SDF-1 entrapped or 10 ng/mL of immobilized SH-SDF-1 were introduced into the newly formed defects. A) MicroCT scans were performed two days after the surgeries. A representative image is shown above, where the red areas denote regions where the levels of optical density did not meet the threshold consistent with bone. B) Representative images of Masson's Trichrome stain are shown where the edges of the original defect area are marked by black arrows. Qualitatively, increased cellularity was observed in

conditions with immobilized SH-SDF-1. C) Histological scoring of the cellularity within the middle of the defect sections was performed by independent and blind observers, where 0 is low cellularity, 1 is medium cellularity, and 2 is high cellularity. SH-SDF-1 was observed to have a significantly higher mean score of 1.3 ± 0.3 , relative to soluble SDF-1 with a score of 0.5 ± 0.7 . D) Similar scoring was performed on the edge of the defect, where again the immobilized SH-SDF-1 had a higher score of 1.3 ± 0.6 relative to soluble SDF-1 with a score of 0.3 ± 0.6 . mean \pm S.D. $**p < 0.1$118

Figure 5.5 BMP-2 thiolation and antibody recognition. A) After modification, the concentration of free thiols per BMP-2 molecule was measured through fluorescent labeling and quantification of the fluorescent signal. It was found that SH-BMP-2 had 0.84 ± 0.02 thiols per molecule, and BMP-2 was found to contain no free thiols. B) Primary antibody recognition was measured by ELISA and no difference was observed for SH-BMP-2 (0.94 ± 0.06) and non-thiolated BMP-2 (1.00 ± 0.10). Mean \pm S.D. $* p < 0.05$119

Figure 5.6 Tunable immobilization of BMP-2 within thiol-ene hydrogels Thiolated BMP-2 was incorporated into the hydrogels via a thiol-ene solution photopolymerization at concentrations of $12 \mu\text{g mL}^{-1}$ and $24 \mu\text{g mL}^{-1}$ and a modified section ELISA was performed. For the $12 \mu\text{g mL}^{-1}$ hydrogels, 2.33 ± 0.03 ng/section was found or 49% of the initially loaded SH-BMP-2. For the $24 \mu\text{g mL}^{-1}$, 7.13 ± 0.02 ng/section was found or 76% of the initial loading. Dashed lines represent initial loading concentrations. Mean \pm S.D. $p < 0.05$120

Figure 5.7 Covalently immobilized SH-BMP-2 retains bioactivity and directs MSC osteogenesis. MSC were encapsulated within thiol-ene hydrogels with 1) no BMP-2 (Blank), 2) 1000 ng/mL of soluble BMP-2 (Soluble) or 3) 1000 ng/mL of SH-BMP-2 immobilized to the hydrogel scaffold (Immobilized) delivered to the cells at the start of culture time. Alkaline phosphatase levels were measured after 3 days of culture and plotted relative to the blank control (1.00 ± 0.19). Soluble BMP-2 induced a relative ALP activity of 4.74 ± 0.04 , while immobilized BMP-2 still retained bioactivity with a relative ALP activity reading of 3.54 ± 0.71 . plotted: mean \pm S.D. $*p < 0.05$122

Figure 5.8 Bone growth in critical sized rat calvarial defects. Bone growth over 4 weeks was measured using microCT scans. Four conditions were tested 1) soluble SDF (10 ng/mL) entrapped within the hydrogel, 2) immobilized SH-SDF (10 ng/mL), 3) immobilized SH-BMP-2 (1000 ng/mL), and 4) immobilized SH-SDF (10 ng/mL) and SH-BMP-2 (1000 ng/mL). A) Shown on the left are representative images for each condition at week 0 and 4. B) On the right, is the average percent area defect closure for 3 animals per condition. The immobilized SH-BMP-2 saw the highest increase in bone fracture healing over the four-week period relative to the other conditions. mean \pm S.D.124

Figure 5.S1 SH-BMP-2 retains bioactivity. A) A C2C12 reporter cell line was dosed with two concentrations (100 ng mL^{-1} , 10 ng mL^{-1}) of BMP-2 and SH-BMP-2 on TCPS and luciferase production was normalized to the negative control. There was a slight decrease in luciferase production for the thiolated BMP-2 at 100 ng mL^{-1} , 21.8 ± 1.4 fold increase (BMP-2) vs. 15.8 ± 2.2 fold increase (SH-BMP-2); however, no decrease was seen at the lower concentration (10 ng mL^{-1}), 3.5 ± 0.6 (BMP-2) and 3.2 ± 0.3 (SH-BMP-2). This shows that SH-BMP-2 retains high

levels of bioactivity. B) The C2C12s were then encapsulated within PEG hydrogels and treated with either soluble SH-BMP-2 or SH-BMP-2 to the network. After normalization to the negative control, the cells treated with the immobilized SH-BMP-2 had the highest levels of luciferase activity (9.0 ± 2.4 fold increase) relative to soluble delivery (5.8 ± 3.6 fold increase). Therefore, SH-BMP-2 retains bioactivity when immobilized to the PEG network. Mean \pm S.D. * $p < 0.05$127

Figure 6.1 Spatial patterning of multiple proteins using bioorthogonal chemistry A) 4-arm PEG-norbornene and MMP-degradable di-thiol peptide react by thiol-ene photopolymerization in the presence of the photoinitiator LAP. B) To enable photopatterning of the bioorthogonal reaction pairs, treatment of tetrazine-PEG-azide converts pendant norbornene moieties within the network into pendant alkynes. C) Using thiol-yne photoconjugation, azide moieties and tetrazine moieties can be sequentially patterned using DLP to spatially control light exposure within the 3D hydrogel. D) After the complementary binding pair is spatially immobilized, treatment of DBCO-labeled proteins and TCO-labeled proteins enables distinct 3D spatial patterning of multiple protein signals.....142

Figure 6.2 User-tuning of light dosage controls immobilized protein concentration. A) DLP was used to control the exposure time and regions of conjugation of the thiolated-azide. The pattern shown above creates a 3×10 array with increasing percentage (10%) of the 40 s light exposure time. B) Confocal microscopy was used to image and quantify protein immobilization. Shown here is a 10x image of the top view of the hydrogel of increasing light exposure from the left to right column of patterned squares of DBCO-BSA-rhodamine. Scale bar = 200 μm . C) Quantification of the level of fluorescence of each square in comparison to known standard samples allowed for the total immobilized protein to be quantified relative to exposure time. A linear increase in the amount of immobilized DBCO-BSA-rhodamine was measured over the 40 s exposure range.....143

Figure 6.3 Patterning of proteins in the presence of complex serum solutions. Protein patterning was performed in gels equilibrated in 0%, 10% or 100% serum, and the concentration of gel-conjugated DBCO-BSA-rhodamine was quantified using fluorescence intensity. Patterning showed high fidelity in all three conditions without a reduction in immobilized protein.....144

Figure 6.4 Immobilized DBCO-BMP-2 retains bioactivity in directing ALP expression in hMSC. DBCO-BMP-2 and CRGDS were patterned in specific regions of the hydrogel and hMSC were seeded on top of these regions and cultured for 5 days. hMSC were fixed and stained for ALP activity (purple) for the two conditions. Increased ALP activity was observed in the presence of immobilized DBCO-BMP-2 relative to no BMP-2 present demonstrating that BMP-2 remains bioactive after modification and immobilization. Scale bar = 100 μm145

Figure 6.5 Screening multi-protein combinations on hMSC behavior Protein signals will be immobilized in highly-defined regions and concentrations to probe their singular and synergistic effects on hMSC behavior. A) The effect of BMP-2 will be measured through image analysis of ALP activity staining. Similarly, image analysis will be used to study the effect of FGF-2 by measuring EdU staining to determine proliferative cells. The depth of individual hMSC invasion

into the hydrogel will be quantified by confocal imaging and image analysis. All of these analysis provide a rapid output that can be quantified computationally. B) Five-by-five arrays will be patterned three-dimensionally in peptide-functionalized hydrogels with an increasing concentration of Protein 1 in the x-axis and an increasing concentration of Protein 2 in the y-axis. This will provide 25 distinct microenvironments for hMSC culture. Additionally, using dynamic light projection multiple arrays can be patterned on a single hydrogel allowing for rapid analysis and increased statistic accuracy.....147

CHAPTER I

INTRODUCTION AND BACKGROUND

Sections as in press in *Annals of Biomedical Engineering*

1.0 Overview

Synthetic cell scaffolds provide versatile platforms to recapitulate important physical and biochemical facets of the extracellular matrix (ECM) for an increasing number of applications: *ex vivo* cell expansion, *in vitro* screening assays of matrix signals and biomolecules that can direct cell function, and delivery vehicles for cells and/or biomolecules (e.g., peptides, proteins) to promote tissue regeneration *in vivo*. Hydrogels are one major class of synthetic scaffolds. Hydrogels are crosslinked polymer networks that imbibe large amounts of water, creating elastic microenvironments that recapitulate many aspects of soft tissues and allow for facile diffusion of exogenously delivered molecules, cell secreted signaling molecules, nutrients, and waste.

While synthetic hydrogels capture many of the biophysical properties of the extracellular matrix, recent advances in bioconjugation chemistries provide numerous strategies to incorporate cell signaling functionalities in the scaffolds, often in a user-tunable manner. With these advancements, researchers can now more intricately probe what ECM cues are important for sustaining and directing cell function, as well as supporting more effective healing *in vivo*. Yet when asking these questions, it becomes important to understand how the contextual presentation of the molecules, the dosage, the spatial presentation, and how the molecules are incorporated (e.g., covalently, physically adsorbed) into the microenvironment, affect the desired outcome.

This following section seeks to introduce recent advances in the incorporation of biological cues into hydrogel scaffolds and begin to elucidate how the temporal and spatial presentation and removal of these cues direct cellular outcomes.

1.1 Setting the context

In our tissues and organs, the extracellular matrix (ECM) is a complex and dynamic structure where cells reside, remodel and interact over a range of length scales to maintain tissue homeostasis, growth and repair [1, 2]. The ECM is bioactive, locally sequestering biomacromolecules that can promote cell adhesion, spreading, survival, proliferation, migration and even, differentiation. The synergistic and antagonistic interplay of these cues, in coordination with the biophysical properties of the surrounding matrix, ultimately directs cell fate. However, how cells receive, process, and exchange information with the ECM is often difficult to elucidate, and it typically involves coordinated presentation of multiple factors that can be presented over multiple time scales.

In the field of regenerative medicine, decellularized ECM matrices have played a long-standing role as scaffolds for tissue engineering [3]. Decellularized ECM scaffolds are typically prepared by treating tissues with detergents to remove cells and antigens, and subsequently repopulated with host cells, allowing them to be transplanted *in vivo* while minimizing the immune response [4]. As an example, Ott et al. used decellularized whole hearts as a structural architecture that was re-populated with cardiac or endothelial cells and the cell-laden matrix led to nascent pumping function [5]. Collagen I and III, laminin and fibronectin were all preserved within the decellularized heart as shown in the immunofluorescence micrographs in Figure 1.1A. While matrices derived from native ECM have the benefit of capturing the complex structure and

composition found in tissues (e.g., a pre-formed vascular network); the ability to recolonize this dense matrix with multiple cell types and to control their functional properties on relevant length and time scales is difficult to achieve and predict.

As a result, there are numerous efforts to engineer materials that recapitulate important facets of the ECM, and synthetic hydrogels represent one such class of materials that have received widespread interest as tissue engineering scaffolds. Hydrogels are crosslinked biomacromolecules that absorb large amounts of water, without dissolving, and this high water content imparts physiologically relevant soft tissue mechanics, and allows facile transport and diffusion of cell secreted molecules. While the structure of synthetic hydrogels can be tuned to allow a range of material properties, the chemistry is devoid of functionalities that are recognized by cells. So when designing suitable hydrogels for culturing cells and regenerating tissues, the question becomes “How simple is complex enough?”. What minimal biological signals are necessary to guide desired cellular functions, and how might temporal addition and/or removal of these matrix cues play an important role in directing bioscaffold design, especially for the regeneration of functional tissues of the future.

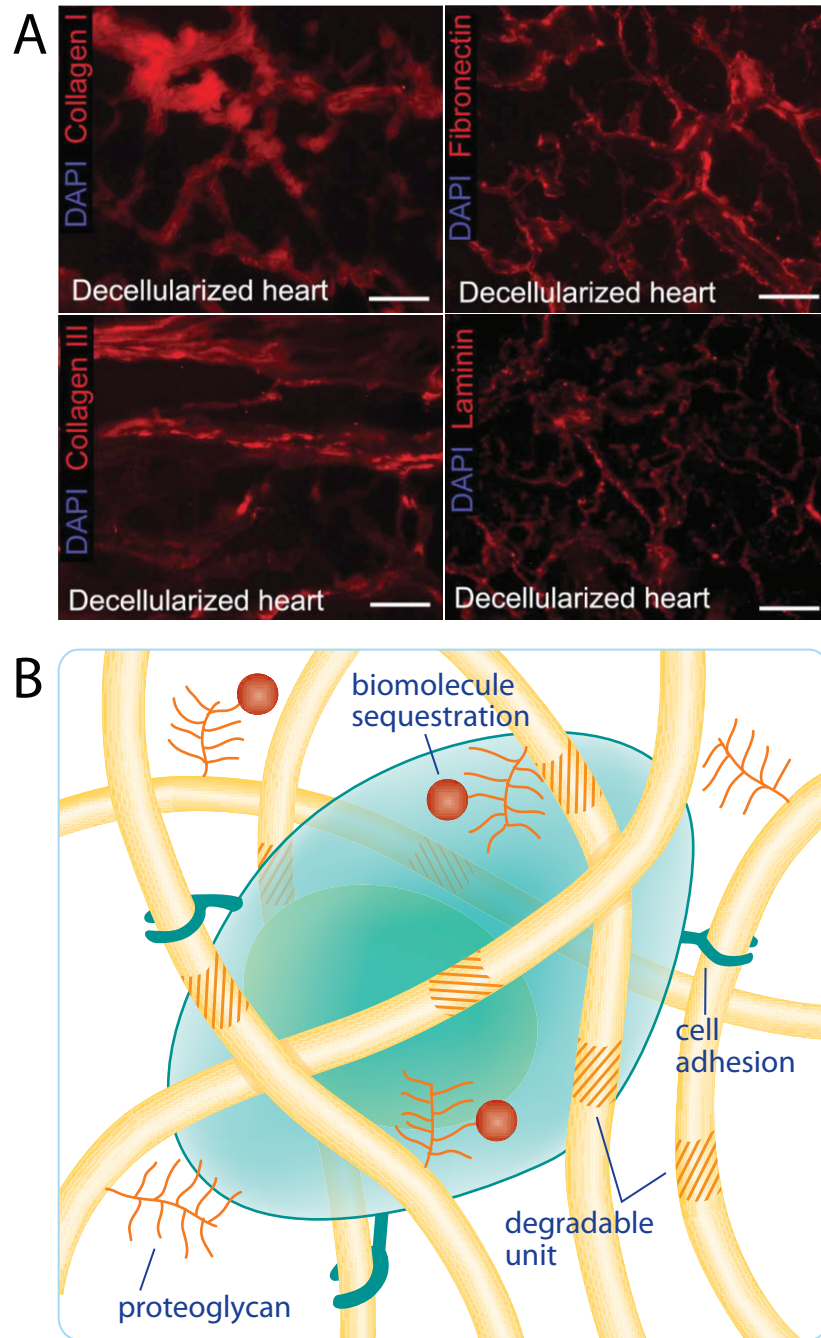


Figure 1.1 A) The extracellular matrix is composed of many different proteins, including collagen, fibronectin, and laminin, which were carefully preserved in decellularized heart tissue in a study by Ott *et al.* [5] B) The cellular microenvironment is a complex biophysical and biochemical environment where cells reside. This microenvironment includes degradable structural fibers, adhesive binding domains, and proteoglycans for biomolecule sequestration.

1.2 The ECM has a complex composition

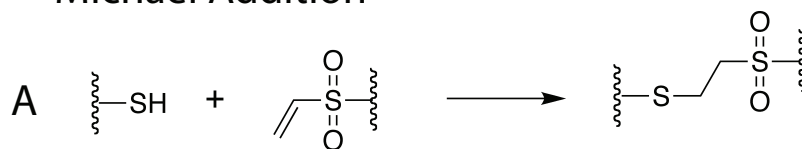
The ECM provides a myriad of cues to resident cells that in combination with cell-cell and cell-matrix signaling regulate functional outputs (Figure 1.1B). The composition of the ECM is complex and consists of high molecular weight proteins (e.g., collagen, fibronectin, and laminin) and branched glycosaminoglycan structures (e.g., heparin sulfate and chondroitin sulfate)[6]. These macromolecules are typically organized into a fibrillar network that provides a unique biophysical and bioactive environment for cells to reside. The most abundant protein in the ECM is collagen, which forms trimeric protein rods that provide tensile strength to the network. Proteoglycans represent another major component of the ECM; these highly branched biomacromolecules arise from covalent attachment of glycosaminoglycans (GAGs) to high molecular weight proteins. Negatively charged GAGs indirectly sequester water molecules through a cationic intermediary, resulting in a water-rich network and unique biophysical properties (e.g., high compressive strength, viscoelastic effects, and streaming potentials).

The multiple ECM components also contain adhesive binding sites for cell binding, such as those found in fibronectin and laminin, which facilitate attachment, spreading, migration, and transduction of mechanical signals from the local microenvironment [7, 8]. GAGs are also known to non-specifically sequester and bind growth factors and signaling proteins that cells interact with through surface receptors, imparting local bioactivity. Finally, the ECM should be considered as a dynamic material, where the local milieu can be remodeled through cell-mediated secretion and deposition of molecules or degraded through cell secreted enzymes called matrix metalloproteinases (MMPs).

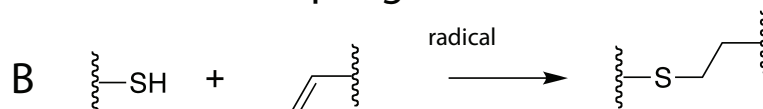
1.3 Synthetic hydrogels as ECM mimics

Synthetic hydrogels can serve as simple platforms to culture primary cells in three-dimensions and test the role of ECM interactions on functional outputs. For example, water soluble polymers, such as poly(ethylene glycol) (PEG), poly(vinyl alcohol), poly(2-hydroxyethyl methacrylate), can be crosslinked to form elastic materials that recreate basic aspects of ECM mechanics of soft tissues [9]. Complementary bioconjugation methods have also been employed to impart biological functionality to these synthetic materials [10]. The relatively bioinert nature and hydrophilicity of PEG, in particular, enables the design of water-rich “blank” cellular microenvironments. Typically, PEG macromolecules are crosslinked or functionalized by modifying the hydroxyl end groups with reactive groups, such as alkenes, alkynes, azides, maleimides, thiols, NHS esters, vinyl sulfones, and norbornenes, which can then be polymerized under cytocompatible conditions via numerous reactions: chain polymerization, Michael addition (Figure 1.2A), thiol-ene (Figure 1.2B), and strain-promoted azide alkyne cycloaddition (Figure 1.2C) [11-14]. The initial macromolecular molecular weight and the functionality of the monomer can be used along with processing conditions to control the final network structure and properties.

Michael Addition



Thiol-ene Coupling



Azide-Alkyne Cycloaddition

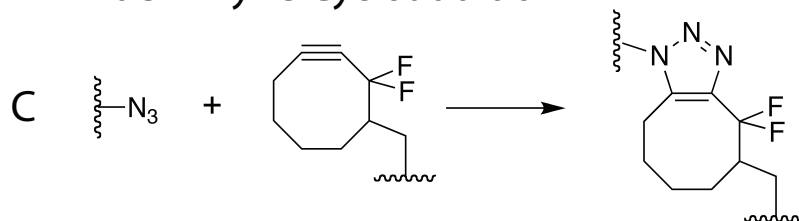


Figure 1.2 Examples of prominent reactions used for bioconjugation and/or hydrogel crosslinking: A) base catalyzed thiol-vinyl sulfone Michael addition, B) radical mediated thiol-ene, C) strain-promoted azide-alkyne cycloaddition (SPAAC).

In this review, focus is first placed on hydrogels as simplified structural mimics of the ECM, capturing basic mechanical aspects and allowing three-dimensional cell culture that direct basic cellular outputs, such as adhesion and morphology (Fig 1.1B). Then, the topic transitions to more complex material environments aimed towards controlling and manipulating cellular processes, such as directing differentiation or *in vivo* engraftment. Clearly, the ECM is a reservoir filled with a rich biochemical context that coordinates to regulate cell function by sequestering growth factors and providing adhesive cellular binding sites. How a cell interprets these bioactive signals can depend on the biophysical inputs a cell is receiving concurrently, so numerous contemporary topics in bioscaffold design focus on understanding and recapitulating the dynamic interplay between cells and their local ECM. In this regard, synthetic hydrogels have been engineered with properties that change with time, such as degrading through specific

mechanisms (e.g., hydrolytic, enzymatic) and on specific time scales. These processes can better capture aspects of cells degrading and/or remodeling their local microenvironment *in vivo*, while simultaneously allowing a researcher to investigate how cells exchange and interpret information received from their niche. However, in designing synthetic hydrogels as ECM mimics, the complex biophysical and biochemical cues present should be motivated by the desired clinical application or hypothesis being tested. The following sections look to explore how these passive and active matrix cues might be incorporated into synthetic hydrogels to better understand how simplified and defined signals affect cell-ECM interactions and then place this in the broader context for the future design of hydrogels as bioscaffolds for tissue engineering applications.

Towards the goal of synthesizing a simplified ECM mimic, initial efforts demonstrated how one could introduce peptide sequences into the network structure to provide integrin-binding sites for adhesion and enzymatically degradable linkers to allow for cell-mediated degradation. Hern *et al.* copolymerized PEG-diacrylate macromolecules with monoacrylated PEGs modified with a pendant RGD sequence to promote adhesion and survival of human foreskin fibroblasts [15]. Specifically, the RGD sequence was coupled to an asymmetric, linear PEG with an acrylate functional group on one end, and an N-hydroxy succinimide ester on the other end. Since this early demonstration, RGD and other adhesive epitopes have been widely used in bioscaffold design to direct cell migration [16-18] or even spatially control cell spreading in three-dimensions [19, 20].

Beyond controlling cell-matrix adhesion, these synthetic methods have also been used to mimic aspects of ECM degradation and remodeling. For example, West and Hubbell incorporated a collagenase-sensitive peptide sequence into a PEG diacrylate crosslinker, rendering it degradable by cell-secreted MMPs. To further control the hydrogel connectivity and

combine both adhesive and degradable functionalities, Lutolf and Hubbell used a base catalyzed Michael addition to react multi-arm PEG with vinyl-sulfone end groups with cysteine containing peptides (e.g., a bis-cysteine peptide that was MMP-cleavable and a mono-cysteine RGD sequence) [21]. This reaction scheme allowed encapsulation of fibroblasts and the study of their invasion into the matrix, as a function of its adhesivity and susceptibility to degradation.

Towards building in complexity and allowing spatial control of matrix functionality others exploited thiol-ene photochemistry to show the versatility of the reaction in forming PEG-peptide ECM mimics [20] with gradient functionalities [22], conjugation of multiple epitopes in spatially distinct scaffold regions [19], and two-photon patterning of complex features [23]. More recent work has expanded the library of “bio-click” chemistries, such as strain-promoted azide-alkyne cycloaddition, that allow sequential and orthogonal reactions for bioconjugation [19]. This reductionist view of the ECM and the expansion of cytocompatible chemistries afford new opportunities to design innovative experiments that should improve the field’s understanding of cell-matrix signaling and the design of the next generation of tissue engineering scaffolds.

1.4 The active role of biophysical cues

The ECM in its simplest interpretation is a 3D structure where cells physically reside. However, cells interact and receive important regulatory cues from the physical properties (e.g., stiff and soft matrices) and structure of the ECM, and these cues in turn direct cell outputs such as spreading, migration, and proliferation (Figure 1.3A). Many of these physical attributes can be engineered and recapitulated within synthetic hydrogels. For example, moderately crosslinked PEG-based hydrogels imbibe large amounts of water (>95%), and this renders them

with properties that can be tuned over a large range of elastic moduli, diffusivity, and structural information. However, this tunability of properties is highly coupled, as all of these properties depend directly on the network crosslinking density.

One of the most widely studied biophysical properties is the matrix elasticity. Although still not fully understood, correlative studies suggest cells interpret elasticity through mechanotransduction and integrin binding to the matrix triggers outside-in signaling cascades. For example, in the seminal work from Engler *et al.*, polyacrylamide hydrogels were used to create substrates with a range of elastic moduli, and this simple biophysical variation was found to manipulate the differentiation of mesenchymal stem cell (hMSC) [24]. Building on this pioneering work, hydrogels with phototunable elasticities were then synthesized to allow users the ability to study the effects of mechanical ‘dosing’ (e.g., culturing cells on TCPS for extended periods of time) on hMSC fate. Work by Yang *et al.* synthesized PEG substrates with elasticities that could be tuned on demand by exposure to light (Figure 1.3B-C) [25]. Briefly, hMSC were cultured on stiff (10 kPa) gels for 1 (Figure 1.3B), 7 (data not shown) or 10 days (Figure 1.3C) and then the hydrogels were softened to 2 kPa *in situ*. The nuclear localization of two transcriptional factors, YAP and RUNX2, was studied, and found to depend upon the time of culture in stiff environments (Figure 1.3B-C). These findings taught that cells may have a ‘memory’ related to their previous culture treatment and highlight the importance of carefully considering the context of cells during their *ex vivo* culture and expansion as this may influence their long-term function after transplantation.

While these studies point to the importance of mechanotransduction, a major unanswered question for the field is how does this signaling occur. Using the same photodegradable hydrogels described above [25], Wang *et al.* identified the PI3K/AKT pathway as one of the key

signaling pathways that regulate mechano-sensing and activation of primary valvular interstitial cells (VICs) [26]. This study showed that through a reduction in the material stiffness the myofibroblast to fibroblast activation of VICs could be reversed. As another example, Gilbert *et al.* also illustrated the efficacy of recapitulating appropriate ECM substrate stiffness on muscle stem cell (MuSC) function [27]. Specifically, PEG-based hydrogel culture platforms that mimicked the elastic modulus of muscle (~12 kPa) were used as a culture platform for MuSC. The MuSC cultured on the muscle-like hydrogel substrates had heightened self-renewal and potency, as well as increased engraftment rates during muscle regeneration compared to MuSC cultured on TCPS.

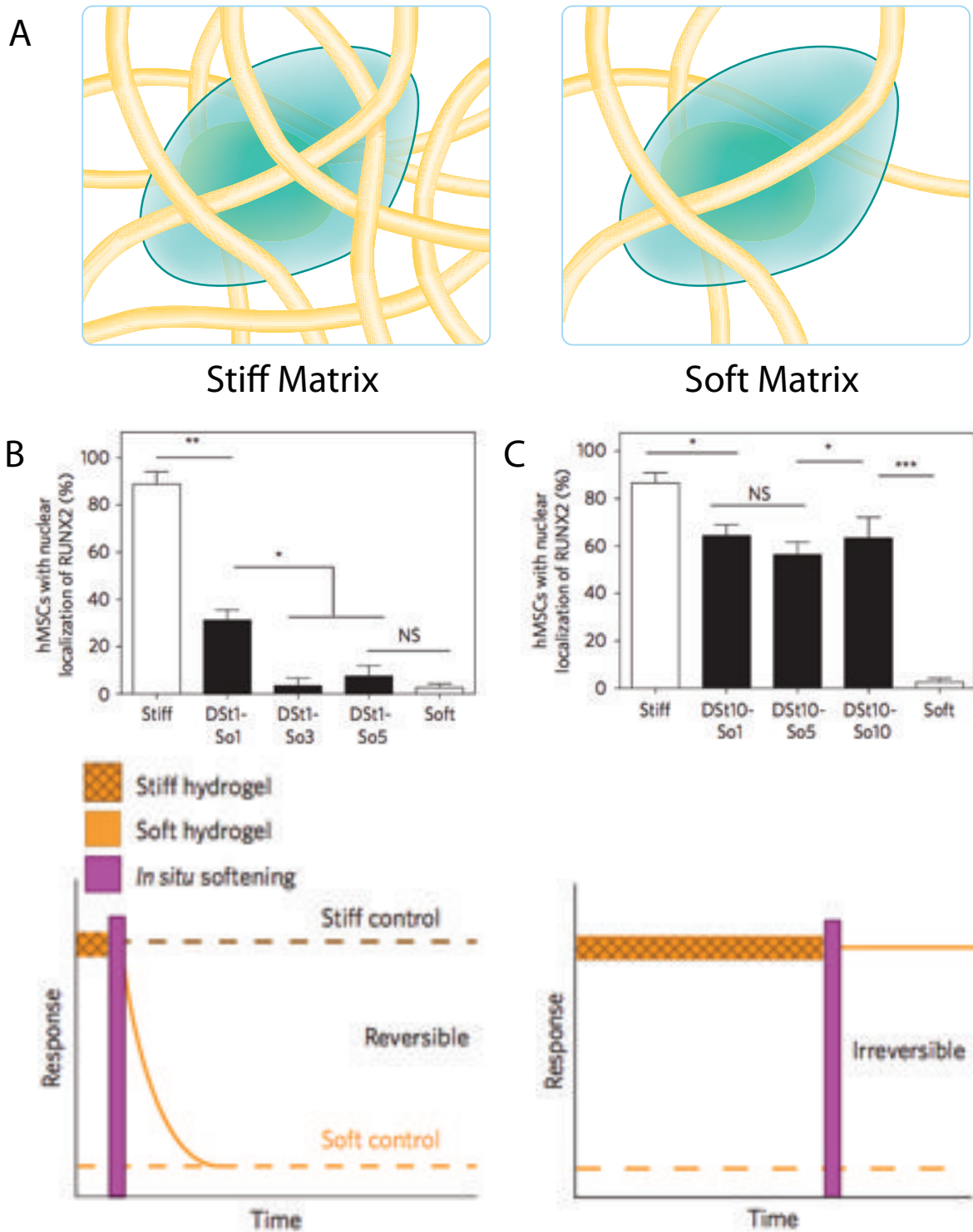


Figure 1.3 A) The ECM provides important biophysical cues, such as matrix elasticity, illustrated here with a stiff, dense matrix (Left) and a soft, loose matrix (Right). Synthetic hydrogels can recapitulate these properties by tuning their mechanical properties. B) Hydrogels

with phototunable elasticity provide a versatile platform to study the role of biophysical cues in directing cell function. Yang *et al.* [25] cultured MSC on stiff substrates for 1 or 10 days and then softened the hydrogels *in situ* using a pre-determined dose of light. RUNX2 and YAP nuclear localization was then observed for up to 10 days, and they both followed similar trends. Shown here, the percent of hMSC with nuclear RUNX2 localization returned to basal levels after being cultured for only 1 day on stiff substrates (DSt1) and different durations on soft substrates. The stiff and soft controls correspond to the average RUNX2 localization for cells only cultured on stiff substrates (i.e., not softened with light) or only on soft substrates (i.e., softened with light) and represent full and basal levels of activation, respectively. C) When hMSC were cultured on stiff substrates for 10 days (DSt10), RUNX2 localization persisted at active levels even after culture on soft substrates, indicating that 10 days on stiff substrates induced irreversible activation of RUNX2. The data are plotted as the mean \pm s.e.m. NS, not significant; *, $p < 0.05$; **, $p < 0.01$; ***, $p < 0.001$

1.5 The ECM as a reservoir of biochemical signals

Beyond serving as a structural framework, the ECM presents a myriad of biochemical cues that regulate cell function and direct macroscopic tissue development and regeneration. These active cues consist of adhesive domains present on ECM proteins (e.g., fibronectin, laminin), soluble molecules that diffuse through the ECM, and others that remain sequestered or substrate-bound. Here, the focus is to review some of the primary methods to present these biochemical signals in hydrogels by functionalizing them with short mimetic peptides of larger proteins or with functionalities that can physically sequester native biomacromolecules through affinity interactions (Figure 1.4A). Finally, the contextual presentation in which cells receive these cues affects the biomolecules efficacy and the cellular output that results; therefore, it is important to understand the interplay between biochemical and biophysical cues.

Within the *in vivo* milieu the ECM is known to sequester and bind many different molecules that then interact with cellular receptors. Recent advances in synthetic hydrogels have provided accessible techniques to recapitulate aspects of this biomolecule sequestration using versatile and bio-orthogonal chemistries for both specific and non-specific binding in a spatially defined manner. Some of these bioconjugation methods include thiol-ene, azide-alkyne,

maleimide-thiol, diels-alder, oxime, hydrazine and hydroxysuccinimide-amine reactions, which enable facile chemical modification of the target molecule and subsequent conjugation to hydrogel scaffolds at physiologically relevant concentrations while retaining the bioactivity of the target molecule [11, 28]. More recent developments in bio-orthogonal “click” chemistries have further enabled highly specific patterning of biomolecules in the presence of cells and biological moieties. For example, 3T3 fibroblast cells were encapsulated in PEG gels using a copper-free azide-alkyne reaction, and the cellular environments were subsequently modified in a spatially defined manner to direct cell migration using a thiol-ene photoconjugation reaction combined with photolithography [17].

For certain applications, peptides provide distinct advantages, compared to utilizing full proteins. Solid phase peptide synthesis allows bioactive cues to be readily synthesized and introduced into a matrix without some of the difficulties in maintaining the bioactivity of the target protein. For example, the adhesive ligand RGDS is routinely incorporated in hydrogels to promote cell attachment and increase survival [29]. Along with RGDS, many other common adhesive binding sites found in the ECM have been incorporated in hydrogels and an excellent review of this topic can be found in Brennan *et al.* [30]. Towards studying the role of matrix binding epitopes on cell secretory properties, Gould *et al.* used a combination of RGDS, VGVAPG, and P15 peptides and showed marked differences in the activation of valvular interstitial cells to myofibroblasts, depending on the ratio of these adhesive ligands [31]. Peptides have also been used as mimics of cell-cell interactions where Bian *et al.* presented covalently-bound N-cadherin mimetic peptides to MSC encapsulated in HA-based gels and observed accelerated chondrogenesis resulting in increased cartilage formation *in vitro* and *in vivo* [32]. Beyond peptide mimics of adhesive ligands, there is also significant effort to identify

sequences that mimic active sites of growth factors, such as stromal derived factor 1 (preserved C terminus and N terminus), a known chemoattractant, and bone morphogenetic proteins (e.g., DWIVA, KIPKASSVPTELSAISTLYL), a potent regulator of MSC differentiation [33-35]. However, peptides do not possess the activity of full proteins and in many instances, designing synthetic ECMs for local protein delivery is critical.

In vivo, many growth factors are physically bound and stored in the ECM through affinity interactions with local macromolecules, such as glycosaminoglycans. This results in localized concentration profiles of the target protein, reduced enzymatic cleavage, and effective presentation of bioactive ligands for cell receptor binding. Building from this notion, synthetic hydrogels have been designed to recapitulate aspects of biomolecule sequestration, where early work in the field demonstrated the use of heparin. Heparin is known to bind growth factors, proteases, and chemokines, and its presentation in hydrogels can be exploited to locally sequester cell secreted molecules to control local signaling [36, 37]. For example, a recent work by Purcell *et al.* used dextran-sulfate, as a heparin mimetic, within an MMP-degradable HA hydrogel to bind to TIMP-3, an MMP inhibitor, through electrostatic interactions [38]. This stimuli-responsive scaffold allowed for cell secreted MMPs to degrade the network and dictate spatially relevant release of TIMP-3. The scaffold was injected into myocardial infarcted (MI) pig hearts and pathophysiological MMP expression was reduced by 14 days post-MI.

Correspondingly, there is a push to develop more highly defined synthetic scaffolds utilizing *specific* binding pairs for sequestration of target molecules in a spatially defined method. Wylie *et al.* took advantage of the specific interactions of barnase-barstar and streptavidin-biotin by spatially patterning barnase and streptavidin into an agarose hydrogel using photolithography (Figure 1.4B) [18]. Next, proteins functionalized with either barstar or

biotin, were swollen into the hydrogel and immobilized only in locations where the binding partner was located to direct 3D adult neural precursor cell invasion. In a complementary approach, Mosiewicz *et al.* used enzymatically degradable hydrogels combined with photopatterning of growth factors to direct MSC migration (Figure 1.4C) [39]. First, MSC clusters were encapsulated in an MMP-degradable PEG hydrogel, and platelet derived growth factor B (PDGF-BB), a known MSC chemoattractant, was conjugated in precise regions near the cell cluster. MSC were shown to migrate in a biased direction towards the conjugated PDGF-BB as quantified through the cell densities within the patterned and unpatterned regions (Figure 1.3C). An interesting facet of this work focused on binding Fc-chimeric proteins to spatially tethered protein A molecules within the hydrogel, which has broad appeal for immobilizing biomolecules as many Fc-chimeric proteins are commercially available.

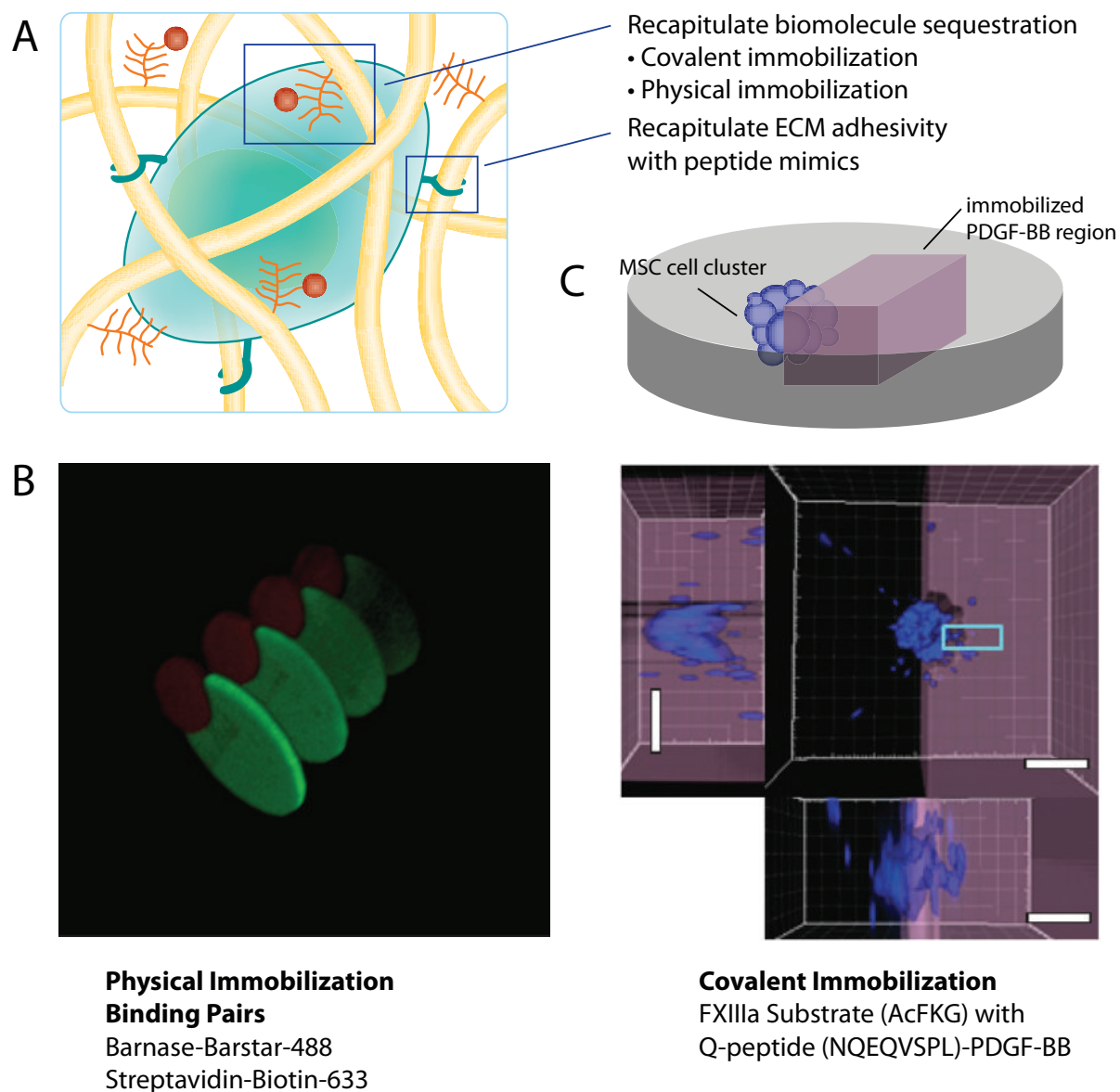


Figure 1.4 A) Techniques based on covalent and physical immobilization are being developed for spatial biomolecule patterning to recapitulate aspects of biomolecule sequestration. Further, peptide mimics have been shown to be effective for recapitulating cell adhesion in otherwise non-adhesive hydrogels. B) Using barstar-barnase and biotin-streptavidin binding pairs, Wylie *et al.* [18] spatially tethered fluorescently labeled sonic hedgehog and ciliary neurotrophic factor into a hydrogel through physical immobilization. C) Mosewicz *et al.* [39] spatially patterned PDGF-BB to direct the invasion of encapsulated MSC. A confocal micrograph shows that MSC, labeled with DAPI (blue), more efficiently invaded the patterned region of a hydrogel with covalently immobilized PDGF-BB (purple).

The context in which these biochemical cues are presented to cells can play a critical role in the efficacy and cellular output. Using highly defined synthetic scaffolds, compelling work is beginning to elucidate the synergistic and antagonistic relationships between biophysical and biochemical cues. For example, work from Chen and coworkers found that varying the rigidity of polyacrylamide gels modified the functional response of TGF- β 1 for mammary gland cells and kidney epithelial cells in inducing higher levels of apoptosis (less rigid substrate) or epithelial-mesenchymal transition (more rigid substrates) [40]. This knowledge is also advancing translational studies for clinical applications. Cosgrove *et al.* showed that inhibition of p38 α and p38 β on soft hydrogel culture platforms promoted higher yields of functional stem cell populations relative to inhibition on TCPS for muscle regeneration application [41]. In this example, the biochemical inhibition and the biophysical hydrogel culture platform worked synergistically, resulting in a desired cellular output for a clinical application. Complementary, there is a focus within the induced pluripotent stem cell community to use hydrogels to retain pluripotency and increase proliferation through the synergistic presentation of biochemical and biophysical cues which is discussed in depth by Dingal *et al.* [42]. Synthetic hydrogels provide a simple, versatile and highly defined culture platform to elucidate the interplay between biochemical and biophysical cues on cell function and further to engineer more effective tissue engineering scaffolds for regenerative medicine applications.

1.6 Cell-directed and user-directed microenvironmental ECM remodeling

The ECM is a highly dynamic environment that is locally degraded and remodeled during development, homeostasis, wound repair, and even pathophysiological events. Degradation of the ECM primarily occurs through enzymatic cleavage by cell-secreted proteases, allowing cells

to remodel their local microenvironment or move through this dense matrix (Figure 1.5A). To capture the dynamic nature of ECM remodeling, synthetic hydrogels are often engineered to degrade through hydrolytic mechanisms, user-tunable mechanisms (e.g., light cleavable, exogenous delivery of chemicals), or enzymatic mechanisms (e.g., protease secretion) [10]. This section will focus on cell-mediated and user-dictated degradation mechanisms, the former allowing the synthesis of hydrogels to observe cells in a native-like environment and the latter allowing user manipulation of the hydrogel to better understand matrix signaling.

To examine how stiffness and structure affect cell function, photodegradable hydrogels were developed that allow for user-tunable material properties in space and time. Photodegradable gels have been used in a number of studies that investigate how temporal manipulation of the synthetic hydrogel regulates cell function. As discussed previously, these user-tunable hydrogels have advanced our understanding of cellular mechanotransduction and mechanical ‘memory’ [25, 26]. Photodegradable hydrogels have also been used to study how cells receive mechanical information from the environment by spatially controlling cell adhesion on a sub-cellular length scale. Tibbitt *et al.* used photodegradable PEG hydrogels to study cytoskeletal pretension through sub-cellular focal adhesion detachment of encapsulated and spread cells within 3D hydrogels [44]. Further, photodegradable hydrogels in combination with two-photon lithography allow for structural changes such as developing 3D channels and shapes to be formed. Kloxin *et al.* used this technique to develop a culture platform that recapitulated the alveolar structure for epithelial lung cell alignment [45]. Using similar techniques, cyst-like and vascular-like structures can be created within a 3D scaffold for tissue regeneration applications.

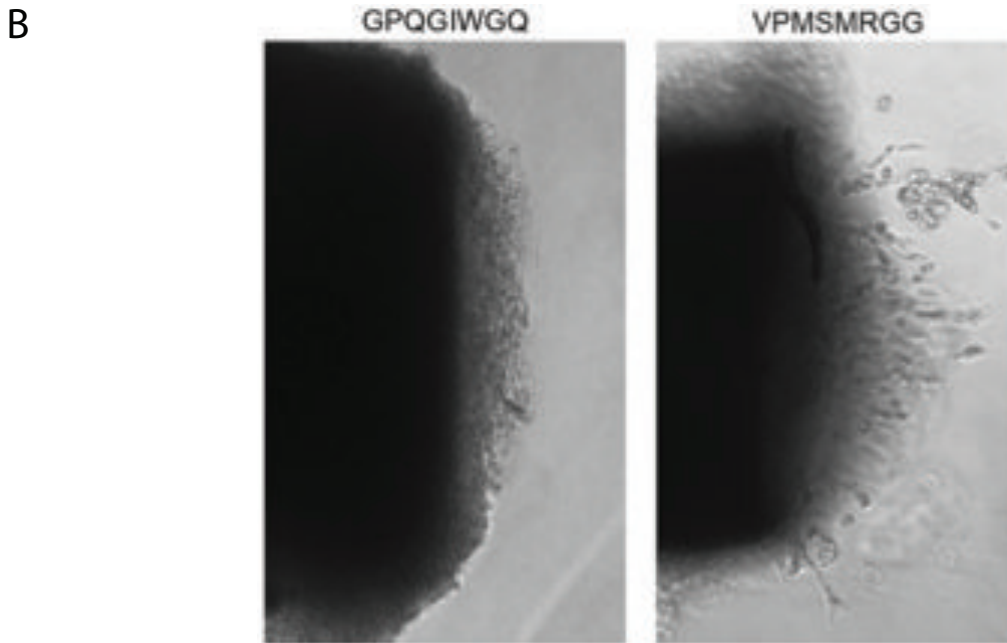
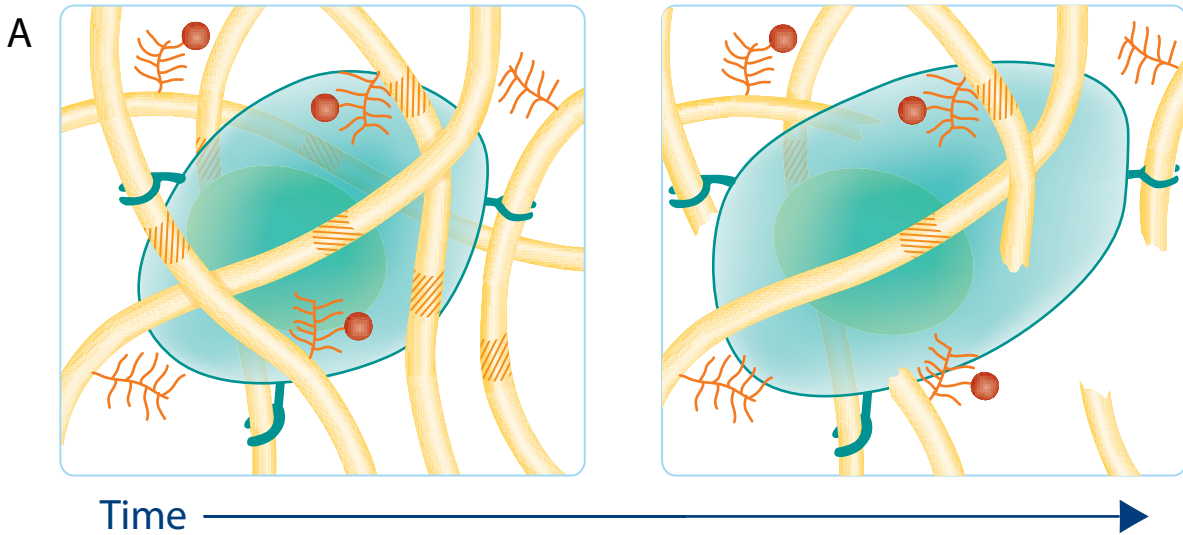


Figure 1.5 A) Cellular remodeling and degradation play an important role in regulating the dynamic nature of the ECM. The introduction of hydrogels that degrade in response to cell-secreted enzymes begins to recapitulate this natural process. B) Patterson *et al.* [43] synthesized PEG hydrogels that were crosslinked with two different peptide sequences that vary in degradation rates. Cells from the aortic chick ring invaded the MMP-degradable network at different rates based on the cleavage rate of the peptide sequence, GPQGIWG (slower) and VPMSMRGG (faster).

Synthetic hydrogels are routinely engineered to degrade in response to cell secreted enzymes, serving as robust *in vitro* models of tissue matrices or useful cell delivery vehicles. Seminal work from Lutolf *et al.* showed that by crosslinking a PEG-based hydrogel with an MMP-cleavable peptide sequence (Ac-GCRD-GPQGIWGQ-DRCG) cells locally degraded the material through a physiological mechanism allowing for cellular invasion into the hydrogel [21]. This ushered in a major advance towards synthetic scaffolds that more closely mimic the ECM. Similar materials and approaches are now being pursued to design biomaterials that can actively promote infiltration by endogenous cells or dispense delivered cells at sites of injury [46].

From a fundamental perspective, these materials are useful as *in vitro* culture platforms where cell-mediated matrix degradation has been implicated in determining cell differentiation fate. Khetan *et al.* encapsulated mesenchymal stem cells into hyaluronic acid (HA) based hydrogels and concluded that differentiation pathways were determined through degradation-mediated cellular traction and not a function of cell shape or elastic modulus of the material [47]. Finally, cell-mediated degradation can be tuned through the introduction of a myriad of enzymatically-degradable peptide sequences with varying cleavage kinetics enabling the design of materials that are application and hypothesis specific through the simple functionalization of effective peptide sequences [43]. For example, Patterson *et al.* studied the degradation rates of a large subset of enzymatically degradable peptides in the presence of MMP-1 or MMP-2 to better engineer hydrogels for 3D cellular invasion from aortic chick rings into PEG based hydrogels. Shown in Figure 1.5B, is cell invasion into a hydrogel with a slower cleaving peptide (GPQGIWGQ) or a faster cleaving peptide (VPMSMRGG) for the MMPs secreted by the migrating cells.

While advances in real time tracking have fueled our understanding of cell matrix interactions in 3D, less is understood about dynamic changes in material properties that occur as a result of degradation of the hydrogel scaffold itself. To this end, fluorescently quenched peptides have been developed as sensors to directly detect cleavage of sequences (un-quenching the fluorescence), as a measure of MMP within a hydrogel matrix [48-50]. These peptides are conjugated as ligands isotropically within the network, and when cleaved become fluorescent and can be visualized using fluorescent microscopy or quantified using a plate reader. There is also a focus on understanding how the material structure in the pericellular region is being degraded and remodeled, and multiple particle tracking is one technique that has emerged to characterize the gel-sol transition surrounding a cell [51, 52]. Cells also attach to the network through focal adhesions and pull on the network to spread and migrate. Here, traction force microscopy has proven to be a useful tool to measure this force in both 2D and 3D hydrogel cultures [47, 53, 54]. Together these microrheological methods and spectroscopic tools for characterizing degradation will provide the field with a much deeper understanding of the complex changes that occur during cell-mediated matrix remodeling.

1.7 Approach of this thesis

The global objective of this thesis is to develop and use thiol-ene PEG-based hydrogels, especially those functionalized with biochemical cues (e.g., peptides, proteins), to recapitulate important facets of the extracellular matrix and understand their role in directing human mesenchymal stem cell (hMSC) migration, differentiation, and proliferation *in vitro* and regulating bone healing *in vivo*. To achieve this objective, Chapter 2 outlines the specific aims of this thesis: characterize hMSC migration in peptide-functionalized PEG hydrogels while

varying biophysical and biochemical cues, measure dynamic cell-material interactions and local network remodeling during 3D hMSC migration in hydrogels, deliver full-length protein signals to direct hMSC behavior and study local protein presentation cell invasion and mineralized tissue formation in a critical sized defect *in vivo*, and exploit bio-click reactions to immobilize multiple protein combinations to screen their synergistic effects on hMSC behavior, which is then followed by four chapters that document the experiments designed to meet these aims. Cell migration is regulated by a myriad of physical and biochemical cues, so in Chapter 3, the focus is placed on characterizing the role of network crosslinking density and adhesive ligand density on permitting hMSC migration in 3D. Experiments are designed to track 3D cell motility in real time using live-cell videomicroscopy and cell spreading, cell attachment, and migration speed and persistence are quantified as a function of matrix properties.

While cell-matrix interactions are known to play an integral role in directing cell behavior (e.g., migration, differentiation), understanding the effect of material properties on hMSC is complex, especially in cellularly-degradable hydrogels. In these materials, bulk property measurements are less likely to be indicative of how a cell is remodeling and interacting with its local microenvironment. Towards addressing this complexity, Chapter 4 introduces microrheological techniques that are used to quantify and characterize material properties in the pericellular region of migrating hMSCs (within the same enzymatically-degradable scaffolds studied in Chapter 3). Several analytical methods are explored with the goal of providing insight into spatial variations that occur in gel properties, at multiple length and time scales, as a result of local cell-mediated degradation and remodeling of the local microenvironment.

During bone development and fracture healing, the extracellular environment presents a complex milieu of protein molecules in soluble and immobilized forms to direct local cell

function (e.g., migration, differentiation, proliferation). In Chapter 5, the aim is to understand how single and multiple protein cues direct hMSC migration and differentiation by exploiting bio-click chemistries to introduce and control protein presentation in PEG hydrogels. Specifically, thiol-ene photo-coupling is utilized to immobilize stromal derived factor 1a (SDF1), a known chemoattractant molecule for hMSC, and bone morphogenetic protein 2 (BMP2), a potent protein to direct hMSC osteogenesis. *In vitro* results show effective immobilization and bioactivity of the two proteins to direct both hMSC invasion and osteogenic differentiation. Finally, as a proof of concept, a biomaterial system is developed to immobilize and deliver these proteins into a rat calvarial critical-sized bone defect model. Migration-permitting hydrogels are selected (Chapter 3) and the effect of local protein presentation in inducing bone healing *in vivo* is measured through histological staining and microCT analysis.

With an appreciation for increasing sophistication in biomaterial design, Chapter 6 investigates bioorthogonal click chemistries and photopatterning methods to develop versatile and biologically relevant methods to screen and study the effects of multiple protein signals on hMSCs. Material chemistries are developed to not only allow spatial patterning of multiple proteins at distinct locations and tunable concentrations, but also in the presence of complex protein solutions that are used during cell culture. These multi-protein patterns are used to study combination and synergistic effects of SDF1, BMP2, and fibroblast growth factor 2 (FGF2) in directing hMSC behavior by measuring cellular invasion, osteogenesis, and proliferation. Finally, Chapter 7 summarizes the key findings from this thesis and provides recommendations as to future directions to build from this research.

1.8 References

- [1] Watt FM, Huck WTS. Role of the extracellular matrix in regulating stem cell fate. *Nat Rev Mol Cell Bio* 2013;14:467-73.
- [2] Lu PF, Weaver VM, Werb Z. The extracellular matrix: A dynamic niche in cancer progression. *J Cell Biol* 2012;196:395-406.
- [3] Moroni F, Mirabella T. Decellularized matrices for cardiovascular tissue engineering. *American journal of stem cells* 2014;3:1-20.
- [4] Faulk DM, Johnson SA, Zhang L, Badylak SF. Role of the extracellular matrix in whole organ engineering. *Journal of cellular physiology* 2014;229:984-9.
- [5] Ott HC, Matthiesen TS, Goh SK, Black LD, Kren SM, Netoff TI, et al. Perfusion-decellularized matrix: using nature's platform to engineer a bioartificial heart. *Nature medicine* 2008;14:213-21.
- [6] Karp G. *Cell and molecular biology : concepts and experiments*. 3rd ed. New York: J. Wiley; 2002.
- [7] Hubbell JA. Biomaterials in Tissue Engineering. *Bio-Technol* 1995;13:565-76.
- [8] Humphries MJ. The Molecular-Basis and Specificity of Integrin Ligand Interactions. *J Cell Sci* 1990;97:585-92.
- [9] Annabi N, Tamayol A, Uquillas JA, Akbari M, Bertassoni LE, Cha C, et al. 25th Anniversary Article: Rational Design and Applications of Hydrogels in Regenerative Medicine. *Adv Mater* 2014;26:85-124.
- [10] Kharkar PM, Kiick KL, Kloxin AM. Designing degradable hydrogels for orthogonal control of cell microenvironments. *Chemical Society reviews* 2013;42:7335-72.
- [11] Azagarsamy MA, Anseth KS. Bioorthogonal Click Chemistry: An Indispensable Tool to Create Multifaceted Cell Culture Scaffolds. *ACS macro letters* 2013;2:5-9.
- [12] Hoyle CE, Bowman CN. Thiol-ene click chemistry. *Angewandte Chemie* 2010;49:1540-73.
- [13] Codelli JA, Baskin JM, Agard NJ, Bertozzi CR. Second-generation difluorinated cyclooctynes for copper-free click chemistry. *Journal of the American Chemical Society* 2008;130:11486-93.
- [14] Hudalla GA, Eng TS, Murphy WL. An approach to modulate degradation and mesenchymal stem cell behavior in poly(ethylene glycol) networks. *Biomacromolecules* 2008;9:842-9.
- [15] Hern DL, Hubbell JA. Incorporation of adhesion peptides into nonadhesive hydrogels useful for tissue resurfacing. *J Biomed Mater Res* 1998;39:266-76.

- [16] DeLong SA, Moon JJ, West JL. Covalently immobilized gradients of bFGF on hydrogel scaffolds for directed cell migration. *Biomaterials* 2005;26:3227-34.
- [17] DeForest CA, Anseth KS. Cytocompatible click-based hydrogels with dynamically tunable properties through orthogonal photoconjugation and photocleavage reactions. *Nature Chemistry* 2011;3:925-31.
- [18] Wylie RG, Ahsan S, Aizawa Y, Maxwell KL, Morshead CM, Shoichet MS. Spatially controlled simultaneous patterning of multiple growth factors in three-dimensional hydrogels. *Nature materials* 2011;10:799-806.
- [19] DeForest CA, Polizzotti BD, Anseth KS. Sequential click reactions for synthesizing and patterning three-dimensional cell microenvironments. *Nature materials* 2009;8:659-64.
- [20] Fairbanks BD, Schwartz MP, Halevi AE, Nuttelman CR, Bowman CN, Anseth KS. A Versatile Synthetic Extracellular Matrix Mimic via Thiol-Norbornene Photopolymerization. *Adv Mater* 2009;21:5005-+.
- [21] Lutolf MP, Lauer-Fields JL, Schmoekel HG, Metters AT, Weber FE, Fields GB, et al. Synthetic matrix metalloproteinase-sensitive hydrogels for the conduction of tissue regeneration: engineering cell-invasion characteristics. *Proceedings of the National Academy of Sciences of the United States of America* 2003;100:5413-8.
- [22] DeForest CA, Sims EA, Anseth KS. Peptide-Functionalized Click Hydrogels with Independently Tunable Mechanics and Chemical Functionality for 3D Cell Culture. *Chem Mater* 2010;22:4783-90.
- [23] DeForest CA, Anseth KS. Photoreversible Patterning of Biomolecules within Click-Based Hydrogels. *Angew Chem Int Edit* 2012;51:1816-9.
- [24] Engler AJ, Sen S, Sweeney HL, Discher DE. Matrix elasticity directs stem cell lineage specification. *Cell* 2006;126:677-89.
- [25] Yang C, Tibbitt MW, Basta L, Anseth KS. Mechanical memory and dosing influence stem cell fate. *Nature materials* 2014.
- [26] Wang H, Tibbitt MW, Langer SJ, Leinwand LA, Anseth KS. Hydrogels preserve native phenotypes of valvular fibroblasts through an elasticity-regulated PI3K/AKT pathway. *Proceedings of the National Academy of Sciences of the United States of America* 2013;110:19336-41.
- [27] Gilbert PM, Havenstrite KL, Magnusson KE, Sacco A, Leonardi NA, Kraft P, et al. Substrate elasticity regulates skeletal muscle stem cell self-renewal in culture. *Science* 2010;329:1078-81.
- [28] Jabbari E. Bioconjugation of hydrogels for tissue engineering. *Current opinion in biotechnology* 2011;22:655-60.

- [29] Perlin L, MacNeil S, Rimmer S. Production and performance of biomaterials containing RGD peptides. *Soft matter* 2008;4:2331-49.
- [30] Brennan AB, Kirschner CM, Society for Biomaterials. Bio-inspired materials for biomedical engineering.
- [31] Gould ST, Darling NJ, Anseth KS. Small peptide functionalized thiol-ene hydrogels as culture substrates for understanding valvular interstitial cell activation and de novo tissue deposition. *Acta biomaterialia* 2012;8:3201-9.
- [32] Bian L, Guvendiren M, Mauck RL, Burdick JA. Hydrogels that mimic developmentally relevant matrix and N-cadherin interactions enhance MSC chondrogenesis. *Proceedings of the National Academy of Sciences of the United States of America* 2013;110:10117-22.
- [33] MacArthur JW, Jr., Purcell BP, Shudo Y, Cohen JE, Fairman A, Trubelja A, et al. Sustained release of engineered stromal cell-derived factor 1- α from injectable hydrogels effectively recruits endothelial progenitor cells and preserves ventricular function after myocardial infarction. *Circulation* 2013;128:S79-86.
- [34] Hiesinger W, Frederick JR, Atluri P, McCormick RC, Marotta N, Muenzer JR, et al. Spliced stromal cell-derived factor-1 α analog stimulates endothelial progenitor cell migration and improves cardiac function in a dose-dependent manner after myocardial infarction. *J Thorac Cardiovasc Sur* 2010;140:1174-80.
- [35] Madl CM, Mehta M, Duda GN, Heilshorn SC, Mooney DJ. Presentation of BMP-2 mimicking peptides in 3D hydrogels directs cell fate commitment in osteoblasts and mesenchymal stem cells. *Biomacromolecules* 2014;15:445-55.
- [36] Liang YK, Kiick KL. Heparin-functionalized polymeric biomaterials in tissue engineering and drug delivery applications. *Acta biomaterialia* 2014;10:1588-600.
- [37] Rabenstein DL. Heparin and heparan sulfate: structure and function. *Natural product reports* 2002;19:312-31.
- [38] Purcell BP, Lobb D, Charati MB, Dorsey SM, Wade RJ, Zellars KN, et al. Injectable and bioresponsive hydrogels for on-demand matrix metalloproteinase inhibition. *Nature materials* 2014;13:653-61.
- [39] Mosiewicz KA, Kolb L, van der Vlies AJ, Martino MM, Lienemann PS, Hubbell JA, et al. In situ cell manipulation through enzymatic hydrogel photopatterning. *Nature materials* 2013;12:1072-8.
- [40] Leight JL, Wozniak MA, Chen S, Lynch ML, Chen CS. Matrix rigidity regulates a switch between TGF- β 1-induced apoptosis and epithelial-mesenchymal transition. *Molecular biology of the cell* 2012;23:781-91.

- [41] Cosgrove BD, Gilbert PM, Porpiglia E, Mourkioti F, Lee SP, Corbel SY, et al. Rejuvenation of the muscle stem cell population restores strength to injured aged muscles. *Nature medicine* 2014;20:255-64.
- [42] Dingal PC, Discher DE. Combining insoluble and soluble factors to steer stem cell fate. *Nature materials* 2014;13:532-7.
- [43] Patterson J, Hubbell JA. Enhanced proteolytic degradation of molecularly engineered PEG hydrogels in response to MMP-1 and MMP-2. *Biomaterials* 2010;31:7836-45.
- [44] Tibbitt MW, Kloxin AM, Dyamenahalli KU, Anseth KS. Controlled two-photon photodegradation of PEG hydrogels to study and manipulate subcellular interactions on soft materials. *Soft matter* 2010;6:5100-8.
- [45] Kloxin AM, Lewis KJ, DeForest CA, Seedorf G, Tibbitt MW, Balasubramaniam V, et al. Responsive culture platform to examine the influence of microenvironmental geometry on cell function in 3D. *Integrative biology : quantitative biosciences from nano to macro* 2012;4:1540-9.
- [46] Kyburz KA, Anseth KS. Three-dimensional hMSC motility within peptide-functionalized PEG-based hydrogels of varying adhesivity and crosslinking density. *Acta biomaterialia* 2013;9:6381-92.
- [47] Khetan S, Guvendiren M, Legant WR, Cohen DM, Chen CS, Burdick JA. Degradation-mediated cellular traction directs stem cell fate in covalently crosslinked three-dimensional hydrogels. *Nature materials* 2013;12:458-65.
- [48] Leight JL, Alge DL, Maier AJ, Anseth KS. Direct measurement of matrix metalloproteinase activity in 3D cellular microenvironments using a fluorogenic peptide substrate. *Biomaterials* 2013;34:7344-52.
- [49] Lee SH, Moon JJ, Miller JS, West JL. Poly(ethylene glycol) hydrogels conjugated with a collagenase-sensitive fluorogenic substrate to visualize collagenase activity during three-dimensional cell migration. *Biomaterials* 2007;28:3163-70.
- [50] Packard BZ, Artym VV, Komoriya A, Yamada KM. Direct visualization of protease activity on cells migrating in three-dimensions. *Matrix Biol* 2009;28:3-10.
- [51] Schultz KM, Anseth KS. Monitoring degradation of matrix metalloproteinases-cleavable PEG hydrogels via multiple particle tracking microrheology. *Soft matter* 2013;9:1570-9.
- [52] Schultz KM, Furst EM. Microrheology of biomaterial hydrogelators. *Soft matter* 2012;8:6198-205.
- [53] Tan JL, Tien J, Pirone DM, Gray DS, Bhadriraju K, Chen CS. Cells lying on a bed of microneedles: An approach to isolate mechanical force. *Proceedings of the National Academy of Sciences of the United States of America* 2003;100:1484-9.

[54] Legant WR, Miller JS, Blakely BL, Cohen DM, Genin GM, Chen CS. Measurement of mechanical tractions exerted by cells in three-dimensional matrices. *Nat Methods* 2010;7:969-U113.

CHAPTER II

THESIS OBJECTIVES

2.1 Overview

Bone marrow derived human mesenchymal stem cells (hMSCs) play a critical role in the complex and coordinated bone fracture healing cascade, and their cellular role has been implicated in the recruitment and colonization of the defect, suppressing the immune response, and even differentiating down osteogenic lineages [1-3]. While bone is a tissue with a natural capacity for healing, large bone defects that do not spontaneously heal, often termed critical sized defects, necessitate clinical intervention [4]. Thus, there is a desire for bioengineering strategies to facilitate healing of these large defects, and one approach is to design bioactive materials that might recruit endogenous hMSC to defect sites and present local osteogenic cues to improve bone regeneration.

While numerous biomaterial scaffolds exist, the focus of this thesis research is on biofunctional poly(ethylene glycol) (PEG) based hydrogels, which have been shown to promote healing of critical sized defects in rat calvarial defects by simply being introduced into fracture sites [5]. PEG hydrogels functionalized with peptides or proteins can serve as synthetic mimics of the extracellular matrix and promote tissue regeneration [6]. However, much remains to be learned about delivery of appropriate osteoinductive and chemoattractant cues, and this necessitates detailed *in vitro* studies that allow one to study how matrix signaling can be used to direct hMSC migration and differentiation. For example, by varying the hydrogel crosslinking

density and/or introducing bioactive peptides and proteins, the physical and biochemical properties of these bioscaffolds can be tuned to direct and manipulate hMSC behavior. Building on this fundamental understanding, the overall goal of this thesis research is to characterize and design biomolecule-functionalized hydrogels that can promote high levels of hMSC migration through tuning of physical properties and engineering strategies to control the contextual presentation and delivery of bioactive peptides and/or proteins. This material design enables one to explore the influence of local bioscaffold properties in directing hMSC migration, invasion, and differentiation through both *in vitro* and *in vivo* assays.

Specifically, we hypothesize that through by controlling the network connectivity and adhesivity of the enzymatically-degradable hydrogels, scaffolds can be designed that permit high levels of hMSC migration can be fabricated. Further, we hypothesize that delivery of a chemotactic protein, such as stromal derived factor 1 α (SDF-1), will afford the ability to direct hMSC migration and invasion into biomaterial niches, and the ability to design multifunctional signals, such as incorporation of osteogenic cues (e.g., BMP-2) within the hydrogels can be designed to locally direct the differentiation of recruited or encapsulated hMSCs. As proof of concept, such scaffolds are tested in a rat calvarial bone defect model to study how local protein presentation affects the complex bone healing cascade in directing bone growth. The complexity of engineering wound healing scaffolds then motivates the development of new materials and *in vitro* screening assays to probe the effects of the presentation of multiple protein cues on hMSC behavior by controlling their introduction in a spatial and dose-dependent manner. Bioorthogonal click reactions are be utilized to spatially pattern and immobilize proteins in a complex, 3D hMSC culture system.

To test all of these hypotheses the specific aims of this thesis are as follows:

Specific Aim 1: Characterize hMSC migration in peptide-functionalized PEG hydrogels as a function of network crosslinking density and adhesivity by quantifying multiple measures of cell migration.

During wound healing and development, hMSC migration is orchestrated by a complex milieu of biophysical (e.g., matrix density, stiffness) and biochemical (e.g., adhesivity, chemoattractant proteins) cues that direct the speed, persistence, and direction of individual migrating hMSC [7, 8]. Peptide-functionalized hydrogels provide a culture platform to recapitulate governing aspects of the hMSC microenvironment to systematically study their role in permitting and promoting three-dimensional migration. Foundational work using biomaterial scaffolds has begun to correlate the role of microenvironmental cues on cell migration in two and three-dimensional contexts; however, there is lack of knowledge in regards to how these cues regulate individual hMSC migration in a 3D context over a broad range of material properties. Understanding how aspects of the hMSC microenvironment direct migration will allow for better-engineered materials to act as cell carrier platforms or as recruitment platforms for endogenous hMSC for bone healing applications. Therefore, the primary goal of Specific Aim 1 is to fabricate a peptide-functionalized PEG hydrogel that permit isotropic 3D migration of encapsulated hMSC, and where the adhesivity and crosslinking density of the hydrogel is varied to quantifiably characterize their role in governing 3D hMSC migration as a function of gel structure.

With this goal in mind, experiments are designed to engineer a 3D platform that promotes high levels of hMSC migration through tuning of the physical (e.g., crosslinking density) and biochemical (e.g., adhesive ligand density) properties of the cellular microenvironment. We

hypothesized that hydrogels with low crosslinking densities, thus reducing the physical barrier of a migrating cell, and high adhesive ligand density, increasing the level of cellular attachment, would promote the highest degree of 3D migration. First, the crosslinking density of the peptide-functionalized hydrogel was varied from 0.18 to 1.6 mM to study its effect on hMSC spreading, attachment, and migration. Variation of the crosslinking density is achieved by the polymerization of off-stoichiometric concentrations of a matrix metalloproteinase (MMP) degradable di-thiol linker (KCGPQG↓IWGQCK) relative to a 4-arm PEG-norbornene. The spreading of the encapsulated hMSC is quantified by imaging cells after 24 hours of culture. Additionally, differences in cellular attachment to the network are visualized through immunostaining of the actin stress fibers and $\beta 1$ integrin. Three-dimensional cell migration is tracked using live-cell videomicroscopy, and the mean square displacements from individual cell tracks are analyzed with a persistent random walk model to elucidate important migration metrics, such as speed, persistence, percent migration, and mean free path. Next, the concentration of adhesive ligand, CRGDS, is varied from 0.001 to 1 mM within a low crosslinked hydrogel ($\rho_{xl} = 0.18$ mM) by varying the concentration of CRGDS in the pre-polymerized solution. Again, hMSC spreading, attachment, and migration is measured to elucidate the effect of ligand density on 3D hMSC behavior.

Specific Aim 2: Measure dynamic cell-material interactions and local network remodeling during 3D hMSC migration in hydrogels on relevant cellular length scales

Three-dimensional cell migration is regulated by local material properties surrounding the cell in the pericellular region; however, traditional matrix property measurements primarily characterize bulk properties of the hydrogel. To date, there is a gap in measuring and

understanding these local material properties during 3D cellular migration in enzymatically-degradable hydrogels where cells exert traction forces, degrade, and remodel the local region. A better-characterized microenvironment will aid in designing biomaterials that more effectively interact in a dynamic manner and direct cell function. Therefore, the focus of Specific Aim 2 is to use microrheological techniques to measure the dynamic changes to material properties within the pericellular region of migrating hMSC within enzymatically degradable hydrogels.

Specifically, microparticles ($D = 1 \text{ } \mu\text{m}$) are encapsulated along with hMSC within enzymatically degradable hydrogels that permit high levels of hMSC migration. Videomicroscopy is used to track the spatial positions of microparticles over time to calculate individual mean squared displacements (MSD) of the microparticles within the pericellular region, which can be related to rheological properties using the Generalized Stoke-Einstein relation. Microparticle displacement maps and particle image velocimetry plots are created to allow for the quantitative visualization of both the spatial and temporal properties of the local network during 3D hMSC migration. To gain a deeper understanding of how the cell-directed matrix remodeling is occurring, inhibition studies are performed to elucidate the role of cell-secreted matrix metalloproteinases (MMPs) and cellular tension on local matrix properties. Finally, to relate the microscopic material changes to macroscopic tunnels formed, fluorescently labeled gels are imaged revealing large defects left behind from migrating hMSC.

Specific Aim 3: Deliver chemotactic and osteogenic cues to direct 3D hMSC migration and differentiation, and explore how the contextual presentation of localized proteins within a thiol-ene hydrogel promote bone formation within a critical-sized calvarial defect model.

The extracellular matrix presents a myriad of proteins and biomolecules that direct hMSC

behavior (e.g., migration, differentiation, proliferation). Oftentimes, these molecules are presented to cells in a locally defined manner, either through endogenous signaling by cell-secreted factors or by local matrix factors that often involve physical interactions of cell-secreted factors with glycosaminoglycans. To direct cell recruitment and invasion within the hydrogel networks, the focus in this thesis is placed on the delivery of small proteins called chemokines, as this can be readily translated to clinical applications for cell recruitment. Additionally, there is a desire to direct the differentiation of cells that have colonized a hydrogel through the presentation of osteogenic cues. Thiol-ene hydrogels provide a simplified and effective platform to present cells with chemokines and osteogenic cues in relevant contexts and concentrations that recapitulate facets of their presentation in the extracellular matrix *in vivo*. Specifically, soluble delivery of biomolecules is achieved by the high water content and large mesh size of the hydrogel allowing for facile diffusion of the chemokines, and immobilization to the matrix is accomplished by thiol-ene conjugation chemistry [9]. For this work, stromal derived factor 1 α (SDF-1) is selected as the chemokine of interest and bone morphogenetic protein 2 (BMP-2) as an osteoinductive factor. The first objective of Specific Aim 3 is to immobilize SDF-1 and BMP-2 using thiol-ene chemistry and measure their bioactivity.

SDF-1 and BMP-2 are reacted with Traut's reagent to convert primary amines found on the molecules into thiol moieties. Thiolated proteins (SH-SDF1 and SH-BMP-2) are incorporated into the hydrogel network through inclusion into the pre-polymerized macromer solution and covalently attaching to the norbornene moieties present on the PEG macromers during gel formation. The structure and immobilization efficiency in user-defined concentrations for both proteins is measured by modified section-ELISA techniques. Next, the bioactivity of SH-SDF-1 is measured by quantification of phosphorylation events on the CXCR4 receptor

found on hMSC. To detect the bioactivity of immobilized SH-BMP2, hMSC are encapsulated into hydrogels with either, no BMP-2 present, soluble BMP-2, or immobilized SH-BMP-2. After 3 days, the presence of alkaline phosphatase (ALP), an early osteogenic differentiation marker, is measured.

To test the efficacy of protein-loaded gels in signaling endogenous cells, a rat calvarial bone defect model is utilized to investigate the performance of various scaffold formulations in bone regeneration *in vivo*. The second goal of Specific Aim 3 is to introduce hydrogels functionalized with SH-SDF-1 and SH-BMP-2 into the critical sized rat calvarial defect model to measure bone formation over time. Hydrogels that permit efficient hMSC migration (Specific Aim 1) are then introduced into critical-sized rat calvarial defects to provide a traditional model of bone fracture healing to determine the effect of local protein presentation on bone growth and tissue development. The following conditions are tested: 1) Entrapped soluble SDF-1 (10 ng/mL), 2) immobilized SH-SDF-1 (10 ng/mL), 3) immobilized SH-BMP-2 (1000 ng/mL), and 4) immobilized SH-SDF-1 (10 ng/mL) and immobilized SH-BMP-2 (1000 ng/mL). MicroCT scans are performed at week 0 and week 4 to elucidate bone formation within the defect. At the week 4 time point, the rats are sacrificed, and the bone defects are excised and analyzed for new tissue formation and cellularity of the defects using histological techniques.

Specific Aim 4: Exploit multiple bio-click reactions to immobilize protein signals in physiologically relevant 3D matrices and screen the effect of localized protein combinations on hMSC proliferation, migration or differentiation.

An hMSC within the *in vivo* microenvironment is presented with a highly complex milieu of biochemical cues making it difficult to isolate individual and synergistic effects of specific

proteins on cell function. However, when designing biomaterials there is a desire to be cognizant of the effective dose, contextual presentation, and interplay of multiple proteins to better engineer platforms for tissue engineering applications (e.g., *ex vivo* cell culture platforms, cell carrier matrices, biomolecule delivery vehicles). To this end, the use of synthetic hydrogels in combination with bio-orthogonal click reactions can result in spatially distinct patterns of multiple proteins functionalized within a matrix to define and tune the local microenvironment a cell resides to better elucidate the biomolecule(s) role in regulating cell behavior. Additionally, we hypothesize that utilizing bio-orthogonal reactions allows the functionalization reactions to occur in cytocompatible solvents to retain high levels of protein bioactivity and effective immobilization in the presence of complex protein solutions. Therefore, the goal of Specific Aim 4 is to develop a series of bio-orthogonal click reactions to functionalize thiol-ene hydrogels (Specific Aim 1) with tunable and spatially distinct multi-protein microenvironments. Then use this versatile platform to probe the isolated and synergistic effects of multiple proteins on directing and regulating hMSC behavior in highly defined microenvironments.

To achieve this goal, thiol-ene and thiol-yne chemistries are used to pattern bio-orthogonal reaction pairs in peptide-functionalized hydrogels using dynamic light projection in spatially defined regions. Subsequently, copper-free strain promoted azide alkyne cycloaddition (SPAAC) and inverse electron demand Diels-Alder (IEDDA) reaction pairs are utilized to “click” proteins into pre-patterned regions in a single step. Initial experiments look to characterize the level of control over the spatial patterns and the immobilized protein concentrations through varying light exposure to specific regions of the hydrogel. The patterning efficiency is then measured in the presence of complex serum protein solutions and quantified with image analysis. To ensure the preservation of the protein bioactivity after immobilization

for both reaction protocols, two common cell assays were chosen: ALP staining of hMSC to detect the presence or absence of immobilized DBCO-BMP2 and an EdU staining to detect hMSC proliferation in response to the presence or absence of immobilized TCO-FGF. Finally, arrays of distinct spatial and concentration doses of two different proteins are created to screen their isolated and synergistic effects on hMSC behavior.

2.2 References

- [1] Uccelli A, Moretta L, Pistoia V. Mesenchymal stem cells in health and disease. *Nature reviews Immunology* 2008;8:726-36.
- [2] Caplan AI, Correa D. The MSC: an injury drugstore. *Cell Stem Cell* 2011;9:11-5.
- [3] Karp JM, Teol GSL. Mesenchymal Stem Cell Homing: The Devil Is in the Details. *Cell Stem Cell* 2009;4:206-16.
- [4] Mistry AS, Mikos AG. Tissue engineering strategies for bone regeneration. *Advances in biochemical engineering/biotechnology* 2005;94:1-22.
- [5] Mariner PD, Wudel JM, Miller DE, Genova EE, Streubel SO, Anseth KS. Synthetic hydrogel scaffold is an effective vehicle for delivery of INFUSE (rhBMP2) to critical-sized calvaria bone defects in rats. *Journal of orthopaedic research : official publication of the Orthopaedic Research Society* 2013;31:401-6.
- [6] Tibbitt MW, Anseth KS. Hydrogels as extracellular matrix mimics for 3D cell culture. *Biotechnology and Bioengineering* 2009;103:655-63.
- [7] Friedl P, Wolf K. Plasticity of cell migration: a multiscale tuning model. *J Cell Biol* 2010;188:11-9.
- [8] Kim H-D, Peyton SR. Bio-inspired materials for parsing matrix physicochemical control of cell migration: a review. *Integrative biology: quantitative biosciences from nano to macro* 2012;4:37-52.
- [9] Hoyle CE, Bowman CN. Thiol-ene click chemistry. *Angewandte Chemie* 2010;49:1540-73.

CHAPTER III

THREE-DIMENSIONAL hMSC MOTILITY WITHIN PEPTIDE-FUNCTIONALIZED PEG-BASED HYDROGEL OF VARYING ADHESIVITY AND CROSSLINKING DENSITY

As published in *Acta Biomaterialia*, **9**, 6381-6392, (2013)

3.1 Abstract

Human mesenchymal stem cell (hMSC) migration and recruitment play a critical role during bone fracture healing. Within the complex 3D *in vivo* microenvironment, hMSC migration is regulated through a myriad of extracellular cues. Here, we use a thiol-ene photopolymerized hydrogel to recapitulate structural and bioactive inputs in a tunable manner to understand their role in regulating 3D hMSC migration. Specifically, peptide-functionalized poly(ethylene glycol) hydrogels were used to encapsulate hMSC while varying the crosslinking density, 0.2 to 1.6 mM, and the adhesive ligand density, 0.001 to 1.0 mM. Using live cell videomicroscopy migratory cell paths were tracked and fit to a persistent random walk model. It was shown that hMSC migrating through the lowest crosslinking density and highest adhesivity had more sustained polarization, higher migrating speeds ($17.6 \pm 0.9 \mu\text{m/hr}$), and higher cell spreading (Elliptical Form Factor = 3.9 ± 0.2). However, manipulation of these material properties did not significantly affect migration persistence. Further, there was a monotonic increase in cell speed and spreading with increasing adhesivity showing a lack of the biphasic trend seen in two dimensional cell migration. Immunohistochemistry showed well-formed actin fibers and $\beta 1$ integrin staining at the ends of stress fibers. This thiol-ene platform provides a highly tunable substrate to characterize 3D hMSC migration with application as an implantable

cell carrier platform or for the recruitment of endogenous hMSC *in vivo*.

3.2 Introduction

Bone marrow derived human mesenchymal stem cells (hMSC) are multipotent cells that are known to be recruited to bone fracture sites and play a significant role in bone regrowth [1, 2]. As a result, there is a growing interest within the orthopedic tissue engineering community to develop materials that could serve as carriers for hMSCs or to recruit endogenous hMSCs to promote the healing of bone fractures and defects [3, 4]. Minimally, the targeted materials must be engineered to permit or promote cell infiltration, so understanding the role of various matricellular signals in regulating migration of hMSC populations (e.g., their speed, persistence) is often essential [5]. In this regard, many synthetic materials have proven useful as tools to study cell motility in three-dimensions, as they can be fabricated to recapitulate desired aspects of extracellular matrix (ECM) properties in a highly tunable and reproducible manner [6, 7]. Here, we exploit one such system, peptide functionalized poly(ethylene glycol) (PEG) hydrogels formed via thiol-ene chemistry, as a versatile matrix to study hMSC migration *ex vivo* and in real time.

During development, wound healing, and other *in vivo* processes, cell migration is governed by a complex milieu of structural [8-10] and bioactive [11, 12] extracellular signals [5]. Pioneering work performed in two dimensions (2D) has provided the field with an understanding of how cell motility depends on these cell-matrix interactions such as substrate stiffness [13-15] and adhesivity [11, 15, 16]. However, more recent literature demonstrates that two-dimensional phenomena may not fully translate to three dimensions, for example Doyle *et al.* compared fibroblast migration on 2D fibronectin substrates with 3D cell derived matrix and saw significant

differences in migration speed and leading edge protrusion rate when differing dimensionality [8]. 3D substrates can better recapitulate aspects of the *in vivo* microenvironment and allow for further understanding of cell migration as 3D does not un-naturally polarize cells and can be designed to require degradation of the matrix by cell-secreted enzymes, such as matrix metalloproteinases (MMP), for local spreading and migration. Natural materials, such as collagen [17] and matrigel [18], provide a heterogeneous, fibrillar platform to observe the role of extracellular cues in regulating cell migration and to discern valuable insight into 3D cell migration; however, there can be a large batch-to-batch variability, as well as complex relationships between adhesivity and mechanical properties that are difficult to deconvolute. Synthetic materials can reproduce many of these cues in a controlled manner *in vitro* and allow one to study systematically their effects on cell migration, but lack biological signals. Therefore, peptide-functionalized synthetic hydrogels can serve as an attractive option as extracellular matrix analogs, providing a platform with tailorable biophysical and biochemical cues to study 3D cell migration [7].

In work by Ehrbar *et al.*, 8-arm poly (ethylene glycol) hydrogels were used to show that the speed of migration of pre-osteoblastic cells was reduced with increasing polymer density[19]. Further, mouse MSCs were observed to undergo collective migration when entrapped in a fibrous clot embedded in a hyaluronic acid gel; the cells also showed reduced migration speeds when surrounded by a matrix of increasing polymer density [20]. Beyond matrix density, another extracellular material property of importance is the mechanism by which the material degrades and its interplay with how a cell locally migrates in relation to local matrix remodeling. Early work by Raeber *et al.* used a 3D culture platform from 4-arm PEG-vinyl sulfone reacted with an MMP-degradable peptide to demonstrate that human foreskin fibroblasts relied on the secretion

of proteases to spread and migrate in a density dependent manner [21]. These results may appear somewhat intuitive, as matrix density often necessitates degradation of the local microenvironment by cell secreted proteases [22], but the relationship can be complex as matrix density also influences the local adhesive ligand density and matrix mechanical properties. Each of these ECM properties can influence cellular functions, such as MMP activity [23, 24] and matrix deposition [25], which in turn can affect cell reorganization of its local matrix density.

Along with mechanical properties of a matrix, the adhesivity of the network plays a significant role in regulating cell spreading and migration. Many cell types simultaneously rely on adhesion to proteins within their extracellular space in addition to matrix degradation before they can migrate through a 3D material microenvironment.¹⁶ Using model surfaces and protein matrices, such as inclusion of the fibronectin peptide mimic RGDS, adhesive ligand density has been shown to play a crucial role in regulating migration of multiple cell types including, fibroblasts [26] and prostate cancer cells [18]. For example, in seminal work from Palecek *et al*, CHO cells cultured on 2D substrates coated with either fibronectin or fibrinogen had a biphasic response in their mean cell speed in relation to substrate adhesivity [11]. This trend was observed also when a fibroblast cell line, HT-1080s, was encapsulated in a three-dimensional MMP-degradable PEG gel [27]. While the speed of migration was dependent on the concentration of the RGDS epitope, the effect was much smaller in three-dimensions and potentially attributed to weaker matrix interactions of this cancer cell line. Finally, collectively migrating MSCs demonstrated a slight monotonic increase in distance traveled from a fibrous clot when the CRGDS concentration range was increased from 0.1 to 1.0 mM in a surrounding hyaluronic acid based gel [20].

Despite this foundational work in correlating cell migration to microenvironmental cues, there is a gap in knowledge as to how these chemical and physical cues regulate individual hMSC migration in 3D, especially over a broader range of material properties. To address this issue, we used photoinitiated thiol-ene reaction to create peptide functionalized PEG hydrogels of varying crosslinking density (0.2 – 1.6 mM) and ligand density (0.001 – 1.000 mM of CRGDS) [28]. Specifically, a 4-arm PEG macromolecule was end-capped with norbornene functionalities and crosslinked with cysteine-containing peptides (KCGPQG↓IWGQCK) through radical-mediated, step-growth photopolymerization to form highly swollen gels (97.3 – 98.4% water). The linker peptide sequence is susceptible to cleavage by matrix metalloproteinases (MMPs) 1,2,3,8, and 9 [29, 30], of which hMSC have been observed to secrete all of these MMPs [31-34], thus providing a substrate that hMSCs can locally degrade. Further, this thiol-ene reaction allows for covalently tethering pendant peptide sequences, such as CRGDS, to promote cell-matrix interactions. Further analysis of actin structure and β 1 integrin spatial distribution is characterized using immunohistochemistry to better understand local cell-matrix interactions. Through manipulation of the macromer solution composition, microenvironments with tailored crosslinking density and adhesive ligand concentration were prepared for 3D hMSC culture, and morphology, speed, polarity, and persistence were monitored in real time as a function of systematic changes to the matrix properties. These results provide valuable insight into hMSC migration, including how individual hMSC interact and attach with their local microenvironment, and how these materials can be manipulated to control the migration phenotype and provide further insight into the role of matricellular signaling on hMSC migration. We believe that this quantitative characterization should prove useful for the

development of scaffold design for hMSC, especially those developed as cell carriers and/or platforms for cell colonization and infiltration.

3.3 Materials and Methods:

3.3.1 Macromer Synthesis

Norbornene acid was conjugated to 4-Arm PEG-hydroxyl (JenKem, USA) as previously described to create 4-arm PEG-Norbornene [28]. In brief, this occurs through the addition of norbornene acid to the PEG-OH by the symmetric anhydride N,N'-dicyclohexylcarbodiimide (DCC) coupling. Norbornene acid was dissolved in dichloromethane and reacted with DCC to couple the norbornenes. This was transferred anhydrously to a second reaction flask. The second reaction flask contained 20,000 kDa 4-arm PEG-OH dissolved in DCM, 4-(Dimethylamino)pyridine, and pyridine and was stirred overnight. The urea byproduct was filtered using a glass-fritted funnel. The filtrate was then washed with alternating glycine buffer and brine wash to remove un-reacted norbornenes. The final product was precipitated and washed with ice-cold diethyl ether. HNMR was used to characterize the purity and functionality (>95% for these studies) of the product (Supplemental Figure 3.10).

Synthesis of the peptide sequences, KCGPQG↓IWGQCK, CRGDS, and CRDGS, was completed on either a 433A solid phase peptide synthesizer (Applied Biosystems) or a Tribute peptide synthesizer (Protein Technologies) using standard solid-phase peptide reagents with Fluorenylmethoxycarbonyl (Fmoc) chemistry on a Rink-amide resin. Peptides were cleaved from the resin and purified using reverse-phase high-performance liquid chromatography (HPLC), and molecular weights were confirmed by matrix-assisted laser desorption ionization (MALDI) mass spectrometry.

3.3.2 Cell Culture

Human mesenchymal stem cells (hMSCs) were isolated from bone marrow aspirates (Lonza). Bone marrow was combined with the ammonium chloride solution (Stem Cell Technologies) vortexed and iced for ten minutes to lyse red blood cells. Cells were then washed twice and plated with growth media (experimental media with 1 ng mL⁻¹ recombinant human fibroblast growth factor-basic (FGF-2, Peprotech). hMSCs were distinguished as the plastic adherent cells and were cultured at 37°C and 5% CO₂. Cells were passaged at ~70 to 80% confluence and passage 2 or 3 were used for these studies.

3.3.3 Gel Formulation and Characterization

The pre-polymerized solution consists of 6 wt% PEG-Norbornene (3 mM, $f = 4$), a specific off-stoichiometric thiol to -ene ratio 0.65, 0.725, and 0.85 (3.9 mM, 4.35 mM, and 5.1 mM respectively) amount of peptide crosslinker (KCGPQG↓IWGQCK, $f = 2$), a 1 mM ratio of CRGDS and CRDGS ($f = 1$), and 0.05% lithium phenyl-2,4,6-trimethylbenzoylphosphinate [35]. CRDGS is a non-bioactive scramble of CRGDS that allows for similar material properties between gels of varying concentration of bioactive CRGDS by keeping the pendant peptide concentration equivalent between all samples. For 3D cell studies, cells were suspended in phosphate buffered saline and added to the pre-polymer solution at a density of 2×10^5 cells/mL. The solutions were placed under 365 nm light at 10 mW/cm² for 3 minutes. *In situ* rheometry demonstrated full gel conversion after 3 minutes (data not shown). These gels were then placed in experiment media (low-glucose DMEM, 10% fetal bovine serum (FBS), 50 U mL⁻¹ each penicillin/streptomycin, 1 µg mL⁻¹ Fungizone antimycotic) for swelling overnight.

The swollen mass of the gels was measured and divided by the theoretical dry mass to calculate the swollen mass ratio (q). Parallel plate rheometry was also performed on an Ares 4400 rheometer (TA instruments) with 10% strain frequency sweep and a 10 rad s⁻¹ strain sweep. Elastic modulus was determined when the gel was in the linear viscoelastic regime for both the frequency and strain sweep.

3.3.4 Real-time Cell Motility Studies

Cell motility in cell-laden hydrogels was characterized using a Nikon TE2000-E microscope with a Nikon environmental chamber and an external heater (In vivo Scientific) and CO₂ regulator (In vivo Scientific). Hydrogels were polymerized and swollen as described previously and then placed in a 24-well culture insert plate (BD Falcon, Fisher) and held in place by a transwell insert (Becton Dickinson) with the bottom removed by a 5 mm biopsy punch. Fresh experimental media was placed in the well at the beginning of each experiment. Real-time tracking was performed using Metamorph software for automated stage control, image collecting and positional cell tracking. After 36 hours in culture, cell centers tracking was commenced and followed for 7 hours. A Matlab (Mathworks) program was used to analyze the positional outputs and fit the data to a Persistent Random Walk model [36]:

$$\langle d^2(t) \rangle = 2S^2P[1 - P(1 - e^{-t/P})]$$

where $\langle d^2(t) \rangle$ is the mean-square displacement (MSD) of the cell calculated using the overlap method, S is the speed of the cell which is calculated by the total distance covered over the tracking window divided by 7 hours, t is time, and P is persistence which is the characteristic time scale a cell migrates in a certain direction. All cell migration tracks were assumed to be isotropic and appropriate scaling of the MSD was applied to account for the z-directional

migration. The individual cell's mean free path, the characteristic length scale a cell migrates in a certain direction, can then be calculated by multiplying the speed by the persistence. Only cells that had a mean free path greater than 3 μm were considered migrating and used to calculate population averages. Metamorph was also used to measure cell length and the perpendicular width to calculate the elliptical form factor as length divided by width.

MSD for each condition were calculated by averaging each cell's individual MSD for a given condition. These were compared to ballistic migration (straight-line migration) and diffusion migration (random migration). These scale with time to the second power and first power, respectively. Turning probabilities were compiled by calculating the change in angle of each cell's movement at each time point. These were then placed in a histogram with bin size of 10 degrees. The percent of forward movements, defined as a turning angle less than 40° , was calculated to more fully elucidate differences between the systems.

3.3.5 Immunostaining

Hydrogels with encapsulated cells were fabricated as previously described. Cells were cultured in these hydrogels for 48 hours, fixed using 4% PFA in PBS for 15 min, rinsed twice with PBS for 5 minutes, permeabilized with 1% Triton X-100 for 1 hour, rinsed twice with PBS for 10 minutes, and blocked using 5% BSA in PBS for 1 hour at room temperature and overnight at 4°C . All steps, unless noted otherwise, were performed at room temperature. Cells were then incubated with $\beta 1$ primary antibody solution (Abcam, 1:20 dilution) with 3% BSA and 0.1% Tween-20 overnight at 4°C . The gels were washed three times with wash buffer, then incubated with goat anti-mouse 488 secondary antibody (Life Technologies, 1:200 dilution in 3% BSA and 0.1% Tween-20 in PBS overnight at 4°C . Gels were washed twice using 3% BSA and 0.1%

Tween 20 for an hour at room temperature and then overnight at 4°C. Gels were then incubated with TRITC-Phalloidin (1:200 dilution) and DAPI (1:1000 dilution) for 1 hour at room temperature. Confocal imaging was performed on an LSM 710 (Zeiss).

3.3.6 Statistical Analysis

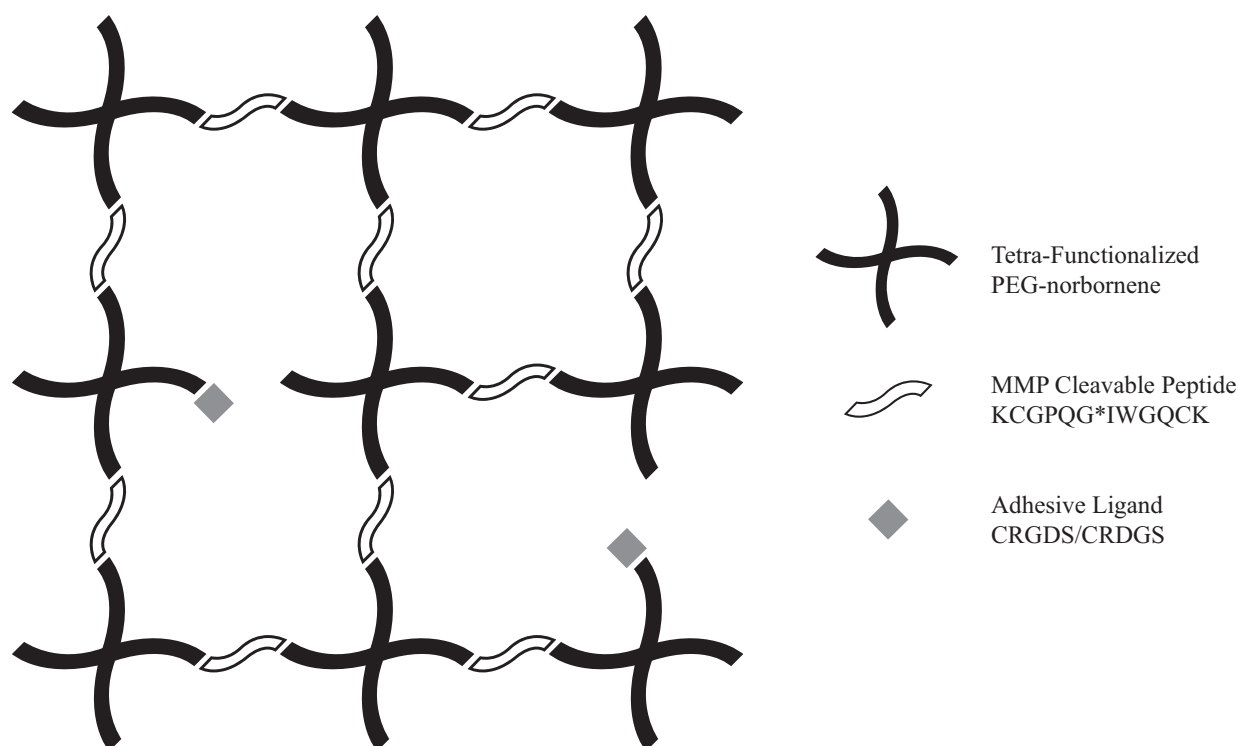
A one-way ANOVA with a Tukey's test ($\alpha = 0.05$) was performed on all data sets to determine statistical significance. For persistence there was extremely high variability for a few points, therefore all points outside of 3 standard deviations from the mean were considered outliers and not used for statistical measurements. For all conditions tested this removed only three cells from the calculations. All experiments were performed three times, and cell metrics were pooled from these different biological replicates for statistical calculations.

3.4 Results and Discussion:

3.4.1 Peptide-Functionalized PEG Hydrogels: Controlling physical and chemical properties

hMSCs were encapsulated within 4-arm PEG-norbornene hydrogels through photopolymerization with a di-thiol, MMP-degradable peptide (KCGPQG↓IWGQCK) linker and the introduction of an adhesive ligand mimic, CRGDS, and its non-bioactive scramble, CRDGS. To control the initial network crosslinking density, the di-thiol linker was added at three different stoichiometric ratios of 0.65, 0.725 and 0.85 thiol to -ene to render low, medium, and high crosslinking density gels, respectively. For organization and simplicity, the gel crosslinking density will be referred to as Low, Medium, or High for the duration of this discussion. The different crosslinking densities showed a decreasing trend in swelling ratio with increasing di-thiol linker concentration from Low to High of 62 ± 1 (98.4% water), 49 ± 1 (98.0%

water), and 37 ± 1 (97.3% water), (Figure 3.1). In general, the higher the gel crosslinking density, which is achieved by increasing the peptide crosslinker content, the denser the polymer network that cells must locally degrade in order to spread and migrate. Note that the network mesh size is orders of magnitude smaller (nanometer size-scale) than the size of a cell (micrometer size-scale). The elastic modulus of gels is directly proportional to the network crosslinking density, and the Low, Medium and High gels demonstrated an increase in elastic modulus with increasing di-thiol concentration of 110 ± 10 Pa, 360 ± 10 Pa, and 1180 ± 30 , respectively (Figure 3.1). Over large ranges of elasticity, material stiffness has been shown to affect hMSC attachment, spreading, and differentiation on 2D substrates [37]; however, less is known about how substrate elasticity influences hMSC morphology, phenotype, and migration in 3D.



	Low (0.65:1)	Medium (0.725:1)	High (0.85:1)
q	62 ± 1	49 ± 1	37 ± 1
% Water	98.4 ± 0.1	98.0 ± 0.1	97.3 ± 0.1
G' (Pa)	110 ± 10	360 ± 10	1180 ± 30
ρ_{xl} (mM)	0.18 ± 0.02	0.54 ± 0.01	1.60 ± 0.04

Figure 3.1 Thiol-ene photopolymerization of a tetra-functionalized PEG-norbornene, MMP cleavable peptide (KCGPQG↓IWGQCK), and adhesive ligands (CRGDS, CRDGS) occurs through a radically mediated step growth reaction to encapsulate hMSC within a 3D tunable microenvironment. The table presents mass swelling ratio (q), % water, shear modulus (G'), and crosslinking density (ρ_{xl} , calculated from Rubber Elasticity Theory) while the thiol:ene ratio was varied to produce Low, Medium, and High gels. As thiol:ene ratio increases, mass swelling decreases, % water slightly decreases, and shear modulus and crosslinking density increase.

By applying rubber elasticity theory and the experimentally measured equilibrium swelling ratio and elastic modulus, a crosslinking density was calculated for each of the three systems and found to be 0.2 mM, 0.5 mM, and 1.6 mM with increasing di-thiol concentration

[38]. These calculated values varied from what is expected theoretically for ideal networks that are free of loops and entanglements and completely reacted at these stoichiometric levels. The predicted crosslinking density for ideal networks is 0.43 mM for the Low, 0.74 mM for the Medium, and 1.44 mM for the High. This implies that there are non-idealities present in the system for the lower two gel systems, which results in a larger mesh size than expected and potential gel defects, such as dangling ends or loops. Interestingly, at the highest stoichiometric ratio/crosslinking density, the value calculated based on experimental measurements of the gel properties was higher than that predicted, possibly indicating the role of entanglements acting as effective crosslinks. Regardless, these defects are still orders of magnitude smaller than a cell body and do not interfere with the degradability of the gel. On a relative basis, these networks are much more ideal than chain polymerized PEG gels that are widely used for 3D cell culture [39-41]. Despite the non-idealities and deviation from theoretical predictions, the characterization of these gels indicates that one can systematically manipulate the polymer density and elasticity of the networks by simple variations in the amount of di-thiol peptide in the pre-polymer solution.

3.4.2 Effect of Crosslinking Density on Cell Spreading and Morphology

To understand the effect of crosslinking density on hMSC morphology and spreading in three-dimensions, hMSC were photoencapsulated in PEG-norbornene hydrogels at Low, Medium, and High crosslinking densities with 1 mM CRGDS to promote cell-matrix interactions. At early time points (30 hours), the high crosslinking density in the gels limits cell spreading, as observed by a decrease in the elliptical form factor (EFF) with increasing crosslinking density (Figure 3.2). Specifically, the EFF decreased with increasing crosslinking

density from 3.9 ± 0.2 (Low) to 2.9 ± 0.1 (Medium) to 1.6 ± 0.1 (High) (Figure 3.2D). For comparison, fibroblasts within collagen, fibrin and cell derived matrix were reported to have an EFF of ~ 4 , which correlates well with the Low crosslinked gel system.²⁷ In loosely crosslinked gels, hMSCs appeared more uniaxial and highly elongated (Figure 3.2A); however, in Medium crosslinked gels, cells were less spread and only smaller protrusions were observed (Figure 3.2B). Cells encapsulated in the High crosslinked gels were mostly rounded with few if any protrusions (Fig 3.2C). These data indicate that although the polymer density is relatively low in all of the systems (1.6 to 2.7 weight % polymer, Figure 3.1), an increase in the number of crosslinks that a cell must degrade impedes cell spreading.

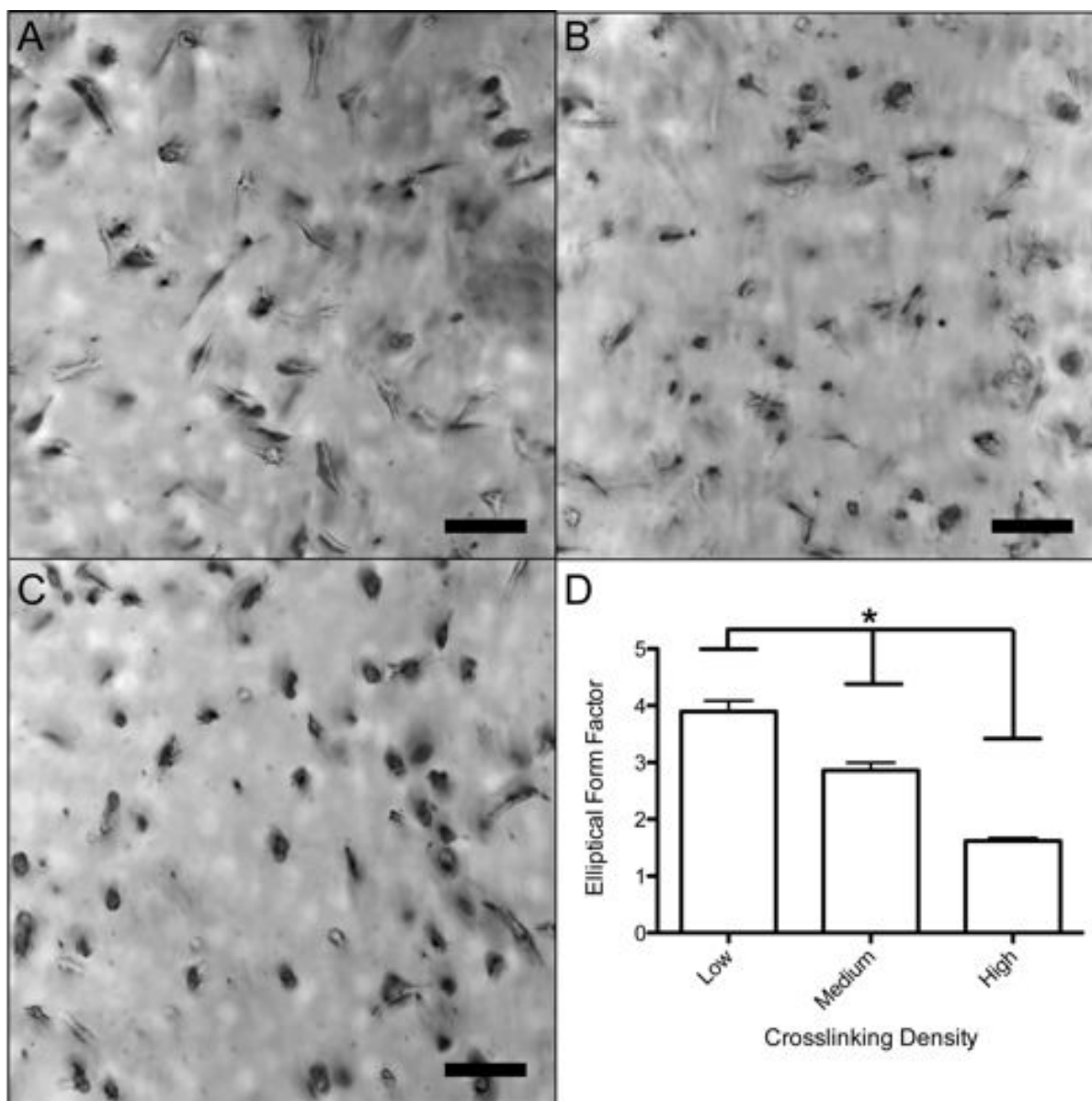


Figure 3.2 Morphology of encapsulated hMSCs cultured for 30 hours in gel systems with varying crosslinking density. A) Brightfield image (10x magnification) of hMSCs in a Low (65%) gel. Cells were found to be well spread and linear. B) Brightfield image (10x magnification) of hMSCs in a Medium (72.5%) gel. Cells were found spread with many protrusions. C) Brightfield image (10x magnification) of hMSCs in a High (85%) gel. Cells were rounded with little or no protrusions. D) An elliptical form factor was calculated by dividing the length and perpendicular width of each cell. There is a significant (* $p < 0.05$) decreasing trend found from a one-way ANOVA and Tukey's Test. Scale bar represents 100 μm .

3.4.3 Effect of Crosslinking Density on hMSC Motility

Along with cell morphology, single cell migration was analyzed using live-cell videomicroscopy in each of the hydrogels. Cell tracks were followed for a continuous 7 hours. Tracking was commenced after the cells had been cultured for 30 hours post-encapsulation in the gels; this time point was selected to allow cells to recover from trypsinization and encapsulation, as well as to allow for some local matrix remodeling before monitoring migration. Isotropic motility was observed over the range of crosslinking densities studied from 0.2 – 1.6 mM, as hypothesized based on the lack of polarizing cues within the material or media. Mean square displacements (MSD) were calculated from the cell tracks for each cell and were averaged over all migrating cells for an aggregate MSD for each gel composition. Comparisons are shown for ballistic migration, which scales to the second power with time, and diffusive migration, which scales to the first power with time. Ballistic migration is a cell that migrates persistently in a straight line, whereas diffusive migration describes a cell moving in a completely random path. All three slopes fall in-between a completely persistent and completely random migration, prompting further analyses of the persistence of the cells.

During cell migration, motile cells polarize to direct their migration spatially, and this process plays a key role in how persistent a cell migrates. The degree of cell polarization can be quantified indirectly within our system by calculating the probability of a cell to migrate in a specific direction relative to the previous direction it migrated. Using this type of analysis, polarized cells sustain their polarity in a fixed direction while randomly migrating cells have unbiased isotropic turning probabilities. Therefore, a cell that has a sustained polarization in a certain direction during migration will have a high probability of very low turning angles. Conversely, a cell that has a highly transient polarization will have an equal probability to turn in

any direction. All three systems demonstrated a similar bias toward polarized cells with migration continuing in a certain direction (Figure 3.3B). To quantify this further, a critical angle of 40° was defined to calculate the percent of turns where a cell continued in a similar direction to their previous movement and therefore stayed polarized (Grey area on Figure 3.3B). The percent of turning angles that were 40° or less were 38.9%, 36.3%, and 37.8% with increasing crosslinking density. These values are quite similar and argue that varying the crosslinking density does not manipulate a cell's ability to sustain polarization while migrating in a 3D network. This result is a bit counterintuitive in that it would seem that in increasing the network density, a cell would need to degrade more of the local network to continue in a sustained direction and therefore would be less likely to stay polarized. However, the observed independence of polarization on crosslinking density may instead be correlated to the fact that speed is affected by network density, but hMSC remain polarized for equivalent time frames. Greater insight into local quantification of the network's stiffness and crosslinking density (i.e., how hMSCs have remodeled and altered the local material properties) would help better elucidate these effects on cell migration.

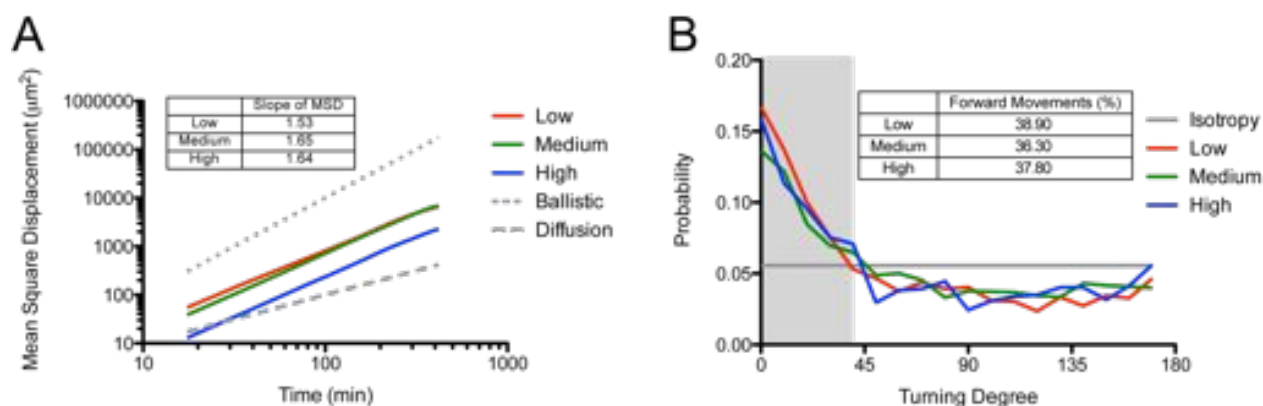


Figure 3.3 hMSC migration was followed over 7 hours using live cell videomicroscopy. Effect of varying crosslinking density on hMSC mean square displacement and sustained cell polarity was calculated from the cell tracks measured using Metamorph. (A) Mean-square displacement

was similar for low and medium gels, but differed for cells in high crosslinked gels. All three gels had slopes that fell between 1 (random migration) and 2 (ballistic migration) (B) Sustained cell polarity showed a similar bias for all three systems, and a similar percentage of sustained steps.

Complementary to the above analyses, key metrics from this data were obtained by fitting the MSD data to a Persistent Random Walk model. This approach allows for the calculation of the speed, persistence, and mean free path of migrating hMSCs as a function of gel properties [36]. hMSC speed correlated similarly with morphology, as average speed decreased from $17.6 \pm 0.9 \mu\text{m/hr}$ to $13.6 \pm 1.0 \mu\text{m/hr}$ to $7.9 \pm 0.5 \mu\text{m/hr}$ as the network density decreased (3.4A). The percentage of cells migrating followed the same trend, as migrating cells decreased from 59%, 42%, and 20% with increasing crosslinking density (Figure 3.4C). Collectively, these data corroborate the hypothesis that denser networks inhibit hMSC migration, as cells must locally degrade more crosslinks in their pericellular space in order to spread and migrate. This results in slowing both the speed at which hMSCs can migrate and the overall number of cells that can overcome the physical barrier to migrate. Interestingly, cell persistence over the range of crosslinking densities studied did not show any statistically significant differences (Figure 3.4B). This correlates well with the cell polarity data (Figure 3.3B). The mean free path of the cell's motility was also equivalent for the three crosslinking densities (Figure 3.3D). This lack of statistical significance found in cell motility might also relate to the higher amount of heterogeneity of persistences observed for each cell population; hMSCs are primary cells and there is typically heterogeneity in the differentiation potential of the populations as well [1]. Interestingly, despite slower speeds in more highly crosslinked networks, it was still observed that cells moved on a similar characteristic time and length scales over this range of crosslinking density.

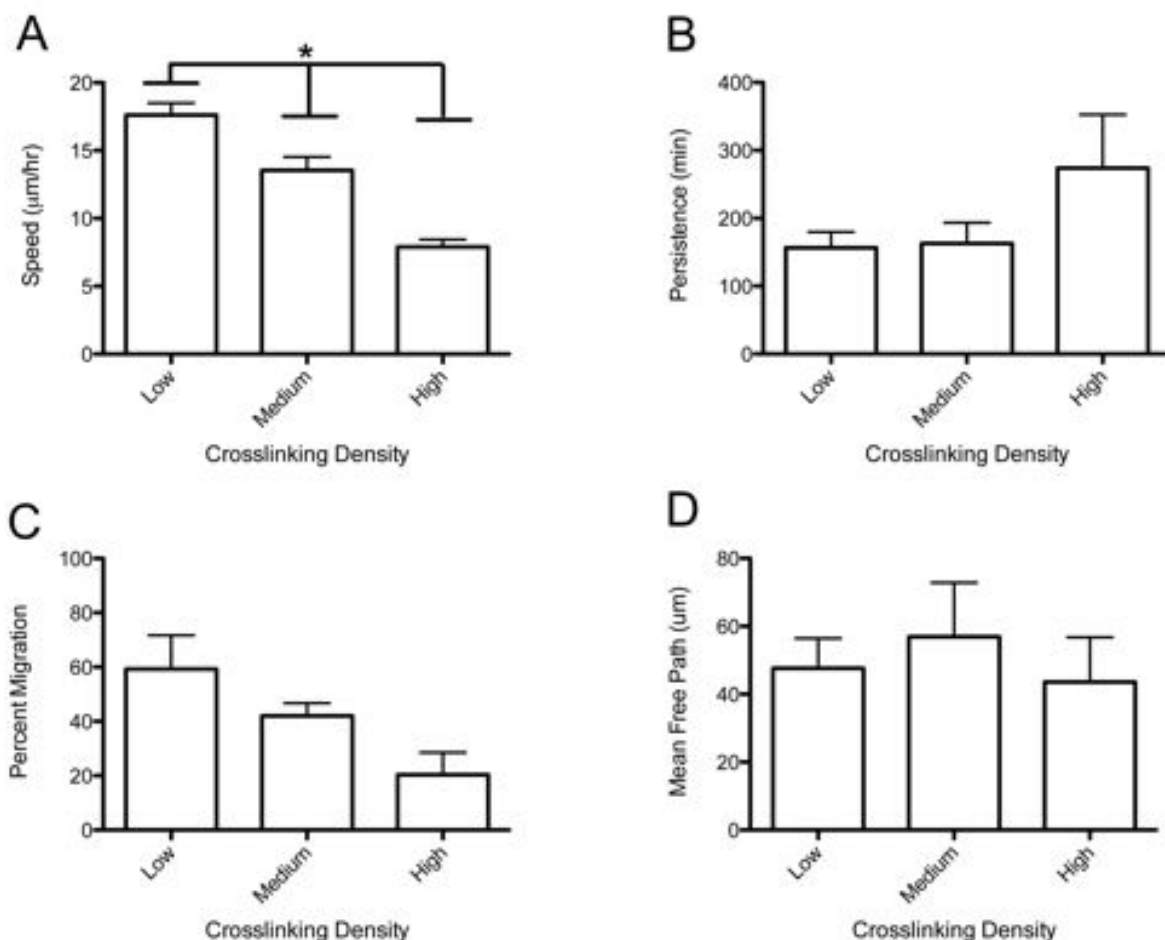


Figure 3.4 Cell tracks from hMSC migration in 3D are modeled using a Persistent Random Walk model (PRW). Effect of varying crosslinking density on hMSC migration. (A) Cell speed shows a decreasing trend with increasing crosslink density. (*Significance $P < 0.05$) (B) Persistence shows no statistical difference over the varying crosslink densities. (C) Percent migration shows a decreasing although not statistically significant difference. (D) Mean free path was not affected by varying the crosslinking density.

3.4.4 Actin Cytoskeleton and $\beta 1$ Integrin Organization and Structure

Cells spread and migrate within 3D networks through adhesion to the matrix via integrin binding. To further understand how hMSCs interact with pendant adhesion functionalities (i.e., R3GDS) when encapsulated in thiol-ene hydrogels, immunohistochemistry was used to visualize actin cytoskeleton organization and $\beta 1$ integrin distribution for cells entrapped in gels of varying

crosslink densities. As mentioned previously (Figure 3.2), there was a distribution of cell spreading and morphologies within the three different systems; and Figure 3.5 provides more detailed characterization of the cell cytoskeleton. In brief, hMSCs had numerous actin stress fibers in all gels, regardless of crosslinking density.

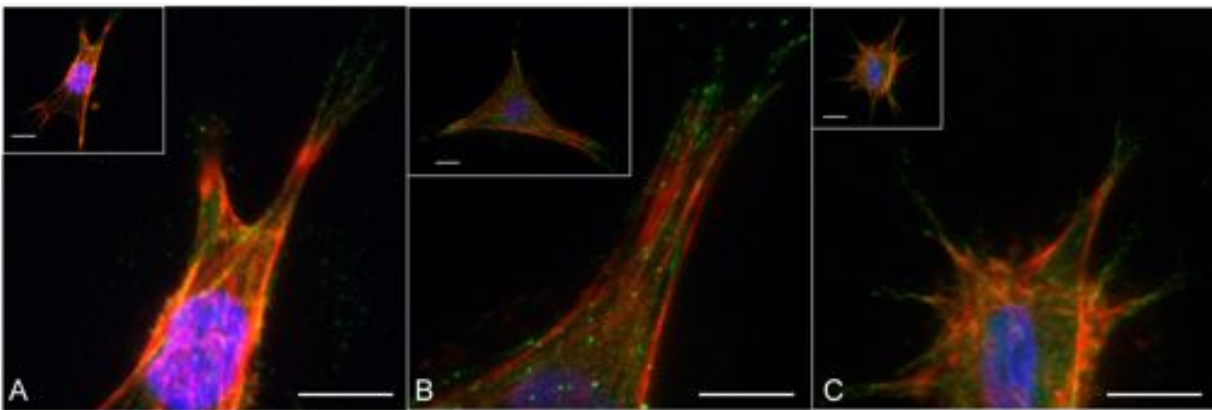


Figure 3.5 Encapsulated hMSCs were cultured in gels at the three different crosslinking densities for 48 hours and immunostained for actin (red), $\beta 1$ integrin (green) and DAPI (blue). A) Low Crosslinking B) Medium Crosslinking C) High Crosslinking. Spread hMSC in all three gels systems show actin fiber formation and punctate $\beta 1$ integrin at the ends of these fibers over this range of crosslinking densities. Scale bars represent 50 μm .

Immunostaining for $\beta 1$ integrin was performed to better understand the effect of crosslinking density on the ability of hMSCs to adhere and interact with matricellular cues in the gels. $\beta 1$ integrin plays a prominent role in cell motility and is one of the primary integrins that

binds to the adhesive RGD motif [42]. $\beta 1$ integrin was localized to punctate foci at the end of actin stress fibers for all three crosslinking densities, illustrating strong cell adhesion to the network (Figure 3.5). The actin stress fibers and $\beta 1$ integrins appear similar to what has been reported for fibroblasts in 3D environments composed of cell derived matrix, collagen and fibrin [43]. Therefore, although the thiol-ene gels are synthetic matrices, they seem to appropriately recapitulate some of the critical factors present in natural materials to promote cell attachment and spreading in these 3D environments. Furthermore, the observance of similar integrin staining in 3D for all of the three gel systems prompted us to pursue a more in-depth study into varying the adhesivity of the network and its effect on cell migration.

3.4.5 Effect of RGD Density on Cell Morphology

Along with substrate stiffness and crosslinking density, substrate adhesivity has been shown to affect MSC migration in 2D and collective MSC migration in 3D. Wu *et al.* showed that in 2D the concentration of fibronectin, vitronectin and collagen coated on glass slides affected MSC speed [44]. Also, Lei *et al.* reported that collective migration of mouse MSCs in 3D hyaluronan gels showed slight differences in overall distance migrated from a fibrin clot while varying the adhesivity of the network [20]. Here, hMSCs were encapsulated in gels containing varying CRGDS concentrations to study how ligand concentration alters single cell morphology and migration in an isotropic network. While this work provides one of the first characterizations of MSC migration in 3D, experiments with natural materials are confounded by the fact that material density and adhesivity are fully coupled in natural gels. In the thiol-ene gel system, these parameters can be decoupled, enabling the systematic investigation of ligand density on cell migration for each gel composition. Here, a non-bioactive scramble of CRGDS

was introduced to keep the total pendant peptide concentration equivalent while varying the concentration of the bioactive CRGDS so that the crosslinking density and resulting gel elasticity remained similar for the various systems. Swelling studies were also performed on all gels to ensure similar water contents.

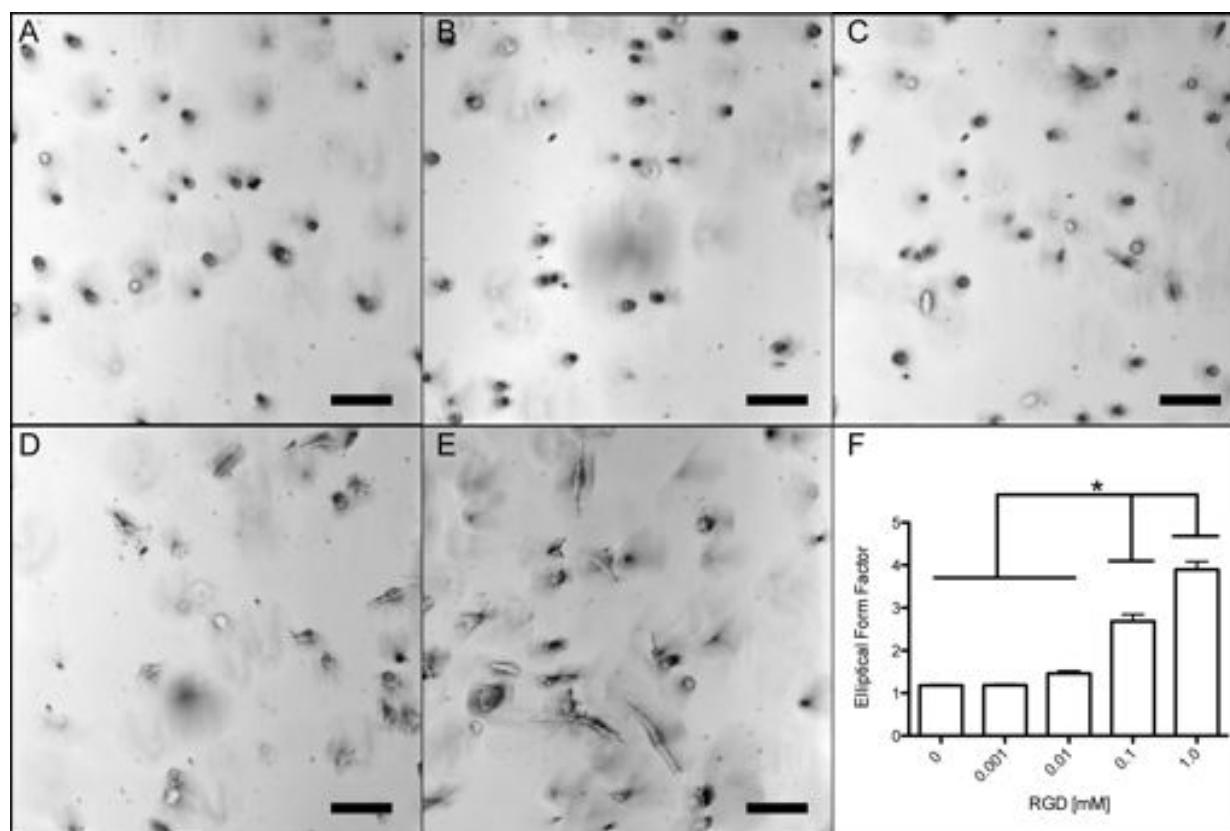


Figure 3.6 Morphology of encapsulated hMSCs cultured for 30 hours in gel systems with varying CRGDS. A) Brightfield image (10x magnification) of hMSCs in 0 mM CRGDS gel. Cells were rounded. B) Brightfield image (10x magnification) of hMSCs in 0.001 mM CRGDS gel. Cells were rounded. C) Brightfield image (10x magnification) of hMSCs in 0.01 mM gels. Cells were rounded with little or no protrusions. D) Brightfield image (10x magnification) of hMSCs in 0.1 mM CRGDS gel. Cells were spread and linear. E) Brightfield image (10x magnification) of hMSCs in 1.0 mM CRGDS gel. Cells were more spread and linear. F) An elliptical form factor was calculated by dividing the length and perpendicular width of each cell. There is a significant ($*p < 0.05$) increasing trend found from a one-way ANOVA and Tukey's Test between the first three systems with the 0.1 mM and 1.0 mM systems. Scale bar represents 100 μm .

The effect of changing CRGDS ligand density on hMSC morphology, migration, and cellular interaction was observed in the Low crosslinked gels, as these gels facilitated the highest degree of spreading and migration. This selection allowed for easier elucidation of differences in outputs when ligand density was varied. Brightfield images and elliptical form factor calculations of the cells show significant increases in cell spreading with increasing CRGDS after 30 hours (Figure 3.6). At 0 mM and 0.001 mM CRGDS concentrations, hMSCs were rounded with no visible protrusions (Figure 3.6A, 3.6B). An increase to 0.01 mM CRGDS showed cells that still were quite rounded but had protrusions emerging from the rounded cells (Figure 3.6C). At 0.1 mM and 1.0 mM, the large majority of cells were highly spread, elongated, and uniaxial (Figure 3.6D, 3.6E). These changes in cell shape are also reflected through quantification of EFF values with significant increases between 0.01 mM to 0.1 mM and 0.1 mM to 1.0 mM (Figure 3.6F). In general, below a certain threshold at low CRGDS concentration, cells are rounded, presumably because of limited adhesions to the matrix, but as the CRGDS concentration is increased to 0.1 mM and beyond, cell attachment appears to increase as observed through dramatic changes in morphology and spreading.

3.4.6 Actin Cytoskeleton and β 1 Integrin Organization and Structure

To more fully characterize and understand the implications of these changes in hMSC morphology, immunohistochemistry was performed to study actin cytoskeletal formation and β 1 integrin distribution as indicators of cell-material interactions. Decreasing RGD concentration resulted in a notable decrease in actin stress fiber formation and β 1 integrin staining at the end of actin stress fibers (Figure 3.7). For cells within 0 mM and 0.001 mM, no spread cells were observed in the representative images, and cells were primarily rounded with only diffuse actin staining and little to no β 1 integrin staining (Figure 3.7A). Within 0.01 mM gels, hMSCs

showed small protrusions, but little if any $\beta 1$ staining at the end of the small actin fibers with much of it found on the rounded cell edges (Figure 3.7B). Increasing to 0.1 and 1.0 mM, spread cells have well-formed actin fibers with punctate $\beta 1$ staining at the end of fibers significantly present for the 1.0 mM gels (Figure 3.7C, 3.7D). This correlates well with the EFF data, and further argues that over this large range of CRGDS that lower concentrations of CRGDS lead to low levels of cell interactions with the matrix resulting in a less-developed actin cytoskeleton, whereas higher concentrations promoted high cellular interactions and development of numerous actin stress fibers. With these significant changes in cell morphology and interactions as a function of matrix composition, we hypothesized that significant variations may exist in hMSC migration over this range of adhesive ligand density.

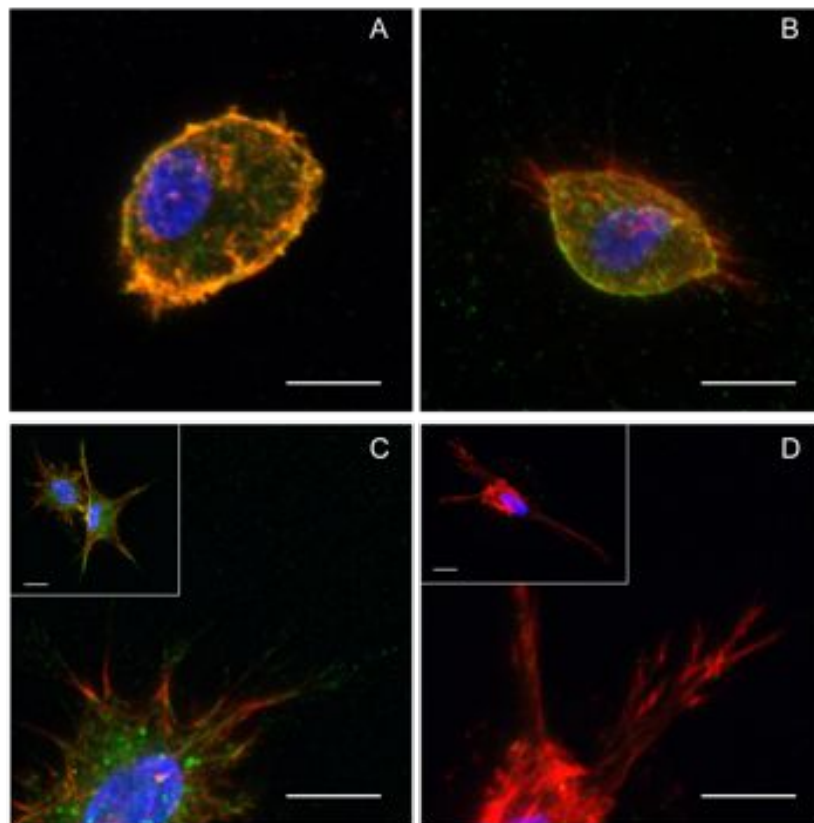


Figure 3.7 Encapsulated hMSCs were cultured in gels with varying CRGDS concentration for 48 hours and immunostained for actin (red), $\beta 1$ integrin (green) and DAPI (blue). A) For 0.001 mM gels, cells remain rounded and show little if any $\beta 1$ integrin even on the rounded edges of the cell B) For 0.01 mM gels, actin protrusions are present although limited with few $\beta 1$ integrin staining on actin fibers C) For 0.1 mM gels, cells are spread with large, protrusive actin fiber formation with $\beta 1$ integrin staining on protrusions. D) For 1.0 mM gels, cells are similar to the 0.1 mM cells with protrusive actin fibers however, the $\beta 1$ integrin staining seems more localized to the ends of actin fibers. Scale bar represents 50 μm .

3.4.7 Effect of RGD on hMSC Motility

hMSC migration was followed through live-cell videomicroscopy over the same range of CRGDS densities for 7 hours. Again, cell tracks were monitored and MSD was calculated using the overlapping method [36]. In contrast to the results with crosslinking density, we observed an increasing trend in the MSD slopes with increasing CRGDS concentration, except for the interesting decrease in slope for cells encapsulated within the 0.1 mM CRGDS functionalized gels (Figure 3.8A). All slopes similarly fall in-between the ballistic and diffusive slopes prompting further quantification and study of the persistence of individual cell migration.

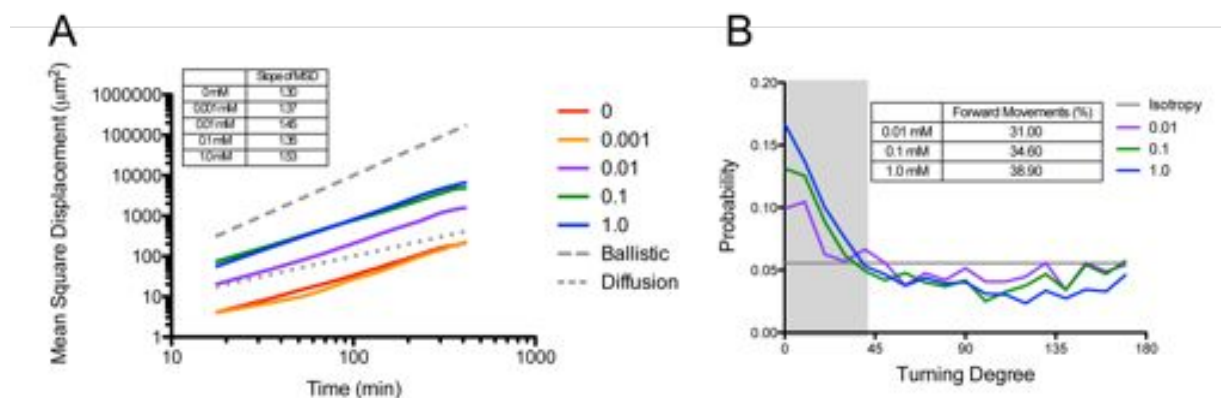


Figure 3.8. hMSC migration was followed over 7 hours using live cell videomicroscopy. The effect of varying CRGDS concentration on hMSC mean square displacement and sustained cell polarity was calculated from the cell tracks measured using Metamorph. (A) Mean-square displacement was similar for 1.0 mM and 0.1 mM gels, and 0 mM and 0.001 mM gels were also similar. All five gels had slopes that fell between 1 (random migration) and 2 (ballistic migration) (B) Sustained cell polarity showed a similar bias for all three systems, and a similar percentage of sustained steps.

The directional turning probabilities for the three highest CRGDS concentrations are presented in Figure 3.8B. The hMSCs encapsulated in gel formulations with CRGDS concentrations between 0 mM and 0.001 mM were not plotted in this figure due to too few migrating cells ($n=6$, $n=5$, respectively), as well as the fact that hMSCs in these gels showed very low cell speeds (~ 5 $\mu\text{m/hr}$). Speeds of ~ 5 $\mu\text{m/hr}$ correlate with cells that are essentially not moving but have non-zero speeds due to error from inadequately tracking the exact center of a cell. The plot shows an increasing trend in sustained cell polarity with increasing CRGDS concentration. Again, looking at the percent of forward movements (turning angle $< 40^\circ$), results illustrate a decrease in polarization with decreasing CRGDS content from 38.9% (1 mM) to 34.6% (0.1 mM) to 31.0% (0.01 mM). These results suggest that hMSCs are more polarized with increasing CRGDS concentration, presumably related to increased cell-matrix interactions, which should in turn promote higher cell persistence.

The MSD for each cell was then fit using a non-linear least-squares regression to the Persistent Random Walk model to gain insight into cell speed, persistence and mean free path while varying CRGDS concentration. Trends in cell speed indicated increasing speed with increasing CRGDS concentration at lower concentrations with a plateau at 16.9 ± 1.1 $\mu\text{m/hr}$ and 17.6 ± 0.9 $\mu\text{m/hr}$ (0.1 mM and 1.0, respectively) (Figure 3.9a). It is speculated that this occurs through the stochastic ability of a cell to garner significant attachment to the network, allowing actin cytoskeletal tension to produce migration. Put differently, when the network is more adhesive, a cell can likely attach and spread more easily in order to provide the necessary tension to perform persistent migration. The classic biphasic trend was not observed over this range of ligand densities and is more similar to the monotonic increase observed in the distance migrated

for collective mouse MSC migration in 3D [20]. Not surprisingly, these speeds are less than half the speed of hMSCs migrating in 2D found by Wu *et al.*, as cells in 2D do not need to degrade a matrix as part of their motility mechanism [44]. Requiring cells to locally degrade their microenvironment, which is typical of many *in vivo* tissues, provides a significant barrier to their migration speed in comparison to cell migration on 2D surfaces.

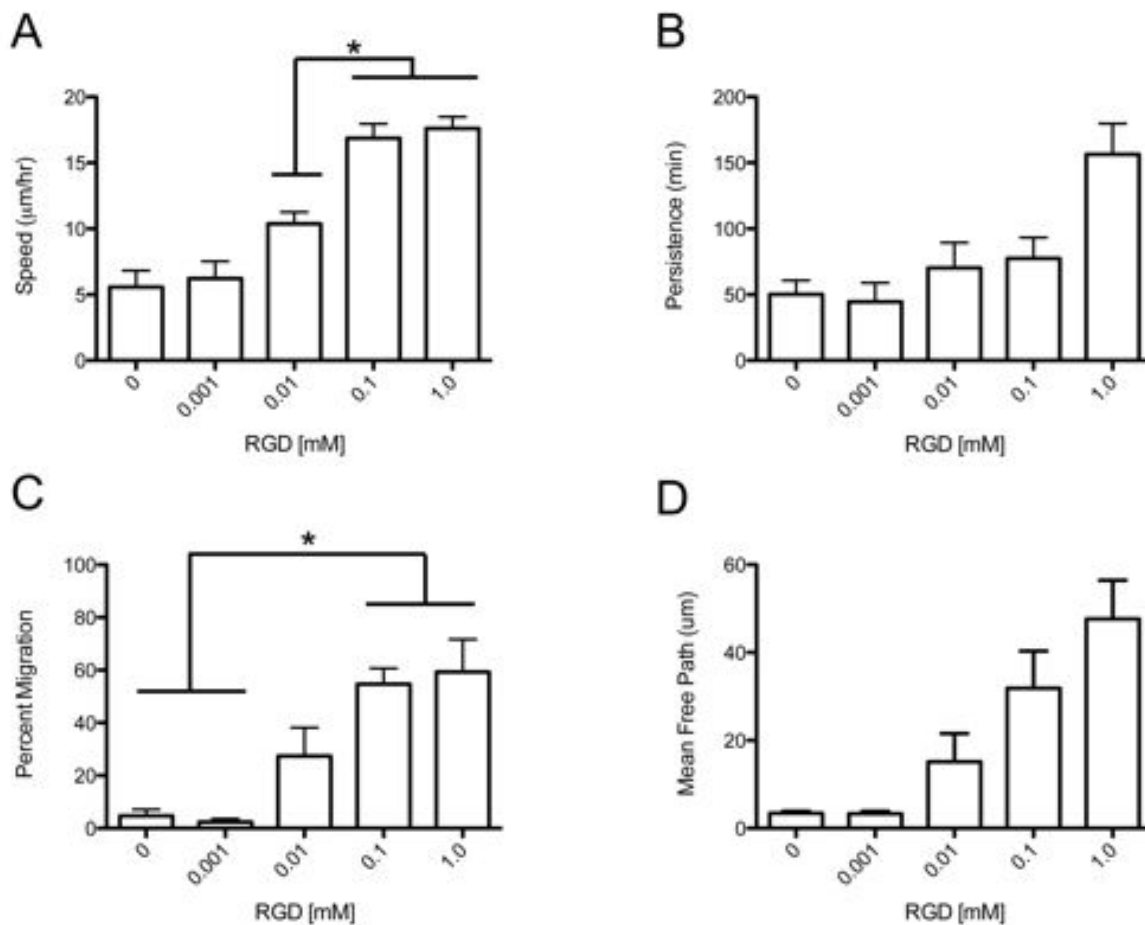


Figure 3.9 Cell tracks from hMSC migration in 3D are modeled using a Persistent Random Walk model (PRW). Effect of varying CRGDS concentration on hMSC migration was studied. (A) Cell speed shows an increasing trend with increasing CRGDS concentration. (*Significance $P < 0.05$) (B) Persistence shows no statistical difference over the varying CRGDS (C) Percent migration shows an increasing trend with increasing CRGDS concentration that plateaus for 0.1 mM and 1.0 mM gels. (*Significance $P < 0.05$) (D) Mean free path was not affected by varying the CRGDS concentration.

The percentage of cells migrating also increased over this range with a plateau observed in the number of migration cells, slightly less than 60% for cells in gels with 0.1 and 1.0 mM CRGDS (Figure 3.9C). Very few cells migrated within the 0 mM and 0.001 mM, which correlates well with the spreading data in Figure 3.6 ($n = 6$, $n=5$, respectively). Therefore, it is believed that the concentration of 0.001 mM CRGDS is below a threshold where cells interact with and form significant attachments to the network to allow spreading, and therefore, lose their ability to migrate as well. Persistence and mean free path were not found to be statistically different over the range of CRGDS concentrations studied (Figure 3.9B, 3.9D). The large variability in persistence is partially explained by the heterogeneity in the cell population. The 3D values of persistence found for cells in this study are roughly twice as large as values observed in 2D for hMSCs, and a similarly high variability was observed in both platforms [44]. Finally, it should be noted that the 2D studies used full proteins instead of peptide mimics, which certainly affects the strength of integrin interactions, so more in-depth comparisons of these numbers are potentially confounded.

Thiol-ene networks allow for facile synthesis of peptide functionalized PEG hydrogels with readily manipulated material properties. Since the chemistry is cytocompatible, it provides for a versatile system to study and observe cell migration, and here we report on hMSC morphology and migration speed as a function of matricellular properties [28]. We believe that such fundamental knowledge will prove helpful in the engineering of materials to serve as cell carriers or for the colonization of endogenous hMSCs into a bone defect site. Interestingly, the structural and bioactive inputs tested here do not manipulate the time and length scales over which hMSCs migrate in a persistent manner. This motivates future work to design more complex systems, such as gradient presentation of soluble growth factors or specific tethered

cues to promote recruitment and persistent anisotropic hMSC migration. Further, thiol-ene hydrogels provide an interesting platform as they are photochemically controlled, which can enable spatial and temporal control of mechanical properties and bioactive presentation through photopatterning [45]. This might allow for further study of physical and biological complexity on different time scales to be introduced within the network, and it would be interesting to use such an approach to manipulate cellular microenvironment to elicit desired migration responses.

3.5 Conclusions

Thiol-ene photopolymerized hydrogels allow for the facile introduction of important structural and bioactive inputs that govern hMSC migration within the *in vivo* microenvironment. In this work, the effects of matrix crosslinking density and ligand density on hMSC migration were studied to provide insight for strategies to better engineer materials for hMSC carrier platforms and materials to recruit endogenous hMSC to fracture sites. It was shown that hydrogels with low crosslinking density (0.2 mM) and high adhesivity (1 mM CRGDS) permitted higher cell speeds ($17.6 \pm 0.9 \mu\text{m/hr}$), higher cell spreading ($\text{EFF} = 3.9 \pm 0.2$), and more sustained polarization. Also, there was a monotonic increase in cell speed relative to an increase in ligand density, lacking the biphasic trend seen in 2D. Further, it was shown that manipulating crosslinking density and ligand density did not significantly affect persistence. Thiol-ene photopolymerized hydrogels provide a valuable tool to study hMSC migration in 3D environments, and this knowledge should provide valuable insight into future engineered materials.

3.6 Supplemental Information

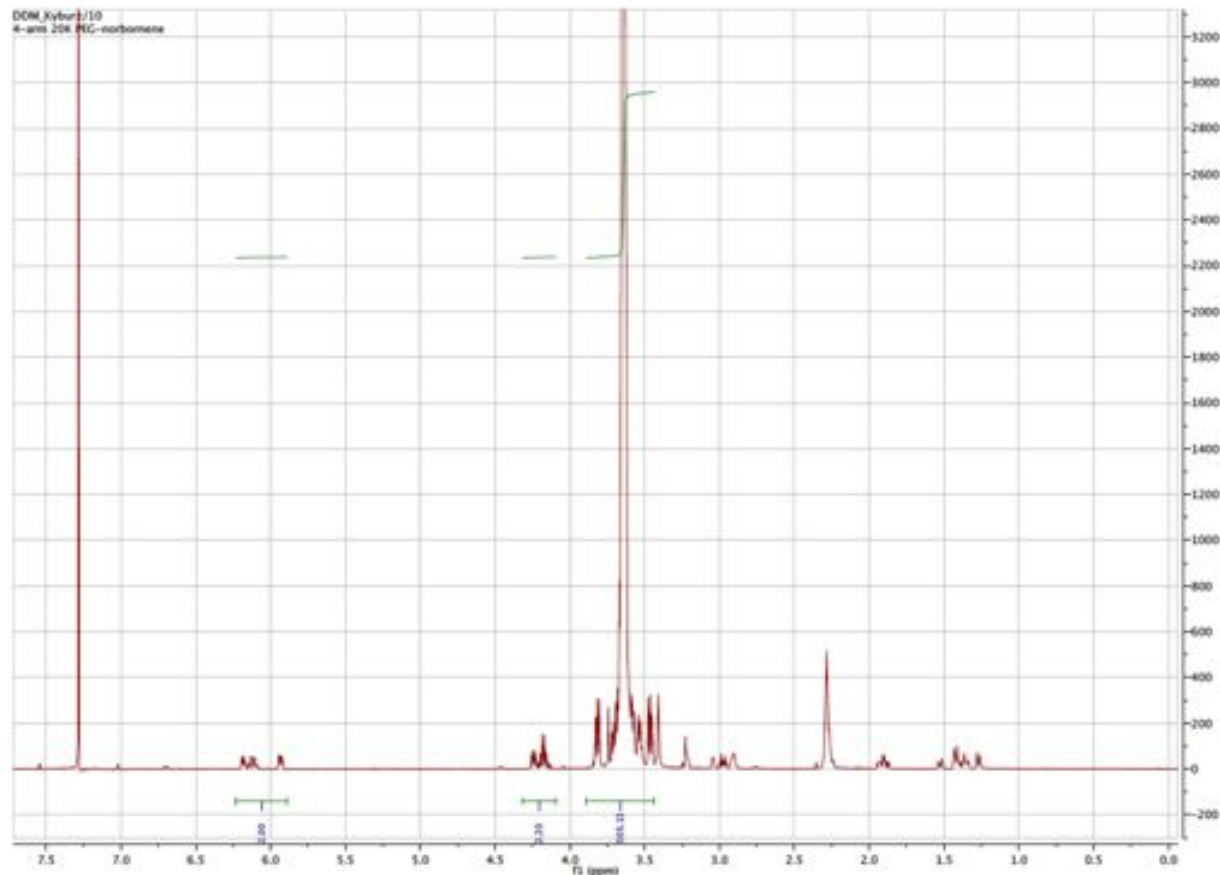


Figure 3.S1 hNMR spectra of PEG-Norbornene. Functionalization was calculated by dividing the norbornene alkene peaks by the PEG alkyl peaks.

3.7 References

- [1] Uccelli A, Moretta L, Pistoia V. Mesenchymal stem cells in health and disease. *Nature Reviews Immunology* 2008;8:726-36.
- [2] Salem HK, Thiemermann C. Mesenchymal Stromal Cells: Current Understanding and Clinical Status. *Stem Cells* 2010;28:585-96.
- [3] Discher DE, Mooney DJ, Zandstra PW. Growth Factors, Matrices, and Forces Combine and Control Stem Cells. *Science* 2009;324:1673-7.
- [4] Chen F-M, Wu L-A, Zhang M, Zhang R, Sun H-H. Homing of endogenous stem/progenitor cells for in situ tissue regeneration: Promises, strategies, and translational perspectives. *Biomaterials* 2011;32:3189-209.
- [5] Friedl P, Wolf K. Plasticity of cell migration: a multiscale tuning model. *J Cell Biol* 2010;188:11-9.

- [6] Lutolf MP, Gilbert PM, Blau HM. Designing materials to direct stem-cell fate. *Nature* 2009;462:433-41.
- [7] Kim H-D, Peyton SR. Bio-inspired materials for parsing matrix physicochemical control of cell migration: A Review. *Integrative Biology* 2012;4:37-52.
- [8] Doyle AD, Wang FW, Matsumoto K, Yamada KM. One-dimensional topography underlies three-dimensional fibrillar cell migration. *J Cell Biol* 2009;184:481-90.
- [9] Peyton SR, Kalcioğlu ZI, Cohen JC, Runkle AP, Van Vliet KJ, Lauffenburger DA, et al. Marrow-derived stem cell motility in 3D synthetic scaffold is governed by geometry along with adhesivity and stiffness. *Biotechnology and Bioengineering* 2011;108:1181-93.
- [10] Peyton SR, Putnam AJ. Extracellular matrix rigidity governs smooth muscle cell motility in a biphasic fashion. *J Cell Physiol* 2005;204:198-209.
- [11] Palecek SP, Loftus JC, Ginsberg MH, Lauffenburger DA, Horwitz AF. Integrin-ligand binding properties govern cell migration speed through cell-substratum adhesiveness. *Nature* 1997;385:537-40.
- [12] Purcell BP, Elser JA, Mu A, Margulies KB, Burdick JA. Synergistic effects of SDF-1 α chemokine and hyaluronic acid release from degradable hydrogels on directing bone marrow derived cell homing to the myocardium. *Biomaterials* 2012;33:7849-57.
- [13] Pelham RJ, Jr., Wang YI. Cell locomotion and focal adhesions are regulated by substrate flexibility. *Proc Natl Acad Sci USA* 1997;94:13661-5.
- [14] Lo C-M, Wang H-B, Dembo M, Wang Y-I. Cell Movement Is Guided by the Rigidity of the Substrate. *Biophysical Journal* 2000;79:144-52.
- [15] Engler A, Bacakova L, Newman C, Hategan A, Griffin M, Discher D. Substrate Compliance versus Ligand Density in Cell on Gel Responses. *Biophysical Journal* 2004;86:617-28.
- [16] Maheshwari G, Brown G, Lauffenburger DA, Wells A, Griffith LG. Cell adhesion and motility depend on nanoscale RGD clustering. *J Cell Sci* 2000;113:1677-86.
- [17] Grinnell F, Petroll WM. Cell Motility and Mechanics in Three-Dimensional Collagen Matrices. *Annual Review of Cell and Developmental Biology* 2010;26:335-61.
- [18] Zaman MH, Trapani LM, Sieminski AL, MacKellar D, Gong H, Kamm RD, et al. Migration of tumor cells in 3D matrices is governed by matrix stiffness along with cell-matrix adhesion and proteolysis. *PNAS* 2006;103:10889-94.

- [19] Ehrbar M, Sala A, Lienemann P, Ranga A, Mosiewicz K, Bittermann A, et al. Elucidating the Role of Matrix Stiffness in 3D Cell Migration and Remodeling. *Biophysical Journal* 2011;100:284-93.
- [20] Lei Y, Gojgini S, Lam J, Segura T. The spreading, migration and proliferation of mouse mesenchymal stem cells cultured inside hyaluronic acid hydrogels. *Biomaterials* 2011;32:39-47.
- [21] Raeber GP, Lutolf MP, Hubbell JA. Molecularly Engineered PEG Hydrogels: A Novel Model System for Proteolytically Mediated Cell Migration. *Biophysical Journal* 2005;89:1374-88.
- [22] Raeber GP, Lutolf MP, Hubbell JA. Mechanisms of 3-D migration and matrix remodeling of fibroblasts within artificial ECMs. *Acta Biomaterialia* 2007;3:615-29.
- [23] Zhang YH, Zhao CQ, Jiang LS, Dai LY. Substrate stiffness regulates apoptosis and the mRNA expression of extracellular matrix regulatory genes in the rat annular cells. *Matrix Biology* 2011;30:135-44.
- [24] Hanjaya-Putra D, Yee J, Ceci D, Truitt R, Yee D, Gerecht S. Vascular endothelial growth factor and substrate mechanics regulate in vitro tubulogenesis of endothelial progenitor cells. *Journal of Cellular and Molecular Medicine* 2010;14:2436-47.
- [25] Gould ST, Darling NJ, Anseth KS. Small peptide functionalized thiol-ene hydrogels as culture substrates for understanding valvular interstitial cell activation and de novo tissue deposition. *Acta Biomaterialia* 2012;8:3201-9.
- [26] Gaudet C, Marganski WA, Kim S, Brown CT, Gunderia V, Dembo M, et al. Influence of type I collagen surface density on fibroblast spreading, motility, and contractility. *Biophysical Journal* 2003;85:3329-35.
- [27] Schwartz MP, Fairbanks BD, Rogers RE, Rangarajan R, Zaman MH, Anseth KS. A synthetic strategy for mimicking the extracellular matrix provides new insight about tumor cell migration. *Integrative Biology* 2010;2:32-40.
- [28] Fairbanks BD, Schwartz MP, Halevi AE, Nuttelman CR, Bowman CN, Anseth KS. A Versatile Synthetic Extracellular Matrix Mimic via Thiol-Norbornene Photopolymerization. *Advanced Materials* 2009;21:5005-10.
- [29] Nagase H, Fields GB. Human matrix metalloproteinase specificity studies using collagen sequence-based synthetic peptides. *Biopolymers* 1996;40:399-416.
- [30] Patterson J, Hubbell JA. Enhanced proteolytic degradation of molecularly engineered PEG hydrogels in response to MMP-1 and MMP-2. *Biomaterials* 2010;31:7836-45.

- [31] Ho IAW, Chan KYW, Ng W-H, Guo CM, Hui KM, Cheang P, et al. Matrix metalloproteinase 1 is necessary for the migration of human bone marrow-derived mesenchymal stem cells toward human glioma. *Stem Cells* 2009;27:1366-75.
- [32] Halfon S, Abramov N, Grinblat B, Ginis I. Markers distinguishing mesenchymal stem cells from fibroblasts are downregulated with passaging. *Stem Cells Dev* 2011;20:53-66.
- [33] Parikka V, Väänänen A, Risteli J, Salo T, Sorsa T, Väänänen HK, et al. Human mesenchymal stem cell derived osteoblasts degrade organic bone matrix in vitro by matrix metalloproteinases. *Matrix Biol* 2005;24:438-47.
- [34] Djouad F, Delorme B, Maurice M, Bony C, Apparailly F, Louis-Plence P, et al. Microenvironmental changes during differentiation of mesenchymal stem cells towards chondrocytes. *Arthritis Res Ther* 2007;9.
- [35] Fairbanks BD, Schwartz MP, Bowman CN, Anseth KS. Photoinitiated polymerization of PEG-diacrylate with lithium phenyl-2,4,6-trimethylbenzoylphosphinate: polymerization rate and cytocompatibility. *Biomaterials* 2009;30:6702-7.
- [36] Dickinson RB, Tranquillo RT. Optimal estimation of cell movement indices from the statistical analysis of cell tracking data. *AIChE Journal* 1993;39:1995-2010.
- [37] Engler AJ, Sen S, Sweeney HL, Discher DE. Matrix elasticity directs stem cell lineage specification. *Cell* 2006;126:677-89.
- [38] Rubinstein M, Colby RH. *Polymer Physics*. 9 ed. New York: Oxford University Press Inc.; 2003.
- [39] Sakai T, Matsunaga T, Yamamoto Y, Ito C, Yoshida R, Suzuki S, et al. Design and fabrication of a high-strength hydrogel with ideally homogeneous network structure from tetrahedron-like macromonomers. *Macromolecules* 2008;41:5379-84.
- [40] Malkoch M, Vestberg R, Gupta N, Mespouille L, Dubois P, Mason AF, et al. Synthesis of well-defined hydrogel networks using Click chemistry. *Chemical Communications* 2006:2774-6.
- [41] Yang T, Long H, Malkoch M, Gamstedt EK, Berglund L, Hult A. Characterization of Well-Defined Poly(ethylene glycol) Hydrogels Prepared by Thiol-ene Chemistry. *Journal of Polymer Science Part a-Polymer Chemistry* 2011;49:4044-54.
- [42] Humphries JD, Byron A, Humphries MJ. Integrin ligands at a glance. *J Cell Sci* 2006;119:3901-3.
- [43] Hakkinen KM, Harunaga JS, Doyle AD, Yamada KM. Direct comparisons of the morphology, migration, cell adhesions, and actin cytoskeleton of fibroblasts in four different three-dimensional extracellular matrices. *Tissue Eng Part A* 2011;17:713-24.

[44] Wu S, Wells A, Griffith LG, Lauffenburger DA. Controlling multipotent stromal cell migration by integrating “course-graining” materials and “fine-tuning” small molecules via decision tree signal-response modeling. *Biomaterials* 2011;32:7524-31.

[45] DeForest CA, Anseth KS. Photoreversible Patterning of Biomolecules within Click-Based Hydrogels. *Angewandte Chemie International Edition* 2012;51:1816-9.

CHAPTER IV

MEASURING DYNAMIC CELL-MATERIAL INTERACTIONS AND REMODELING DURING 3D HMSC MIGRATION IN HYDROGELS

As in review in the Proceedings of the National Academy of Sciences

4.1 Abstract

Biomaterials that mimic aspects of the extracellular matrix by presenting a 3D microenvironment that cells can locally degrade and remodel are finding increased applications as wound healing matrices, tissue engineering scaffolds and even substrates for stem cell expansion. *In vivo*, cells do not simply reside in a static microenvironment, but instead, they dynamically re-engineer their surroundings. For example, cells secrete proteases that degrade extracellular components, attach to the matrix through adhesive sites, and can exert traction forces on the local matrix, causing its spatial reorganization. Although biomaterials scaffolds provide initially well-defined microenvironments for three-dimensional culture of cells, less is known about the changes that occur over time, especially local matrix remodeling that can play an integral role in directing cell behavior. Here, we use microrheology as a quantitative tool to characterize dynamic cellular remodeling of peptide-functionalized poly(ethylene glycol) (PEG) hydrogels that degrade in response to cell-secreted matrix metalloproteinases (MMPs). This technique allows measurement of spatial changes in material properties during migration of encapsulated cells, and has a sensitivity that identifies regions where cells simply adhere to the matrix, as well as the extent of local cell remodeling of the material through MMP-mediated degradation. Collectively, these microrheological measurements provide insight into microscopic, cellular

manipulation of the pericellular region that gives rise to macroscopic tracks created in scaffolds by migrating cells. This quantitative and predictable information should benefit the design of improved biomaterial scaffolds for medically-relevant applications.

4.2 Introduction

Synthetic hydrogel scaffolds have been designed to serve as mimics of the native extracellular matrix (ECM) with the goal of promoting desired cell functions (e.g., proliferation, migration, differentiation), especially for applications in wound healing [1], tissue regeneration [2] and stem cell culture [3, 4]. For example, poly(ethylene glycol) (PEG) hydrogels can serve as blank slates in which peptide cues can be systematically introduced in the scaffold to allow integrin-binding [5, 6], proteolytic degradation [7, 8] and even local sequestering of growth factors [9]. Furthermore, it is well known that cells respond to mechanical stimuli (e.g., stiffness) in their local microenvironment, the so-called pericellular region, and tuning of a scaffold's mechanical properties, can influence how a cell degrades and remodels its surroundings [10, 11, 12]. The complex cell-matrix interactions that occur in the native extracellular matrix (ECM) are often mimicked in peptide-functionalized hydrogels through the incorporation of adhesive binding peptides (e.g., RGDS, IKVAV) and enzymatically degradable peptide cross-linkers (e.g., GPQGIWGQ, GPLGLWAR), both of which are necessary for cell attachment, spreading [13] and motility [14, 12]. However, changes in the local material properties as a result of this cell-mediated remodeling have largely remained a “black box”, limiting interpretation of data and confounding the design of more advanced biomaterials.

Macroscopically, cells degrade micron-sized channels into scaffolds as they move, an event that begins with microscopic remodeling of their pericellular region and eventually

permanently reengineering the scaffold architecture and material properties on a larger scale. If one seeks to design synthetic ECM environments to direct cellular processes, such as migration, it is important to better understand how these inputs are dynamically altered on the local length scale. Such information can help advance biomaterial design, especially for applications focused on the delivery or recruitment of cells, where directing cell-material interactions and migration can be critically important. At present, cell matrices are generally engineered to have certain initial material properties, but the resulting cell motility and cell-material interactions are often only empirically correlated with these design parameters [7, 15]. To overcome this obstacle and provide an in situ measurement of scaffold degradation, microrheological measurements have been used to fingerprint and understand changes in material properties in the pericellular region during cell motility.

Although real time measurements of material properties near a cell are difficult, investigations have focused on developing techniques to access this information. In two-dimensions, forces that cells exert when seeded on hydrogel surfaces have been measured using deflection of beds of microneedles [15] and deformation of gel surfaces [16]. For example, Tan *et al.* developed a measurement technique that exploits independent deflection of microneedles of varying lengths (and therefore stiffnesses) to measure the distribution of subcellular traction forces of both smooth muscle cells and fibroblasts. The main conclusion was that cellular spreading and morphology control the magnitude of the traction forces [15]. The traction force of confluent cell sheets interacting with a gel surface was also analyzed, towards understanding how cellular processes are coordinated over large length scales. Using endothelial, epithelial and breast cancer cell sheets, results showed that collective migration was due to a transmittance of normal stress across cell-cell junctions with migration orientated in the direction of the minimal

intercellular shear stress [16].

While two-dimensional studies add to our understanding of cell-matrix interactions, 2D environments can un-naturally polarize cells, and some aspects of cell motility can be quite different in 2D versus 3D environments [17, 18]. For these reasons, recent developments have focused on strategies to measure cell-material interactions in 3D (e.g, cell-laden hydrogels). Traction force microscopy measures spatial interfacial forces by quantifying the elastic deformation of a substrate [17]. If the modulus of the material is known, this technique quantifies the forces cells exert in 3D calculated from embedded bead displacement. This approach has identified patterns of forces generated around distinct morphological regions during cellular invasion into a scaffold [17]. Additionally, Bloom *et al.* investigated the degradation of a collagen scaffold during the migration of a fibrosarcoma cell line (HT1080s) using embedded particle displacements. The authors showed that the hydrogel was reversibly deformed at the cell's leading edge, but irreversibly remodeled at the trailing edge [19]. Collectively, these pioneering investigations have provided insight into aspects of the complex interplay between cells and scaffold materials; however, complementary techniques that allow characterization of dynamic and local changes in mechanical properties, degradation and scaffold erosion would be beneficial in further advancing our understanding of mechanotransduction, mechanisms of cell motility and even biomaterials design.

In this contribution, multiple particle tracking microrheology (MPT) is used to measure how human mesenchymal stem cells (hMSCs) remodel peptide cross-linked PEG hydrogels as they migrate. hMSC migration is characterized by significant remodeling of the local environment through attachment, enzymatic degradation and cellular traction. Further, hMSCs are observed to degrade the synthetic network through two pathways, matrix metalloproteinase

(MMP) secretion that cleaves the peptide cross-linker and myosin II regulated adhesion and reversible remodeling of the network. We find that MPT has the sensitivity to capture the temporal transition of the hydrogel from an elastic gel to a viscous liquid, during hMSC-mediated degradation. MPT simultaneously provides information about the spatial region, proximal to the cell, over which this matrix remodeling occurs. The technique and measurements enhance our understanding of cell-material interactions in 3D and enable visualization of dynamic cell mediated matrix degradation, the so-called fourth dimension. On longer time scales, these microscopic changes give rise to the creation of macroscopic channels in the hydrogel that are important for hMSC motility. We believe that this approach and characterization can provide an important link for better understanding outside-in signaling experienced by cells when embedded in 3D environments.

4.3 Results and Discussion

4.3.1 Microrheological characterization of hydrogel degradation and remodeling during hMSC migration

To characterize hMSC remodeling of their local environment when embedded in MMP-degradable hydrogels, we use multiple particle tracking microrheology (MPT). The sensitivity of MPT in the low moduli range (10^{-3} - 4 Pa) of hydrogels enables measurements of transitions from loosely cross-linked networks to viscoelastic polymeric fluids, an important critical state transition that correlates to many macroscopic changes in cell behavior (e.g., morphology, motility, secretory properties). MPT measurements use video microscopy for data collection, capturing spatial information about changes in hydrogel properties with time. This technique enables one to resolve both temporal and spatial information about the cellular

microenvironment, and here, we report on the characterization of the remodeling and degradation of MMP-degradable PEG-peptide hydrogels by 3D encapsulated hMSCs.

Microrheology measures the Brownian motion of embedded probe particles ($2a \cong 1 \mu\text{m}$) and relates this motion to rheological properties, such as viscosity and creep compliance, using the Generalized Stoke-Einstein relation (GSER),

$$\langle \Delta r^2(t) \rangle = \frac{k_B T}{\pi a} J(t) \quad (1)$$

Here $\langle \Delta r^2(t) \rangle$ is the mean-squared displacement, t is time, $k_B T$ is the thermal energy, $J(t)$ is the creep compliance and a is the probe particle radius [20, 21, 22, 23]. The state of material, i.e. sol or gel, can be determined using the logarithmic slope of the mean squared displacement, $\alpha = d \log \langle \Delta r^2(t) \rangle / d \log \tau$, and the critical relaxation exponent, n . Probe particles freely diffusing in a liquid have a value of $\alpha = 1$. When $\alpha \rightarrow 0$, probe particles are completely arrested in the gel network. All values of α between 0 and 1 are an elastic solid or viscoelastic liquid, and this transition is defined by the critical relaxation exponent, n . The value of n has been previously determined from measurements of the kinetics of degradation analyzed using time-cure superposition [24, 25, 26, 27]. To determine the state of a material, α is compared to n ; if $\alpha > n$, the material is a viscoelastic fluid, and if $\alpha < n$, the material is an elastic solid [24]. The value of n for the hydrogel studied here is $n \approx 0.2$ [24].

In general, PEG hydrogel scaffolds have been designed with a complexity that allows physical and chemical cues to be locally presented to encapsulated cells and elicit desired functions [12, 10, 11]. The hydrogel used in this work was formed via a photoinitiated thiol-ene polymerization of norbornene functionalized PEGs cross-linked with thiol containing peptides (Figure 1a) [28, 29]. Specifically, a four arm star PEG (M_n 20,000) was end functionalized with norbornene; PEG was chosen due to its hydrophilicity, resistance to non-specific protein

adsorption and the ability to tailor cell-material interactions by conjugation of selected peptide sequences [30, 31, 29]. Here, the PEG was cross-linked with a matrix metalloproteinase (MMP) degradable peptide, KCGPQG↓IWGQCK, which is cleaved at a high rate by MMP-1, 2, 3, 8 and 9 on a time scale relevant for 3D cell culture [12, 8, 32]. A schematic of the hydrogel formation and the specific formulation used for cell encapsulation experiments is shown in Figure 1a. Included in the hydrogel scaffold is an adhesive ligand (1 mM CRGDS) that promotes hMSC adhesion and motility in the otherwise bioinert PEG scaffold. Upon irradiation with ultraviolet light (3 min, 365 nm light at 10 mW cm⁻²) in the presence of a photoinitiator (lithium phenyl-2,4,6-trimethylbenzoylphosphinate), the norbornene and thiol functionalities undergo alternating propagation and chain transfer reactions via a step-growth mechanism to yield a covalently cross-linked network [28, 29]. Previous work has shown the usefulness of this material chemistry for culture of cells in two and three dimensions, rendering it a suitable material for studying how degradation induced matrix changes influence cell motility in 4D (i.e., 3D space and time) [12, 14].

All cell monitoring experiments were performed using a hydrogel with a low cross-linking density (0.18 ± 0.02 mM), which was achieved by tuning the stoichiometric ratio to 0.65 thiol:ene. hMSCs encapsulated at a density of 2×10^5 cells/mL in this gel formulation survive, spread and migrate. Figure 1b-d shows examples of real time cell tracking experiments, where hMSC migration was followed for a period of 6 hours, Figure 1b. Cell tracking was used to calculate speed, persistence and percent of cells migrating, which were $18 \pm 1 \mu\text{m h}^{-1}$, 156 ± 23 mins and $59 \pm 12\%$, respectively [14]. During 3D migration, hMSCs were observed to move over large distances in the matrix (10 to 150 μm over 6 hours), which implies significant cell-mediated network degradation and of nanometers) than the size of a cell (tens of micrometers).

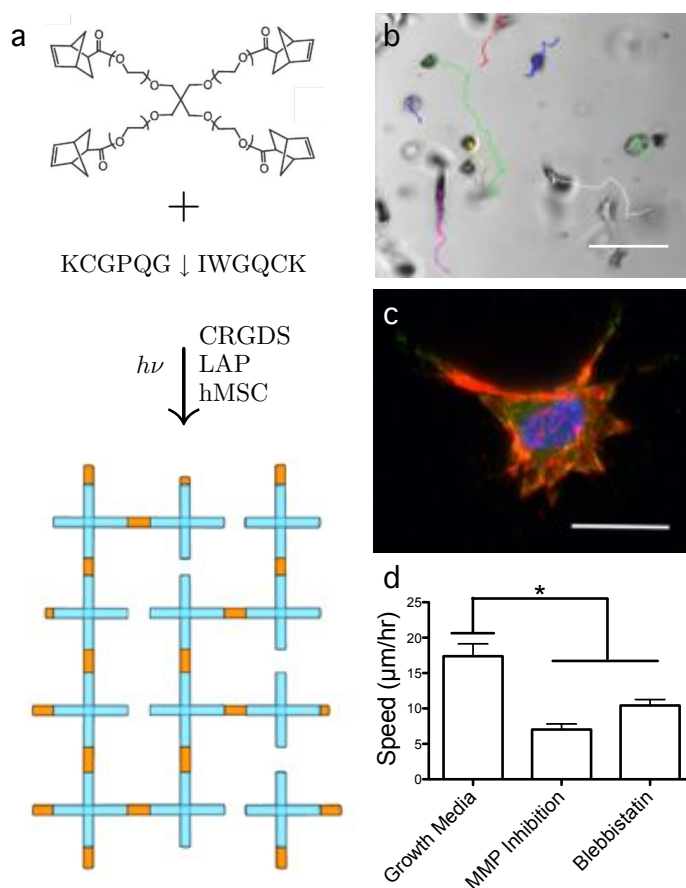


Figure 4.1 Human mesenchymal stem cells (hMSCs) migrate and form focal adhesions within the MMP-degradable thiol-ene hydrogel. (a) Schematic of network formation for the MMP-degradable PEG-norbornene hydrogel scaffold (0.65 thiol:ene, 3 mM 4-arm PEG-norbornene M_n 20,000 $g\ mol^{-1}$ $f = 4$, 3.9 mM KCGPQG↓IWGQCK M_n 1,305 $g\ mol^{-1}$, $f = 2$, 1mM CRGDS). (b) hMSCs were encapsulated at a density of 2×10^5 cells/mL, and the motility of individual cells was followed in real time for a period of 6 hours, scale bar: 100 μm , phase contrast image. (c) Representative image of an encapsulated hMSC immunostained for actin (red), $\beta 1$ integrin (green), and DAPI (blue). 48 hours after encapsulation, hMSCs spread within the gel and form actin stress fibers and punctate $\beta 1$ integrin staining as observed at the end of these fibers, scalebar: 20 μm . (d) The migratory speed of hMSCs decreased when cells were treated with either an MMP inhibitor (InSolutionTM GM 6001, 10 μM , immediately after encapsulation) or blebbistatin (50 μM , 2 hours post encapsulation). * $p < 0.05$.

As further evidence of cell-matrix interactions, immunostaining was performed, Figure 1c. Punctate $\beta 1$ integrin staining (green) at the ends of actin stress fibers (red) was observed, indicating strong cellular attachment and spreading of the hMSCs in these PEG

microenvironments. Additionally, hMSC migration was inhibited by the addition of either an MMP inhibitor, which limits cell-mediated degradation of the matrix, or with blebbistatin, which inhibits cytoskeletal tension. In both cases, cell migration was significantly reduced compared to untreated hMSCs, Figure 1d. These controls further emphasize the importance of cell-mediated degradation and cellular tension on microenvironmental remodeling and subsequently regulating the hMSC migration process within these materials.

4.3.2 Cell-mediated degradation during early stages of motility

Using MPT to characterize hMSC-laden gels, we measured the changes in material properties, temporally and spatially, in the pericellular region of individual cells as they attach, spread and begin to migrate in MMP-degradable hydrogels. MPT data during cellularly-dictated changes in the hydrogel scaffold were collected over 25 – 60 minutes, while hMSCs were migrating. Initially and immediately after encapsulation, hMSCs were essentially embedded in a largely elastic solid gel environment, and representative, surrounding probe particle trajectories are depicted in Figure 2a. However, tens of minutes after encapsulation, the hMSCs began to spread, remodel and degrade their local hydrogel microenvironment; in this region, the material begins to transition from an elastic solid to a viscoelastic fluid, and the probe particle trajectories become significantly longer, Figure 2b. At much longer time scales, the hMSC morphology is highly extended and relatively fast migration is observed, presumably through regions that are largely in a polymeric liquid state, as observed by probe particle trajectories illustrated in Figure 2c.

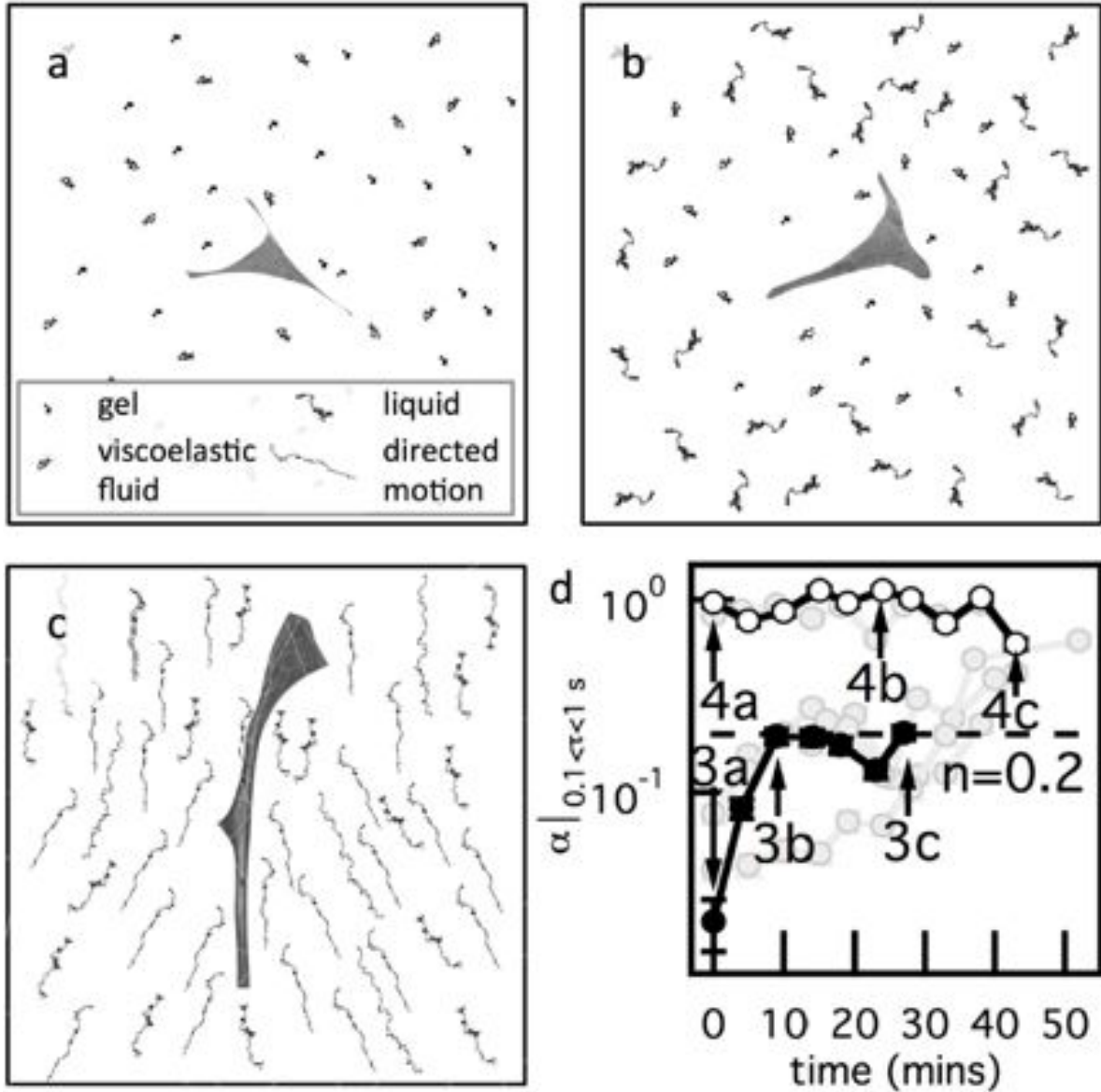


Figure 4.2 hMSC remodeling and degradation of peptide cross-linked PEG hydrogels. Schematic image of changes that occur in cell-laden hydrogels, where the changes in the gel properties are captured by MPT probe particle trajectories. (a) Initial state, before hMSCs have caused any substantial changes in the local material properties and the cells experience a solid gel environment (b) during cell spreading, the local environment degrades in response to cellular activity and the material begins to transition from a gel to a sol in a local region and (c) at longer time scales, the pericellular region is extensively degraded, becoming a sol, and cell motility is observed. (d) Logarithmic slope of the mean-squared displacement ($\alpha|_{0.1 < \tau < 1 \text{ s}} = \frac{d \log \langle \Delta r^2(\tau) \rangle}{d \log \tau} |_{0.1 < \tau < 1 \text{ s}}$) of probe particles in the pericellular region during hMSC migration. The gel-sol transition occurs at the critical relaxation exponent, $n = 0.2$. Values of $\alpha > 0.2$ represent materials that are a sol and $\alpha < 0.2$ are gelled materials. Data are highlighted for two stages of cell motility that will be described in detail in Figure 3 and 4. 3a-c shows a cell that is spreading and starting to degrade the pericellular region and 4a-c is a cell that is very motile in a sol.

The logarithmic slope of the MSD, α , was calculated for each of these time points and collected in the pericellular region. Measurements were repeated over 4 – 10 cells for each condition, and each data set on the graph (Figure 2d) represents measurements around an individual cell. Clearly, degradation on the microscopic length scale has macroscopic implications related to cell mediated scaffold architectural reengineering that facilitates motility. For hMSCs migrating through the MMP-degradable gels, we measured cells at two different time points. Initially in the migration process, we calculated that $\alpha \approx 0$, where the cell is encapsulated in the gel network prior to any remodeling. Over the next 15 – 30 minutes, hMSCs begin to attach and spread in the network, a process that necessitates some degree of local scaffold degradation. MPT measurements capture this remodeling, as an increase in α over $n = 0.2$, the value where the gel-sol transition occurs. In general, this parameter corresponds to a decrease in network connectivity and the transition of the material from a gel, a sample spanning cross-linked network, to a sol. Once cell-mediated degradation is complete (i.e., the gel to sol transition), rapid migration is observed as detailed below.

Optical fluorescent video microscopy was used to capture MPT data and enabled characterization of spatial changes in the material properties during hMSC migration. With these measurements, we aimed to identify regions where a cell adheres to the network during MMP secretion and matrix degradation, as well as characterize the distances over which this hMSC matrix remodeling occurs. As an example, Figure 3a-c maps the material properties surrounding an hMSC embedded in a gel and measures degradation of the environment through time. The color of each ring is the logarithmic slope of the MSD, α , calculated from the motion of particles within that area. Warm colors indicate that $\alpha \rightarrow 0$, and the region is basically a solid gel state;

light blue represent where $\alpha = 1$ and indicative of Brownian diffusion; cooler colors are $\alpha \approx 1.6$, indicating ballistic or directed motion. Concentric rings on the map are centered on the original cell position, which was defined at the beginning of the video. Here, the central ring has a radius of $r_1 = 150$ pixels $\approx 37 \mu\text{m}$, with each ring having a radius 150 pixels larger than the previous one, i.e. $r_2 = 150 + r_1$. In this scheme, the central circle represents a value of α 150 pixels from the center of the cell area, and the next circle represents a value of α of particles 150 – 300 pixels ($37 - 74 \mu\text{m}$) away from the cell. Each ring represents the movement of particles that are uniquely identified within the specified area from the initial particle position. Figure 3a-c shows the changes in material properties over 27 minutes, during migration of an hMSC that is beginning to spread at the early stages of data collection (these data are highlighted in Figure 2d with closed symbols). Throughout this time period, the area closest to the cell remains a gel until the final time point, indicating that the cell is likely adhering to this region of the scaffold during MMP secretion. In Figure 3b, we measured the transition from a gel to a sol, as annotated by the orange color, and here, the area directly around the cell appears to remain a gel. As we move through time, Figure 3c, we observe that the extent of degradation of the scaffold is highest in regions furthest from the cell. In fact, a gradient in degradation is measured with viscoelastic fluid properties observed furthest from the cell, but transitioning to an elastic solid as one approaches the cell. In Figure 3c, the outer circle indicates that the region has returned to a gel state, and we believe that this likely due to contraction or compaction of gel into the area that was previously degraded.

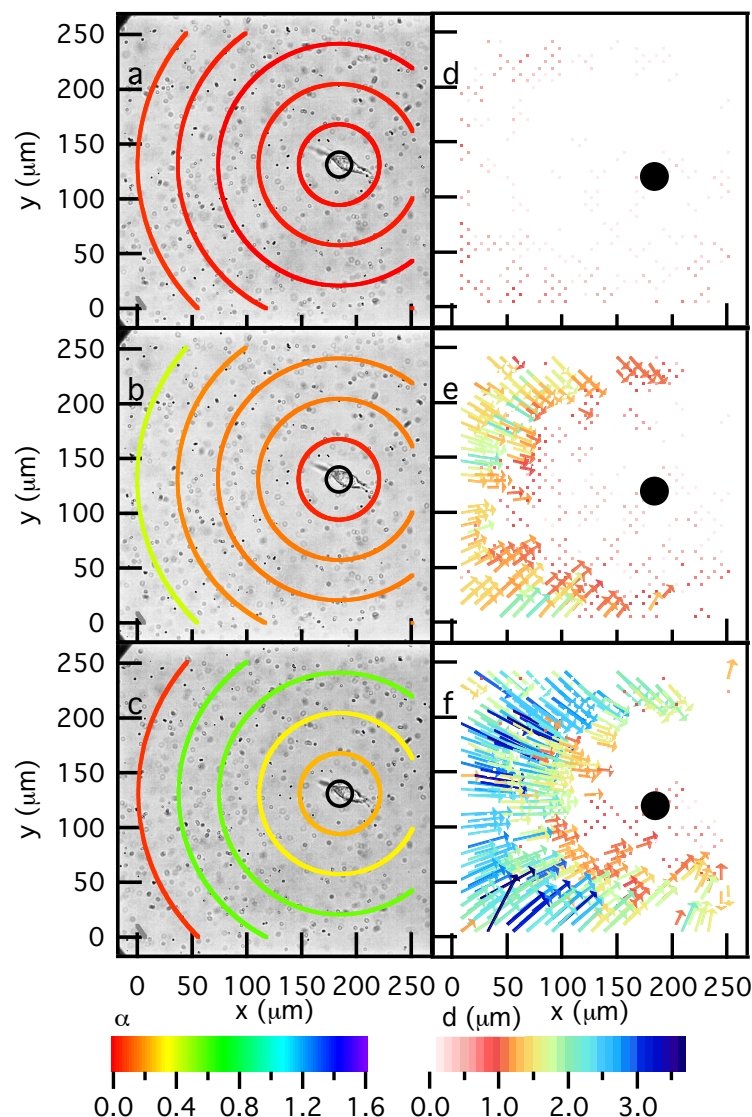


Figure 4.3 Dynamic rheological changes in the pericellular region during migration of an encapsulated hMSC overtime. Data are taken at (a) 0, (b) 9 and (c) 27 minutes after the cell is identified. Particle image velocimetry (PIV) measurements quantify the long time movement of probe particles between (d) 0 – 4, (e) 9 – 14 and (f) 23 – 27 minutes. Every other particle trajectory is displayed on PIV plots for clarity. Brightfield images are set in the background of MPT measurements with mean-squared displacement values calculated spatially as the distance away from the cell. The z axis, indicated by color, is the logarithmic slope of the mean-squared displacement, α , where a slope of 0, red, indicates no particle movement, a slope of 1, light blue, indicates Brownian motion and a slope of 1.6, purple, indicates ballistic motion. PIV measurements show the displacements using color and size of arrows. Warm colors and small arrows indicate small particle displacement, while cool colors and large arrows show large particle displacement. Both of these measurements confirm that through time as the cell is spreading the largest extent of degradation occurs furthest from the cell.

The corresponding images in Figure 3d-f are particle image velocimetry (PIV) measurements of particle movements over long time scales ($\Delta t = 4 - 5$ minutes) where displacement of the particles was measured between two brightfield images separated by several minutes. Warm colors indicate small particle displacements whereas cool colors correlate to larger displacements. Lack of arrows in the PIV map indicates that there is no detectable displacement. In these PIV maps, we quantified particle displacements that agreed with our microrheological measurements and reveal displacements primarily due to cell traction. In Figure 3d, few particle displacements were detected. Over the long time intervals used for PIV, $\Delta t = 4 - 5$ minutes, we measured the largest particle displacement furthest from the cell during spreading. This movement decreased, as characterized in regions closest to the center of the cell. On this time scale, we believe that the particle movement is due to cytoskeletal tension in regions of the scaffold that are degraded. The detected displacement shows that particles are moving in a persistent direction over this interval, which implies cellular remodeling and traction on the remaining porous scaffold. Furthest from the cell, MPT measurements describe an elastic fluid, and PIV measurements agree with MPT but also imply that there is a scaffold structure on length scales greater than accessed with MPT. Together, MPT and PIV analyses illustrate the complex interplay between cellular remodeling due to both cell-matrix interactions leading to traction, as well as cell-secreted enzymatic degradation in the local pericellular region. Both processes play a vital role in understanding dynamic changes in cell laden hydrogel environments and its effects on cell motility.

The gradient in extent of degradation, where the highest extent of degradation was observed furthest from the cell, suggests that the value of the Damköhler number, $Da = \frac{\text{reaction rate}}{\text{diffusive mass transfer rate}}$, is small. This physically indicates that the cell-secreted enzymes

diffuse away from the cell faster than it binds to and cleaves scaffold cross-links. This hypothesis is further supported by the time scales of diffusion and measured MMP degradation. As previously reported, the hydrogel scaffold is completely degraded over 24 – 48 hours in a sample of similar dimensions using varied concentrations (0.1 – 0.3 mg/mL) of collagenase, a mixture of MMPs delivered in bulk solution [24]. The protein diffusion time is approximately 1.35 hours for our gels that are 0.6 mm thick; this value is defined as $t_D \sim \frac{L^2}{D}$ where L is the thickness of the gel and D is the protein diffusivity, calculated as $D = 7.4 \times 10^{-7} \text{ cm}^2 \text{ s}^{-1}$ [24, 33]. Therefore, these length scales would result in a small value of Da because the time scale of the reaction is much slower than the rate of MMP diffusion through the gel. However, one must recognize that all of this must be placed in the context of complexities that arise from cell adhesion and traction in the scaffold during motility. This asymmetric deformation can aid in diffusion of the enzyme contributing to the extent of degradation gradient measured in the pericellular region.

4.3.3 Local hydrogel remodeling by hMSCs during migration.

After culture and initial spreading of hMSCs in MMP-degradable hydrogels, significant migration begins to occur with time, and this cellular degradation and remodeling of the matrix was characterized with MPT. On shorter time scales, hMSC were observed to actively degrade and remodel the pericellular region, creating an environment in which cells not only adhere and spread, but also migrate through the material via MMP-mediated mesenchymal mechanisms. However, at longer times in this process, hMSCs completely erode the hydrogel in the pericellular region, and significantly higher levels of motility (e.g., speed) are observed, as well as a more elongated morphology. The state of the material over the entire data collection

window, 45 minutes, is that of a viscoelastic fluid (open symbols in Figure 2d, $\alpha \rightarrow 1$), and cells in these regions are highly motile.

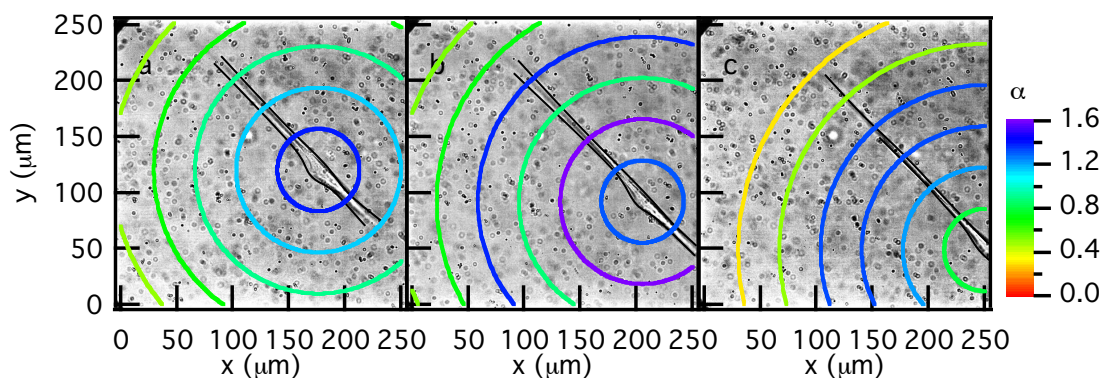


Figure 4.4 Dynamic spatial rheological data of the pericellular region during cell migration. Data are taken through time at (a) 0, (b) 24 and (c) 43 minutes after the cell is identified. This rapidly moving cell is causing the particles to move with the cell (outlined in black) as it migrates through the acquisition window. These measurements indicate that once the cell is spread and begins to move that the scaffold is a viscoelastic fluid.

Spatial measurements of the material properties in the pericellular region show this transition with time, Figure 4a-c. It is important to note that this transition enables rapid motility of hMSCs located in these regions ($\approx 150 \mu\text{m}$), and ballistic or directed motion of the probe particles (values of $\alpha \rightarrow 2$) are measured. As the cell begins to migrate out of the field of view, Figure 4c, we observe that the probe particles start to resume trajectories more indicative of Brownian motion, which we hypothesize is evidence that hMSC motility primarily influences local particle trajectories during this long-range migration.

4.3.4 Visualization of cellularly degraded pathways after migration in 3D hydrogels.

Cell migration in 3D necessitates matrix erosion and remodeling over larger lengths scales, much greater than those measured with microrheology. To complement MPT results, confirm some of the conclusions drawn using the MPT method and directly observe cell-

mediated macroscopic remodeling of the hydrogel, a fluorescently labeled peptide was directly and isotropically tethered to the hydrogel structure to allow direct visualization of matrix erosion. Two-photon laser scanning confocal enables 3D reconstruction of macroscopic material remodeling in hMSC-laden hydrogels. Figure 5 shows a minimum intensity projection of a compressed z-stack of a fluorescently labeled hydrogel to visualize the cell-mediated remodeling of the local matrix during hMSC migration. The cell, initially located at the large void, α , was allowed to migrate for a period of 48 hours resulting in a final spatial position, β , and a distance to origin of $\sim 175 \mu\text{m}$. The final position, β , of the cell can be clearly seen in the complimentary brightfield image (Figure 5b) of the same region. In this image, the initial position of the cell is circled by a dashed line to highlight the total migrated distance. The black regions in the fluorescent image (Figure 5a) represent voids created in the network, as the cell locally remodels and degrades the matrix. These representative images demonstrate that migrating cells lead to large matrix remodeling and erosion in three-dimensions. MPT captures aspects of these tracks in the pericellular space, and this can be directly observed on the macroscale as tracks and tunnels that allow long range motility of hMSCs within covalently cross-linked network. Certain regions of the cell track tunnel (e.g., near the final location of the cell) are on a smaller size scale than cannot be visualized using this method. As both the gel and the cells are deformable, cellular translocation can still occur within these regions despite the small size scale of the pores. Additionally, after a cell has migrated through these small tunnels, local hydrogel swelling and the limitations of visualizing dark regions within a highly fluorescent image may reduce the ability to image void regions. Measuring and characterizing this erosion provides fundamental insight into cell migration, the links between matrix remodeling and migration mechanisms, as well as strategies to direct cell migration through biophysical and biochemical scaffold design.

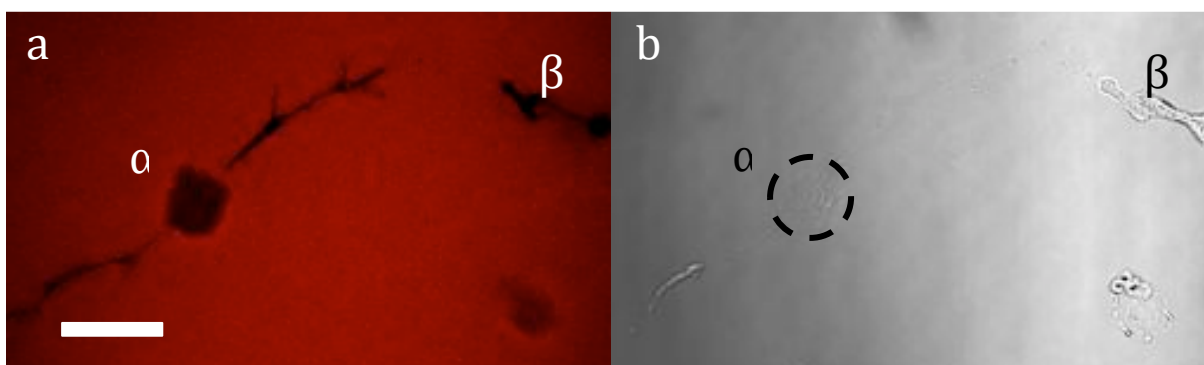


Figure 4.5 Fluorescently labeled hydrogels allow for the visualization of cell-mediated remodeling of the hydrogel during migration. (a) A minimum intensity projection of a compressed z-stack of a fluorescently labeled (AF-546) hydrogel permits visualization of the black (void) regions present in the gel from cellular degradation and remodeling. Over 48 hours, the cell migrated $\sim 175 \mu\text{m}$ from its original location, α , to its final location, β . Void tracks from cell spreading and migration can be seen developing off of this spherical void. (b) The bright field image depicts the initial cell location after polymerization circled with a dashed line, α , and the cell is located at its final position, β , after 48 hours of migration. Scale bar = $50 \mu\text{m}$.

4.4 Conclusions

Microrheological measurements were used to quantify cell-matrix interactions during three-dimensional hMSC migration. Multiple particle tracking microrheology has proven to be a valuable technique to determine the state of cell-mediated scaffold remodeling in the pericellular region with a sensitivity to discriminate between areas of cell adhesion and cell-mediated scaffold degradation. Here, we measured degradation processes on two time scales for hMSCs encapsulated in three-dimensions. On the short timescale, we observed the initial stages of cell-mediated degradation and cell spreading, and that the scaffold was fully degraded in areas farther away from the cell. These observations were attributed to the small Damköhler number (i.e., the

diffusion time scale is much faster than the reaction time scale) of cell-secreted MMPs. Particle image velocimetry was used to characterize particle movement over time intervals of 4 – 5 minutes on length scales greater than those accessible by MPT. PIV measured persistent particle movement in regions farther away from the cell, likely due to cytoskeletal tension on the scaffold. At longer time scales, the pericellular region near the hMSCs is a viscoelastic fluid that cells can rapidly migrate through. This microscopic material degradation is the initiation of much larger macroscopic scaffold reengineering that ultimately results in irreversible tracks that are eroded in the scaffold. Collectively, these methods and results provide links that should help the field better understand the outside-in signaling that a cell experiences during migration, advance the development of biomaterials that manipulate basic cellular processes and improve strategies for biomaterial design for regenerative medicine, wound healing and three-dimensional cell culture applications.

4.5 Materials and Methods

4.5.1 Hydrogel scaffold

All measurements were taken in a photopolymerizable thiol-ene network creating a chemically cross-linked matrix metalloproteinase (MMP) degradable poly(ethylene glycol) (PEG) hydrogel scaffold. Polymer functionalization was performed as described previously [29, 34]. Briefly, the four-arm PEG molecule (M_n 20,000 g mol⁻¹, $f = 4$, JenKem, Inc.) is end functionalized with norbornene ($f = 4$) and is reacted with a matrix metalloproteinase (MMP) degradable peptide (KCGPQG↓IWGQCK, M_n 1,305 g mol⁻¹, $f = 2$). This peptide is highly degradable, easily cleaved by cell secreted MMPs and has been previously used to study three-dimensional cellular migration [14, 12]. An adhesion ligand, CRGDS (M_n 594 g mol⁻¹), is

tethered to the network to promote adhesion and migration by binding to integrin receptors [35]. The reaction is initiated by a highly-water soluble initiator, lithium phenyl-2,4,6-trimethylbenzoylphosphinate (LAP), and a 365 nm light source (34). Carboxylated fluorescently labeled probe particles ($2a = 1.02 \pm 0.03 \mu m$, Polysciences, Inc.) were incorporated into the precursor solution to enable passive microrheological measurements. The hydrogel composition used for all experiments was 3 mM (7.2×10^{-18} -ene functional groups) PEG-norbornene, 3.9 mM (4.7×10^{-17} -SH functional groups) MMP degradable peptide, 1mM CRGDS, 0.04% (solids per volume) probe particles and 2×10^{-5} hMSCs per mL with all components dissolved in 1x Dulbecco's phosphate buffered saline (1x PBS, Life Technologies). This composition is chosen due to previous success studying hMSC migration [14]. Hydrogels are formed in sample chambers (described below) ensuring that the gel has sufficient room to swell during incubation.

4.5.2 Device fabrication and three-dimensional cell encapsulation

Hydrogels with encapsulated hMSCs are made in a device that enables multiple particle tracking microrheology measurements. This device reduces drift of the probe particle as the hydrogel scaffold degrades and enables incubation of the encapsulated hMSCs during data collection. The device consists of a glass bottom petri dish ($d = 0.35$ mm, no. 1.5 glass coverslip, MatTek Corp.) with a polydimethylsiloxane (PDMS, Dow Corning) chamber attached to the glass slide. The PDMS chamber is made using manufacturers instructions, namely, 10:1 silicone elastomer base: cross-linking agent. PDMS is degassed and cured in a flat sheet overnight for $65^{\circ}C$. The cured PDMS is cut using two biopsy punches and creates a circular chamber with an inner diameter of 6 mm and an outer diameter of 10 mm. The chamber is attached to the glass bottom using uncured PDMS and incubating at $65^{\circ}C$ overnight. The sample chambers are

sterilized with ethanol and UV light prior to cell-laden hydrogel formation. Hydrogels are made using the concentrations described above and are cured under UV light (365 nm, 10 mW cm⁻²) for 3 minutes in a sterile hood. The volume of the gel created in the samples is adjusted to 17 μ L enabling complete swelling. Samples are incubated overnight prior to data acquisition.

4.5.3 Human mesenchymal stem cell culture

HMSCs were isolated from bone marrow aspirates (Lonza). The isolation and freezing procedure is described previously [14]. Cells were passaged and passage two and three were used for each experiment.

4.5.4 Multiple particle tracking microrheology and particle image velocimetry measurements

Multiple particle tracking microrheology (MPT) was used to measure the material properties of the hydrogel scaffold during hMSC migration. MPT is a passive microrheological technique in which the Brownian motion of probe particles is measured and related to rheological properties using the Generalized Stokes-Einstein Relation (GSER). Data are collected using optical video microscopy enabling simultaneous measurements of dynamic material properties, such as cell-mediated scaffold degradation, and visualization of the microenvironment. Data were taken using an inverted microscope (Nikon TE2000E, Nikon Instruments Inc.) with a low numerical aperture oil immersion objective at 60x magnification (N. A. 1.4, 1x optovar, Nikon Instruments Inc.). An incubation chamber is connected to the microscope maintaining samples at 37°C and 5% CO₂ to ensure cells remain healthy during data collection. Data were collected at 30 frames s⁻¹ for 800 frames (\approx 27 s) and an exposure time of

1 ms (CMOS high-speed camera, Hi-Spec 3, 1024x1280 pixels, Fastec Imaging Corp.), parameters chosen to minimize the effects of static and dynamic particle tracking errors [23].

MPT measurements were collected of an area directly around a migrating hMSC, the pericellular region. This was done by first identifying a cell using brightfield microscopy. An image of each cell was collected with brightfield microscopy immediately before fluorescence MPT data was taken. Approximately 10 movies were collected in the pericellular region of each cell over approximately an hour. Particle tracking was performed using classic tracking algorithms developed by Crocker and Grier and maintained by Weeks that identify the brightness-weighted centroid of each particle and link the positions together in each frame to create a trajectory [20, 22]. From this data the mean-squared displacement, MSD, of the probe particles was calculated and used to identify the state of the material [24]. For each condition three biological replicates were measured. Within the biological replicates two separate gel stock solutions were measured over two days with 2 – 3 gels made per solution. Hydrogels were also measured in the absence of cells. These gels were made and incubated in an identical manner to cell-laden hydrogels and showed no significant scaffold degradation when incubated.

Particle image velocimetry (PIV) analysis was performed on brightfield images taken of the same observation window as MPT data. Iterative PIV analysis was done using ImageJ (NIH Image) and the PIV plugin [36]. In this analysis the image is broken up into smaller interrogations windows and the cross-correlation between particle movements in these windows is identified and plotted.

4.5.5 Visualizing cell tracks in hydrogel.

For visualizing cell tracks present in the scaffolds, CRGDS was fluorescently labeled

with Alexafluor 546 succinimidyl ester (AF546-NHS). Briefly, AF546-NHS was dissolved in dimethyl formamide and reacted overnight with the peptide before cleavage from the resin. The peptide was then introduced into the macromer solution before photopolymerization at 1 mM. HMSC encapsulation and hydrogel formation was performed as discussed above. After 48 hrs, z-stack images were taken using an LSM 710 confocal microscope (Carl Zeiss AG) at a step size of $0.78\ \mu m$. The z-stacks were compressed and a minimum intensity projection was created using ImageJ (NIH Image). Images presented within the manuscript were cropped and adjusted for contrast and brightness for better illustration of cell tracks.

4.6 Supplemental Information

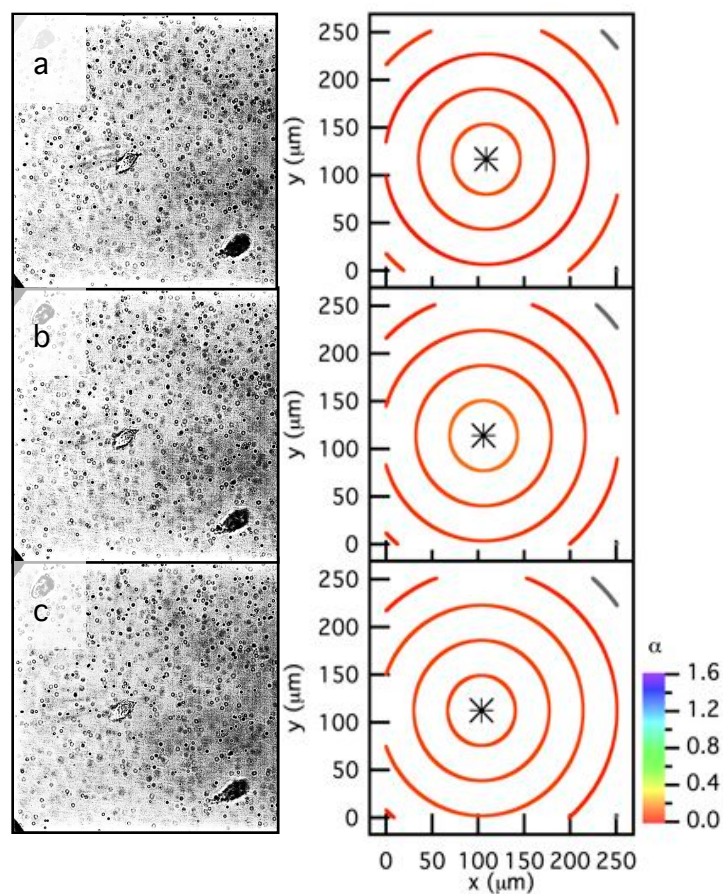


Figure 4.S1 Dynamic rheological data of the material during cell migration of a hMSC treated with a MMP inhibitor. The left panels are brightfield images of the cell encapsulated in 3D. The right panels are measurements of probe particle movement in the same field of view. The z axis, indicated by color of the marker and the rings that are averages of the particles within them, is the logarithmic slope of the mean-squared displacement, dark gray rings indicate that no particles fall within their area. Data are taken through time at (a) 0, (b) 21 and (c) 38 minutes after cell is identified.

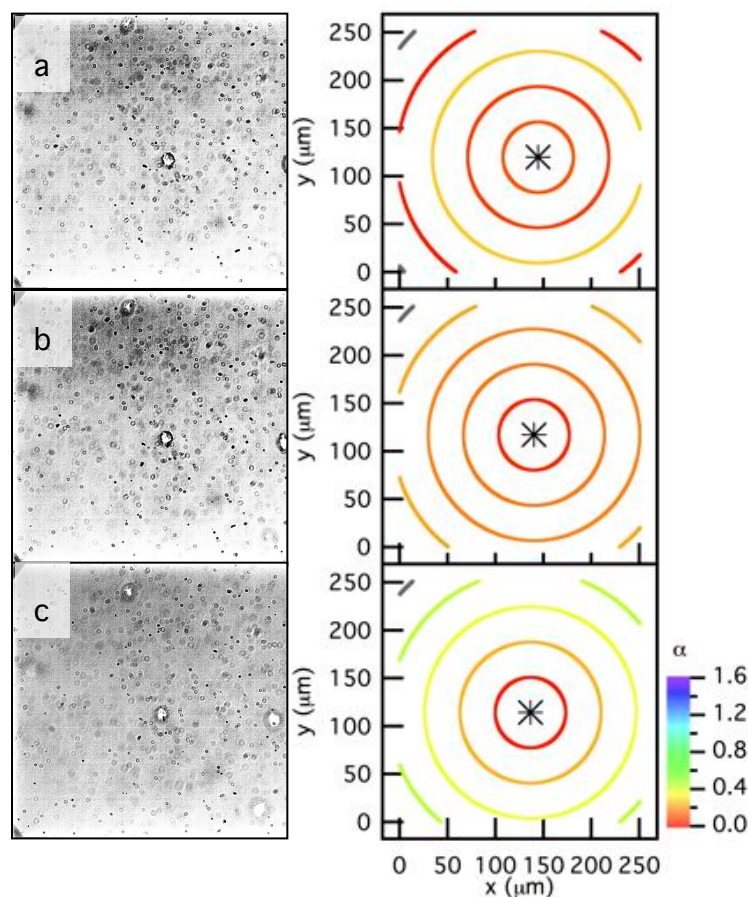


Figure 4.S2 Dynamic rheological data of the material during cell migration of a hMSC treated with blebbistatin, which inhibits myosin II. The left panels are brightfield images of the cell encapsulated in 3D. The right panels are measurements of probe particle movement in the same field of view. The z axis, indicated by color of the marker and the rings that are averages of the particles within them, is the logarithmic slope of the mean-squared displacement. Data are taken through time at (a) 12, (b) 20 and (c) 35 minutes after cell is identified.

4.7 References

- [1] Slaughter BV, Khurshid SS, Fisher OZ, Khademhosseini A, Peppas NA. Hydrogels in regenerative medicine. *Advanced Materials* 2009;21:3307-3329.
- [2] Hubbell JA. Biomaterials in tissue engineering. *Nature Biotechnology* 1995;13:565-576.
- [3] Peppas NA, Langer R. New challenges in biomaterials. *Science* 1994;263:1715-1720.
- [4] Kloxin AM, Kloxin CJ, Bowman CN, Anseth KS. Mechanical properties of cellularly responsive hydrogels and their experimental determination. *Advanced Materials* 2010;22:3484-3494.
- [5] Hern DL, Hubbell JA. Incorporation of adhesion peptides into nonadhesive hydrogels useful for tissue resurfacing. *Journal of Biomedical Material Research Part A* 1998;39:266-276.
- [6] DeLong SA, Moon JJ, and West JL. Covalently immobilized gradients of bfgf on hydrogel scaffolds for directed cell migration. *Biomaterials* 2005;26:3227-3234.
- [7] Lutolf MP, Lauer-Fields JL, Schoekel HG, Metters AT, Weber FE, Fields GB, Hubbell JA. Synthetic matrix metalloproteinase-sensitive hydrogels for the conduction of tissue regeneration: engineering cell-invasion characteristics. *Proceedings of the National Academy of Science* 2003;100:5413-5418.
- [8] Patterson J, Hubbell JA. Enhanced proteolytic degradation of molecularly engineered peg hydrogels in response to mmp-1 and mmp-2. *Biomaterials* 2010;31:7836-7845.
- [9] Lin CC, Boyer PD, Aimetti AA, Anseth KS. Regulating mcp-1 diffusion in affinity hydrogels for enhancing immuno-isolation. *Journal of Controlled Release* 2010;142:384-391.
- [10] Discher DE, Jamney P, Wang Y. Tissue cells feel and respond to the stiffness of their substrate. *Science* 2005;310:1139-1143.
- [11] Engler AJ, Sen S, Sweeney HL, Discher DE. Matrix elasticity directs stem cell lineage specification. *Cell* 2006;126:677-689.
- [12] Schwartz MP, Fairbanks BD, Rogers RE, Rangarajan R, Zaman MH, Anseth KS. A synthetic strategy for mimicking the extracellular matrix provides insight about tumor cell migration. *Integrative Biology* 2010;2:32-40.
- [13] Anderson SB, Lin CC, Kuntzler DV, Anseth KS. The performance of human mesenchymal stem cells encapsulated in cell-degradable polymer peptide hydrogels. *Biomaterials*, 32:3564-3574, 2011.
- [14] Kyburz KA, Anseth KS. Three-dimensional hmsc motility within peptide-functionalized peg-based hydrogels of varying adhesivity and crosslinking density. *Acta Biomaterialia*

2013;9:6381-6392.

[15] Tan JL, Tien J, Pirone DM, Gray DS, Bhadriraju K, Chen CS. Cells lying on a bed of microneedles: An approach to isolate mechanical force. *Proceedings of the National Academy of Science* 2003;100:1484-1489.

[16] Tambe DT, Hardin CC, Angelini TE, Rajendran K, Park CY, Serra-Picamal X, Zhou EH, Zaman MH, Butler JP, Weitz DA, Fredberg JJ, Treppe X. Collective cell guidance by cooperative intercellular forces. *Nature Materials* 2011;10:469-475.

[17] Legant WR, Miller JS, Blakely BL, Cohen DM, Genin GM, Chen CS. Measurement of mechanical tractions exerted by cells in three-dimensional matrices. *Nature Methods* 2010;7:969-973.

[18] Guvendiren M, Burdick JA. Engineering synthetic hydrogel microenvironments to instruct stem cells. *Current Opinion in Biotechnology* 2013;24:841-846.

[19] Bloom RJ, George JP, Celedon A, Sun SX, Wirtz D. Mapping local matrix remodeling induced by a migrating tumor cell using three-dimensional multiple-particle tracking. *Biophysical Journal* 2008;95:4077-4088.

[20] Crocker JC, Grier DG. Methods of digital video microscopy for colloidal studies. *Journal of Colloid Interface Science* 1996;179:298-310.

[21] Mason TG, Ganesan K, van Zanten JH, Wirtz D, Kuo SC. Particle tracking microrheology of complex fluids. *Physical Review Letters* 1997;79:3282-3285.

[22] Crocker JC, Weeks ER. Particle tracking using idl. <http://www.physics.emory.edu/~weeks/idl/index.html>, 2011.

[23] Savin T, Doyle PS. Static and dynamic errors in particle tracking microrheology. *Biophysical Journal* 2005;88:623-638.

[24] Schultz KM, Anseth KS. Monitoring degradation of matrix metalloproteinases- cleavable peg hydrogels via multiple particle tracking microrheology. *Soft Matter* 2013;9:1570-1579.

[25] Schultz KM, Baldwin AD, Kiick KL, Furst EM. Capturing the comprehensive modulus profile and reverse percolation transition of a degrading hydrogel. *Macro Letters* 2012;1:706-708.

[26] Adolf D, Martin JE. Time-cure superposition during crosslinking. *Macromolecules* 1990;23:3700-3704.

[27] Winter HH, Chambon F. Analysis of linear viscoelasticity of a crosslinking polymer at the gel point. *Journal of Rheology* 1986;30:367-382.

- [28] Aimetti AA, Machen AJ, Anseth KS. Poly(ethylene glycol) hydrogels formed by thiol-ene photopolymerization for enzyme-responsive protein delivery. *Biomaterials* 2009;30:6048-6054.
- [29] Fairbanks BD, Schwartz MP, Halevi AE, Nuttelman CR, Bowman CN, Anseth KS. A versatile synthetic extracellular matrix mimic via thiol-norbornene photopolymerization. *Adv. Mater* 2009;10:3114-3121.
- [30] Raeber GP, Lutolf MP, Hubbell JA. Molecularly engineered peg hydrogels: a novel model system for proteolytically mediated cell migration. *Biophysical Journal* 2005;89:1374-1388.
- [31] Kienberger F, Pastushenko VP, Kada G, Gruber HJ, Riener C, Schindler H, Hinterdorfer P. Static and dynamical properties of single poly (ethylene glycol) molecules investigated by force spectroscopy. *Single Molecules* 2000;1:123-128.
- [32] Miller JS, Shen CJ, Legant WR, Baranski JD, Blakely BL, Chen CS. Bioactive hydrogels made from step-growth derived peg-peptide macromers. *Biomaterials* 2010;31:3736-3743.
- [33] Weber LM, Lopez CG, Anseth KS. Effects of peg hydrogel crosslinking density on protein diffusion and encapsulated islet survival and function. *Journal of Biomedical Material Research Part A* 2009;90A:720-729.
- [34] Fairbanks BD, Schwartz MP, Bowman CN, Anseth KS. Photoinitiated polymerization of peg-diacrylate with lithium phenyl-2,4,6-trimethylbenzoylphosphinate: polymerization rate and cytocompatibility. *Biomaterials* 2009;30:6702-6707.
- [35] Nuttelman CR, Tripodi MC, Anseth KS. Synthetic hydrogel niches that promote hmsc viability. *Matrix Biology* 2005;24:208-218.
- [36] Tseng Q. Piv (particle image velocimetry) | imagej plugin. <https://sites.google.com/site/qingzongtseng/piv>, 2014.

CHAPTER V

OSTEOINDUCTIVE THIOL-ENE HYDROGELS THROUGH LOCALIZED PRESENTATION OF SDF-1 AND BMP-2

5.1 Introduction

Synthetic hydrogels provide a versatile platform to engineer cellular microenvironments that recapitulate important physical and biochemical facets of the extracellular matrix (ECM) for directing and regulating cell behavior and healing *in vivo* [1-4]. These platforms act as simplified models of the complex *in vivo* environment to probe the singular and synergistic effects of ECM cues and their interplay with cells in a systematic and tunable manner. Synthetic matrices capture many biophysical properties of the ECM, and recent advances in bioconjugation chemistry provide user-tunable techniques to incorporate cell signaling functionalities in the hydrogel [5, 6]. This work focuses on one class of synthetic matrices, thiol-ene degradable PEG hydrogels, which have been explored as osteoinductive scaffolds for bone regeneration [7]. Through the incorporation of MMP-degradable peptides and adhesive binding peptides these PEG networks permit high levels of cell migration and invasion providing a versatile platform to promote cellular integration and interaction *in vivo* [8, 9]. Building from this work, the aim is to design a biofunctional synthetic scaffold using thiol-ene chemistry to immobilize two proteins relevant to the bone healing cascade, namely SDF-1 and BMP-2. Then, evaluate the ability of the functionalized scaffolds to promote healing of a critical-sized rat calvarial defect.

There is a desire to effectively recapitulate facets of the *in vivo* milieu where cells are presented with a complex environment of proteins, sequestered and physically adsorbed to the

local ECM, to intricately direct and manipulate cell behavior. To this end, proteins have been incorporated into synthetic scaffolds through numerous mechanisms, such as simple loading and entrapment within the network to more sophisticated sequestration through the addition of affinity binding motifs or charged biomolecules [10-12]. However, the challenge is maintaining protein activity and presenting proteins in the appropriate context at the right time and dose. To address this issue, one strategy has focused on immobilization of proteins in degradable hydrogel systems; protein immobilization localizes their presentation and minimizes any bolus [13]. To confer biological signaling within the PEG hydrogels networks, we exploit the thiol-ene photo-click reaction as a bioconjugation technique, which has rapid bioorthogonal reaction kinetics, even in complex aqueous solutions and under physiologically-relevant conditions [6, 14]. Thiol-ene chemistry is a versatile and facile reaction that can be used to functionalize a large library of biomolecules through the presence of a thiol moiety on the molecule of interest that can undergo radical-mediated thiol-ene conjugation to an –ene moiety present within the network. Recent work has looked at utilizing thiol-ene chemistry to covalently immobilize full-length proteins to the hydrogel network. For example, transforming growth factor β (TGF- β) and Interleukin 10 (IL-10) have been immobilized on the surface of a PEG-diacrylate chain-growth hydrogel to reduce the maturation of dendritic cells [15]. Another example again looked at covalently immobilizing TGF- β to direct chondrogenic differentiation of encapsulated MSC [16]. In this work, we seek to locally deliver immobilized proteins within step-growth PEG-based hydrogels to a bone defect to direct the cellular invasion and mineralized tissue formation during bone regeneration in a critical sized bone defect.

Bone fractures that are too large for the body to heal through the natural bone-healing cascade are an area of intense interest for the tissue engineering community [17]. Much research

has focused on the design of biomaterials to deliver mesenchymal stem cell (MSC), which are known to play an integral role in the bone healing cascade through colonization of the defect, immune response regulation, and differentiating down osteogenic lineages to facilitate bone regeneration [18-20]. However, cell delivery approaches require *ex vivo* expansion of MSCs, which increases time and cost of the procedure as well as complicates regulatory issues when translating to clinical applications [21]. Additionally, work is beginning to elucidate that *ex vivo* expansion of stem cells can modify cell phenotype, chemokine receptors present on the cell surface, and engraftment capacity [22-25]. An alternative tissue engineering paradigm seeks to design scaffolds that attract endogenous MSC to bone defects, thereby avoiding some of these disadvantages [21, 26-28]. Recruitment of local, endogenous cells has the ability to promote healing of bone defects through normal healing cascade mechanisms and further promote crosstalk and regulation of neighboring cells through paracrine signaling to effectively govern the defect environment [18, 29].

To study the effect of thiol-ene photoconjugation of proteins to direct cell function in a critical-sized bone defect, the chemokine Stromal Derived Factor-1 α (SDF-1) and the growth factor Bone Morphogenetic Protein 2 (BMP-2) were chosen as they play a critical role *in vivo* directing MSC recruitment and differentiation during the complex bone healing cascade, respectively [30, 31]. SDF-1 is a small 8 kDa chemokine that is a part of the CXC chemokine family and has been shown to be a potent MSC chemokine *in vitro* and *in vivo* through interacting with the cell surface receptor CXCR4 [31-36]. Elegant work has elucidated the important role SDF1 plays in directing CXCR4⁺ progenitor cells to hypoxic environments during wound healing [37]. Furthermore, CXCR4-dependent chemotaxis was found to be necessary to recruit injected MSC to tibial fractures, where the MSC then helped accelerate bone

formation and modulated the inflammatory response [38]. This important role of SDF1 has motivated work that utilizes this chemotactic pathway for engineering drug delivery devices and cell-recruiting scaffolds for translational tissue regeneration applications. For example, Purcell *et al.* combined soluble SDF-1 with hyaluronic acid (HA) based gels to direct MSC recruitment to the myocardium after a myocardial infarction [39]. Similarly, Thevenot *et al.* loaded soluble SDF-1 into hydrolytically degradable poly(lactic-co-glycolic acid) hydrogels, and when the hydrogels were placed within the subcutaneous space of mice an increase in the recruited MSC and hematopoietic stem cell populations were observed at the implantation site [35].

In this work, there is a desire to understand the effects of co-delivery of immobilized SDF-1 with BMP-2 to a bone defect. BMP-2 is apart of the TGF β superfamily of growth factors that bind with serine/threonine kinase receptors to initiate the intracellular SMAD signaling cascade [30]. Additionally, BMP-2 plays an important role during bone fracture repair as it appears at an early time frame (day 1 – 21) to regulate, amongst other cell functions, MSC proliferation and differentiation [30, 40]. Because of its potency, BMP-2 has been delivered to bone fracture sites using many different natural (e.g., gelatin, fibrin) and synthetic (e.g., PLA-PEG, PLG) biomaterial delivery vehicles to increase bone formation [41-46]. Both SDF-1 and BMP-2 are prime candidates for immobilization to hydrogel networks, as they do not need to be internalized to elicit a cellular response. Here, thiol-ene hydrogels that permit high levels of MSC migration are functionalized with SDF-1 and/or BMP-2 to study their effect on cellular invasion and mineralized tissue formation in a rat calvarial defect model *in vivo*. This work begins to elucidate important engineering parameters to better deliver important molecules of the complex bone healing cascade in a local, sustained, and physiologically relevant dose to advance designs of synthetic scaffolds for bone regeneration applications.

5.2 Materials and Methods

5.2.1 Monomer Synthesis and Gel Formulation

Norbornene acid was conjugated to 4-arm PEG-hydroxyl (JenKem, USA), as previously described, to yield 4-arm PEG-norbornene [28]. In brief, norbornene conjugation was achieved by first reacting the norbornene acid with 0.5 molar equivalents of N,N'-dicyclohexylcarbodiimide (DCC) in anhydrous dichloromethane (DCM) for ~45 min at room temperature to produce an activated symmetric norbornene anhydride. The crude product was transferred anhydrously to a second reaction flask that contained 20 kDa 4-arm PEG-OH dissolved in DCM, 4-(dimethylamino)pyridine and pyridine, and was stirred overnight at room temperature. The urea by-product was removed via filtration using a glass-fritted funnel. The filtrate was then washed with glycine buffer and then brine to remove unreacted norbornene. The final product was precipitated and washed with ice-cold diethyl ether. Proton nuclear magnetic resonance ($^1\text{H-NMR}$) was used to characterize the purity and functionalization (>90% for these studies) of the product. The peptide sequences KCGPQG↓IWGQCK and CRGDS were purchased from the American Peptide Company and reconstituted in deionized water at working concentrations.

The pre-polymerized solution consisted of 6 wt.% PEG-norbornene (3 mM, $f = 4$), an MMP-degradable peptide crosslinker (KCGPQG↓IWGQCK, 3.7 mM, $f = 2$) with an off-stoichiometric thiol to ene ratio of 0.6, 1 mM CRGDS ($f = 1$), and 0.05% lithium phenyl-2,4,6-trimethylbenzoylphosphinate (LAP) [47]. SH-SDF-1 (1000 ng mL⁻¹ for section ELISA, 10 ng mL⁻¹ for *in vivo*) and SH-BMP-2 (12 and 24 μg mL⁻¹ for section ELISA, 1000 ng mL⁻¹ for *in vivo*) were included in the pre-polymerized solutions for studies related to their conjugation into the thiol-ene network. For cell encapsulation studies, cells were reconstituted in PBS and

introduced into the macromolecular monomer solutions. The solutions were then placed under 365 nm light at 2 mW cm⁻² for 3 min to initiate polymerization and hydrogel formation. *In situ* rheology measurements of the shear modulus evolution demonstrated full gel conversion before 3 min (data not shown).

5.2.2 Thiolation of SDF-1 and BMP-2

To study the effects of immobilized SDF-1 (Peprotech) and BMP-2 (Medtronic) on bone regeneration, the proteins were thiolated with 10X molar excess of Traut's reagent (Pierce) following the manufacturer's protocol. SH-SDF-1 was reconstituted in PBS at 1 μM and SH-BMP-2 was reconstituted in PBS at 1.5 mg/mL, and kept at -70°C until needed. The extent of thiolation was measured using Measure-IT™ Thiol Assay Kit (Life Technologies) following the manufacturer's protocol. To immobilize either protein into the hydrogel, the thiolated protein was introduced into the macromer solution at specific concentrations before photopolymerization.

5.2.3 Cell Isolation and Culture

Human mesenchymal stem cells (MSCs) were isolated from bone marrow aspirates from a single donor (Lonza), by first adding an ammonium chloride solution (Stem Cell Technologies), followed by vortexing and incubation on ice for 10 min to lyse the red blood cells. The cells were then washed twice and plated in media (low-glucose Dulbecco's modified Eagle's medium, 10% fetal bovine serum (FBS), 50 U ml⁻¹ each of penicillin and streptomycin, and 1 μg ml⁻¹ Fungizone antimycotic (all purchased from Life Technologies)). MSCs were distinguished as the plastic adherent cells and cultured at 37 °C and 5% CO₂. After 72 h, the non-

adherent cells were washed away using medium., and cell culture media was exchanged every 2–3 days to remove non-adherent cells,. After the resulting MSCs reached ~70–80% confluency, they were trypsinized and frozen in a solution of 95% FBS and 5% dimethyl sulfoxide (Sigma-Aldrich). For all experiments, MSCs were thawed and passaged at ~70–80% confluence with medium (including 1 ng ml⁻¹ recombinant human fibroblast growth factor-basic (FGF-2, Peprotech)) changed every 2–3 days. For all studies, MSCs at passages lower than three were used.

5.2.3 ELISA and Modified Section ELISA

To characterize SDF-1 immobilization, SH-SDF-1 was introduced at 1000 ng/mL into 30 µL of pre-polymerized macromer solution and photopolymerized using 365 nm light at 2 mW cm⁻² for 3 min. For BMP-2 immobilization, SH-BMP-2 was introduced similarly at concentrations of 12 and 24 µg mL⁻¹. The increased concentration of SH-BMP-2 was used as the primary antibody detection level was lower. The hydrogels were then allowed to swell in PBS for at least 4 hrs and then in HistoPrep (Fisher Scientific) overnight. The hydrogels were placed in cryomolds with HistoPrep and flash frozen in liquid nitrogen. A Leica CM1850 cryostat was used to take 20 µm cross-sections of the hydrogel, which were subsequently adhered to SuperFrost® Plus Gold slides (Fisher Scientific). To quantify the amount of SDF-1 and BMP-2 in each section, a modified ELISA was used [48]. Briefly, the sections were washed in wash buffer (0.01% bovine serum albumin (BSA), 0.05% Tween-20 in PBS) and blocked in 5% BSA for 2 hrs at room temperature. They were subsequently washed three times with wash buffer and then incubated with a rabbit anti-SDF-1 primary antibody (Abcam, 1:1000 dilution) or rabbit anti-BMP-2 primary antibody (Abcam, 1:200 dilutions) overnight at 4° C. They were then

washed three times, followed by incubation with a goat anti-rabbit HRP secondary antibody (Abcam, 1:2000 dilution) for two hours at room temperature. The sections were washed again five times before a hydrophobic boundary was drawn around each section with a ImmunoPen (Calbiochem). They were then incubated with 100 μ L of peroxidase and 3,3',5,5'-tetramethylbenzidine substrate for 30 min at room temperature. The reaction was stopped with 100 μ L of 2 M sulfuric acid, and the absorbance at 450 nm was read on a Synergy H1 microplate reader (BioTek). Standard curves were made by preparing a 96-well high binding clear plate with 0 – 10 ng mL⁻¹ of SDF-1 or 0 – 200 ng mL⁻¹ of BMP-2, and the absorbance from the blank condition was subtracted from all of the values in the standard curve.

The theoretical amount of SDF-1 in each section was calculated by assuming that each section was a cylindrical disc with a diameter of 5 mm and height of 20 μ m. It was also assumed that there was a uniform distribution of SDF-1 throughout the hydrogel. With , the ratio of the volume of each section to the total volume of the hydrogel was calculated and used in conjunction with the molecular weight of SDF-1 ($M_n=8,000$ g mol⁻¹) and BMP-2 ($M_n = 26,000$ g mol⁻¹) to determine the theoretical amount of SDF-1 and BMP-2 per section of the hydrogel.

5.2.4 Alkaline Phosphatase Assay

MSCs were encapsulated at 5×10^6 cells mL⁻¹ within the peptide-functionalized hydrogels by mixing them with the pre-polymerized macromer solution. Three conditions were tested: a negative control with no BMP-2 present, soluble BMP-2 entrapped within the hydrogel, and thiolated SH-BMP-2. For the soluble and immobilized BMP-2 conditions, 1000 ng mL⁻¹ of BMP-2 or SH-BMP-2 was introduced into the pre-polymer solution. Gels were formed as discussed above. On day 3 of MSC culture the hydrogels were washed in PBS for 15 min, and

then placed into 1.7 mL epistubes with 200 μ L of RIPA lysis buffer (Millipore) and the gel is degraded with a handheld homogenizer. Cell lysates were then spun down for 5 minutes at 14,000 rpm to pellet the gel material in the bottom of the tube. Duplicate wells of a clear 96 well plate were filled with 50 μ L of cell lysate for each triplicate sample of each condition. Next, 50 μ L of p-nitrophenyl phosphate was introduced as an alkaline phosphatase (ALP) substrate. Finally, mean velocities of the change of absorbance were calculated as relative ALP activity from a kinetic study that measured the change in absorbance of the solution at 405 nm over 10 min using a multi-mode, microplate reader (Synergy H1, Biotek®).

5.2.5 Phospho-CXCR4 Western Blot

To detect phosphorylation of CXCR4, MSCs were seeded at 7.5×10^4 cells mL^{-1} in 6 well plates and cultured overnight in 1% FBS low-glucose DMEM and then serum starved for 4 hrs. Cells were then dosed with either blank, 1000 ng mL^{-1} of SDF-1, or 1000 ng mL^{-1} of SH-SDF-1 in serum free low glucose DMEM for 5 min. Samples were rinsed once with PBS and lysed on ice with RIPA buffer (Thermo Scientific), 1X Complete protease inhibitor, and 1X PhosStop phosphatase inhibitor (Roche). Lysate was collected and centrifuged at 14,000 RPM for 10 min at 4°C. The protein concentration was determined by the micro BCA Protein Assay Kit (Pierce, Thermo Scientific). At least 18 μ g of total protein was loaded into each lane of a 10% Bis-Tris NuPAGE precast gel (Life Technologies) and electroblotted onto a PVDF membrane (Bio-Rad Laboratories, Inc.), blocked with 5% bovine serum albumin (BSA, Sigma-Aldrich) in tris-buffered saline in 0.05% Tween 20 (Sigma-Aldrich) (TBST). CXCR4 was probed with specific antibodies (1:1000 Anti-CXCR4 (pSer339) or 1:1000 Anti-CXCR4, Assay Biotech), and GAPDH (1:1000, Cell Signaling Technologies) was used as a loading control. To probe for

GAPDH, CXCR4 antibodies were stripped from the PVDF membrane using the Restore Western Blot Stripping Buffer (Pierce, Thermo Scientific) for 20 minutes at room temperature, two 10 min washes, followed by GAPDH immunoblotting. Proteins were detected using donkey anti-rabbit horseradish peroxidase-conjugated antibodies (1:5000, Jackson ImmunoResearch) and SuperSignal West Dura (Pierce, Thermo Scientific). Western blots were visualized with a GE ImageQuant LAS 4000 and quantified using ImageJ.

5.2.6 Rat Calvarial Bone Defect Model

All work performed with animals was done with the approval and guidance of the University of Colorado Denver IACUC. Eight ten-week old male Sprague-Dawley rats were anesthetized by intraperitoneal injection of ketamine hydrochloride (40 mg/kg) and xylazine (10 mg/kg). The hair covering the top of the head was shaved and an incision was made along the sagittal suture. The periosteum was elevated from the skull, and two 5 mm circular calvarial defects were created with a 4 mm coarse diamond burr (Stryker). The defect was then filled with pre-polymerized hydrogel discs. The periosteum and skin was then closed over the defects with resorbable sutures. Animals were sacrificed after 4 weeks and tissue samples were sectioned and stained using Masson's Trichrome as previously described [7]. Histological scoring was performed by two independent and blind groups who were shown 8X magnification images and assessed total cellularity on a scale of 0 (low cellularity), 1 (medium cellularity), 2 (high cellularity). Images from both the edge of the bone defect and in the middle of the bone defect were randomly presented. Histological scores were averaged for the different conditions and each bone defect regions and plotted as mean \pm standard deviation. Micro-Computed Tomography (microCT) was used to assess bone formation at 0 and 4-week time points. Each

animal was scanned within 4 days of the initial surgery to establish the original defect area and then at week 4 to assess new bone formation within that area. MicroCT analysis of tissue mineralization was completed as previously described [7], and the mean percentage of bone closure after 4 weeks for each condition was plotted.

5.2.7 Statistical Analysis

A one-way analysis of variance (ANOVA) and post hoc comparisons with Tukey's test ($\alpha = 0.05$) or t-tests in Prism 5 (GraphPad) were performed when applicable on all data sets to determine statistical significance unless otherwise noted.

5.3 Results and Discussion

5.3.1 MSC attach and migrate within peptide-functionalized hydrogels

PEG hydrogels synthesized via a thiol-ene photo-click polymerization lead to versatile scaffolds that can be readily functionalized with biomolecules to recapitulate key aspects of the ECM (e.g., cell adhesive sites, enzymatically-degradable matrix). Here, we synthesized gels with a pendant adhesive peptide, CRGDS, and a matrix metalloproteinase degradable peptide, KCGPQG↓IWGQCK, to facilitate MSC attachment and migration (Figure 1A) [8]. Figure 1B shows a Brightfield image of MSCs migrating in a typical gel, over a 6 hour culture period; x-y cell tracks are highlighted by individual colored lines. Basal migration markers were quantified, including speeds of $18 \pm 1 \mu\text{m h}^{-1}$, persistence values of $156 \pm 24 \text{ min}$, and a mean free path of $48 \pm 9 \mu\text{m}$. These were observed and quantified through modeling MSC migration as a persistent random walk. As thiol-ene matrices support local MSC remodeling, we next sought to direct basal MSC migration and invasion through the introduction of a chemotactic cue, SDF-1.

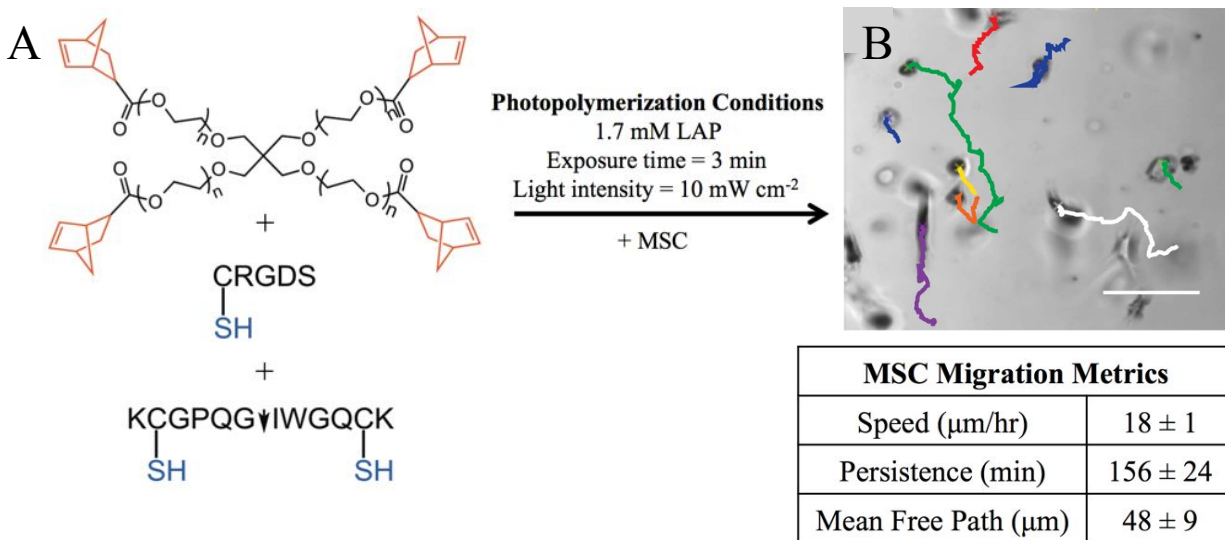


Figure 5.1 MSC attach, migrate three-dimensionally, and remain viable within peptide-functionalized thiol-ene hydrogels. A) Four-arm PEG Norbornene (M_n 20,000, 3 mM) is photopolymerized with a di-thiol MMP-degradable peptide (thiol:ene = 0.65:1) and mono-thiol adhesion peptide (1 mM) with 1.7 mM LAP and 3 minutes of 10 mW cm⁻². B) MSC were encapsulated within the hydrogel and cultured for 24 hours. Live-cell videomicroscopy was performed and cell movement was tracked over a 6-hour period. Mean-squared displacements for individual cells were then modeled with a persistent random walk to elucidate important migration metrics. The mean cell speed for 3D MSC migration was 18 ± 1 , the persistence was found to be 156 ± 24 , and a mean free path of 48 ± 9 . Mean \pm S.E.

5.3.2 Functionalization of SDF-1

The thiol-ene reaction mechanism provides a robust method to conjugate thiol-containing biomacromolecules (e.g., peptides, proteins) into hydrogels with pendant -ene functionalities. To immobilize SDF-1, the protein was thiolated using a commercially available Traut's reagent that converts primary amine moieties found on lysine residues or at the protein N-terminus into free thiols. For SDF-1, there are nine lysines sites that could be modified, and after reaction, results show incorporation of 2.7 ± 0.2 thiols per molecule (Figure 2A). However, it is important to note that the extent of thiolation is always a balance between the desire for high levels of conjugation to the hydrogel and not introducing modifications at a key protein binding sites. To

ensure that thiolation of SDF-1 did not significantly disrupt the structure of the protein, an ELISA was performed to verify that a primary antibody could still recognize and bind to SH-SDF-1 (Figure 2B). Results show a slightly reduced level of binding, 0.65 ± 0.02 relative to SDF-1. This likely indicates that small structural changes occur to the proteins during the modification step, especially at this level of thiolation, but a majority of the SDF-1 still retains its structure and is recognized by a binding epitope.

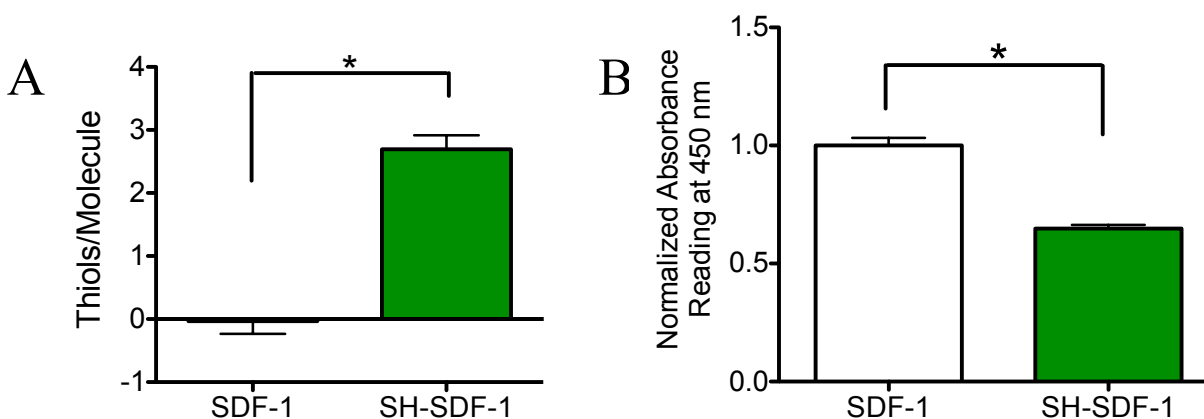


Figure 5.2 SDF-1 Thiolation and antibody recognition. A) The concentration of thiols per SDF-1 and SH-SDF-1 was measured using the commercially available Measure-IT™ Thiol Assay Kit (Life Technologies). SDF-1 had no free thiols present before modification, but SH-SDF-1 was found to have 2.7 ± 0.2 thiols/molecule. B) An ELISA was performed to determine recognition of SH-SDF-1 by a primary antibody. Absorbance values were normalized to the native protein, SDF-1. The SH-SDF-1 protein was 0.65 ± 0.02 relative to the unmodified SDF-1, indicating that the modified SH-SDF-1 is recognized by the primary antibody, but at a reduced level. Mean \pm S.D. * $p < 0.05$

5.3.3 Bioactivity and Immobilization of SH-SDF-1

Along with characterizing the protein structure, it is imperative to ensure that modified proteins retains bioactivity and can signal to cells when immobilized in a hydrogel environment. SDF-1 interacts with the chemokine receptor CXCR4 through inducing a phosphorylation event that initiates subsequent downstream effects [49]. CXCR4 is present on MSC to varying extents [22], so to test the bioactivity of SH-SDF-1, MSC were dosed with SH-SDF-1 and SDF-1 and levels of phosphorylation of the CXCR4 receptor measured by western blot (Figure 3). In this analysis, phosphorylated-CXCR4 was normalized to total CXCR4 expression levels. The modified, SH-SDF-1 had an elevated value of phosphorylation, a 1.22-fold increase, over the blank control that was not dosed with SDF-1. For comparison, unmodified SDF-1 had a 1.45-fold increase over the control. Collectively, these results indicate loss of SDF activity with modification, but a significant fraction can still signal to cells and induce a phosphorylation event on CXCR4.



	Blank	SDF	SH-SDF
phospho CXCR4			
total CXCR4			
Phospho/Total	1.00	1.45	1.22

Figure 5.3 SH-SDF-1 retains bioactivity post-modification. To detect SH-SDF-1 bioactivity, a western blot was performed to measure the elevated levels of phospho-CXCR4 on MSC after dosing with SDF-1 and SH-SDF-1. Phospho-CXCR4 was normalized to total levels of CXCR4 and a fold-increase of 1.22 was found for SH-SDF-1, and a fold-increase of 1.45 was found after dosing with SDF-1.

Since the modified SH-SDF-1 retained high levels of its structure and bioactivity, the protein was incorporated into hydrogels at a concentration of 1000 ng mL^{-1} via a thiol-ene solution polymerization. Covalent immobilization into the hydrogel network was confirmed by a modified hydrogel-section ELISA. Specifically, $20 \text{ }\mu\text{m}$ cryosections of functionalized hydrogels were prepared, and the SDF-1 content quantified using an indirect ELISA. Results confirm that $86 \pm 10\%$ of the SH-SDF-1 present in the initial solution was covalently bound to the hydrogel network. Overall, this demonstrates that thiol modification of primary amine-containing proteins provides a simple, but versatile protocol to immobilize proteins at biologically relevant concentrations, while maintaining activity, using thiol-ene reaction mechanisms. The resulting protein-functionalized hydrogels allow one to recapitulate facets of the contextual presentation of ECM-sequestered proteins *in vivo*, and we posit that this approach will allow signaling to endogenous cells and promote wound healing *in vivo*. More specifically, protein-immobilization in bioscaffolds provides opportunities to introduce proteins in a local manner and sustain their presentation at physiologically relevant concentrations.

5.3.4 Assessing SDF-1 functionalized hydrogels and the ability to promote cell infiltration *in vivo*

To test whether or not immobilized SH-SDF-1 could locally signal and influence cellularity *in vivo*, hydrogels with SDF-1 entrapped or with locally immobilized SH-SDF-1 were implanted into a critical-sized bone defect created in the rat calvarium. Specifically, a hydrogel formulation was selected that was crosslinked with a proteolytically degradable crosslinker (KCGPQG↓IWGQCK) and modified with 1 mM of CRGDS; this formulation was previously demonstrated to support high levels of MSC motility[8]. The gels were then modified by either

entrapment of 10 ng mL⁻¹ of SDF-1 (soluble delivery) or 10 ng mL⁻¹ of SH-SDF-1 that was locally conjugated to the matrix. Figure 4A shows a top-down axial microCT scan of a rat skull one week post-transplantation, where gray represents mineralized tissue and red represents absence of a threshold of mineralization. Figure 4A illustrates the size and location of the two surgically created defects where the hydrogels were implanted. After four weeks, the animals were sacrificed and the skulls were sectioned and stained with Masson's Trichrome to visualize tissue regeneration in the bone defect regions (Figure 4B). Black arrows demarcate the approximate locations of the original wound margins, and the region between the arrows highlights the new tissue growth. Initial observations reveal a striking pattern of increased cellularity within the defect regions for treatments with the immobilized SH-SDF relative to the entrapped SDF. As a first approach to quantify this, a histological scoring of cellularity was performed by independent and blinded observers. The cellularity of two regions of the defects, the edge and middle of the bone defects, were scored on a scale of 0 to 2: 0 (low cellularity), 1 (medium cellularity), or 2 (high cellularity). An increase in cellularity was observed in the middle of defects treated with localized SH-SDF-1 relative to entrapped SDF-1 treatment with histological scores of 1.3 ± 0.3 and 0.5 ± 0.7 , respectively. Complementary, scoring of at the edge of the defects revealed a similar pattern as immobilized SH-SDF-1 treatments scored a 1.3 ± 0.6 while the soluble delivered only scored 0.3 ± 0.6 . These results suggest that localized delivery of SH-SDF-1 retains high levels of bioactivity *in vivo* and more effectively induces cellular invasion into the defect site relative to soluble and entrapped SDF-1 delivery.

These results support the hypothesis that local and sustained presentation of SH-SDF-1 more effectively recruits cells over a longer time period contrary to entrapment of unmodified SDF-1 (MW = 8 kDa), that can readily diffuse away from the hydrogel due to its low molecular

weight. Interestingly, it also suggests that contextual presentation of proteins (e.g., soluble, immobilized) has a significant effect on directing cell behavior *in vivo*; however, we acknowledge that Masson's Trichrome limited some of the visualization and quantification of the cellularity of a tissue. Current studies will address this issue by staining with hematoxylin and eosin along with appropriate image processing to better quantify the number of invaded cells into the defect areas as a function of the treatment condition.

Interestingly, despite the observed increase in cellularity at the defect sites, complementary microCT scans (Figure 8) showed limited mineralized tissue formation, with only 10-20% closure of the defect after 4 weeks. Therefore, though SDF-1 immobilization positively influenced cellular infiltration and colonization, the lack of mineralized tissue suggest that other osteoinductive signals may be required and motivated the design of multifunctional protein gels.

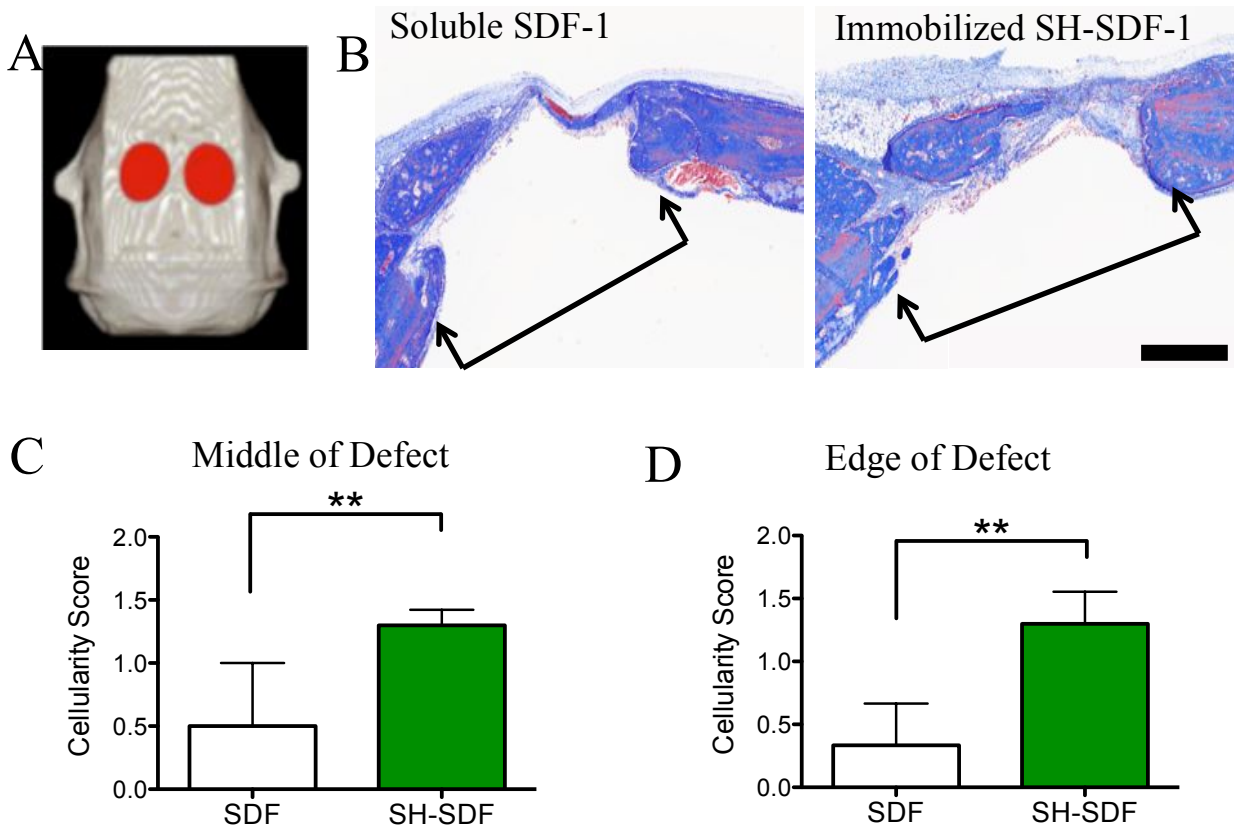


Figure 5.4 Covalently immobilized SH-SDF increases cellular invasion in rat calvarial defects. Two 5 mm critical sized defects were created on the top of a rat cranium and thiol-ene hydrogels with either 10 ng/mL of soluble SDF-1 entrapped or 10 ng/mL of immobilized SH-SDF-1 were introduced into the newly formed defects. A) MicroCT scans were performed two days after the surgeries. A representative image is shown above, where the red areas denote regions where the levels of optical density did not meet the threshold consistent with bone. B) Representative images of Masson's Trichrome stain are shown where the edges of the original defect area are marked by black arrows. Qualitatively, increased cellularity was observed in conditions with immobilized SH-SDF-1. C) Histological scoring of the cellularity within the middle of the defect sections was performed by independent and blind observers, where 0 is low cellularity, 1 is medium cellularity, and 2 is high cellularity. SH-SDF-1 was observed to have a significantly higher mean score of 1.3 ± 0.3 , relative to soluble SDF-1 with a score of 0.5 ± 0.7 . D) Similar scoring was performed on the edge of the defect, where again the immobilized SH-SDF-1 had a higher score of 1.3 ± 0.6 relative to soluble SDF-1 with a score of 0.3 ± 0.6 . mean \pm S.D. ** $p < 0.01$

5.3.5 BMP-2 Thiolation and conjugation into thiol-ene hydrogels

Bone morphogenetic protein 2 (BMP-2) is a potent osteoinductive factor that is known to promote bone regeneration in humans [50]. Based on these findings, thiol-ene hydrogels were modified with BMP-2 in an effort to influence osteogenic properties of colonized cell populations and promote mineralized tissue formation. BMP-2 plays a critical role in the early stages of the bone healing cascade, and is routinely used as a potent osteogenic cue for differentiating MSC [30]. BMP-2, which contains 15 lysine moieties, was thiolated using Traut's reagent and in a similar manner as the SDF-1 modification; results revealed the introduction of 0.84 ± 0.02 free thiols per molecule (Figure 5A). While this modification was a lower conversion than that for SDF-1, the ELISA protocol showed that antibodies bound the SH-BMP-2 in a manner that was statistically indistinguishable from unmodified BMP-2.

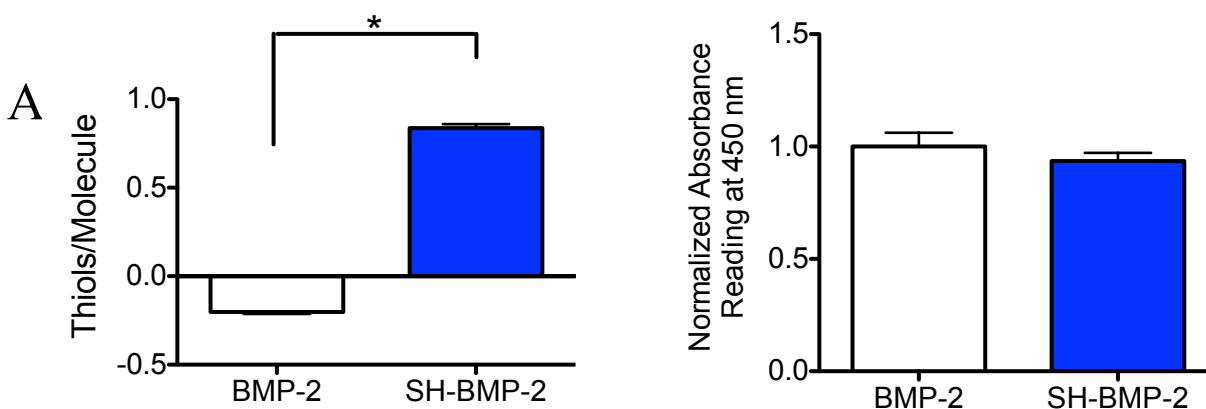


Figure 5.5 BMP-2 thiolation and antibody recognition. A) After modification, the concentration of free thiols per BMP-2 molecule was measured through fluorescent labeling and quantification of the fluorescent signal. It was found that SH-BMP-2 had 0.84 ± 0.02 thiols per molecule, and BMP-2 was found to contain no free thiols. B) Primary antibody recognition was measured by ELISA and no difference was observed for SH-BMP-2 (0.94 ± 0.06) and non-thiolated BMP-2 (1.00 ± 0.10). Mean \pm S.D. * $p < 0.05$

To confirm BMP-2 immobilization into thiol-ene hydrogels at desired doses, a hydrogel-section ELISA was performed on gels synthesized with $12 \mu\text{g mL}^{-1}$ and $24 \mu\text{g mL}^{-1}$ of SH-BMP-2. It was found that the SH-BMP-2 at lower efficiencies than the SH-SDF-1, at 49% ($12 \mu\text{g mL}^{-1}$) and 76% ($24 \mu\text{g mL}^{-1}$), which is thought to be due to the decreased extent of thiolation of BMP-2. Despite the decreased efficiencies, these results still show that the concentration of immobilized SH-BMP-2 can be user-defined based on initial loading of the protein to the pre-polymerized solution.

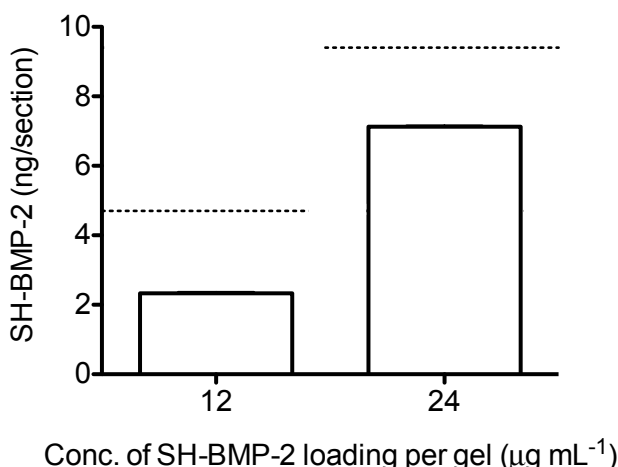


Figure 5.6 Tunable immobilization of BMP-2 within thiol-ene hydrogels Thiolated BMP-2 was incorporated into the hydrogels via a thiol-ene solution photopolymerization at concentrations of $12 \mu\text{g mL}^{-1}$ and $24 \mu\text{g mL}^{-1}$ and a modified section ELISA was performed. For the $12 \mu\text{g mL}^{-1}$ hydrogels, 2.33 ± 0.03 ng/section was found or 49% of the initially loaded SH-BMP-2. For the $24 \mu\text{g mL}^{-1}$, 7.13 ± 0.02 ng/section was found or 76% of the initial loading. Dashed lines represent initial loading concentrations. Mean \pm S.D. $p < 0.05$

5.3.6 BMP-2 bioactivity and cell signaling in thiol-ene hydrogels

Multiple *in vitro* assays were performed to ensure that BMP-2 activity was retained both when in solution and when covalently immobilized to hydrogel networks. First, a C2C12 reporter cell line developed by the Rifkin lab was used that produces luciferase in the presence of

active BMP-2 [51]. On both TCPS and when immobilized into a hydrogel, the SH-BMP-2 was found to retain a high level of bioactivity at multiple concentrations as indicated by luciferase production of the cell line (Supplemental Figure 5.S1A-B). These results support the notion that SH-BMP-2 structure and bioactivity are conserved when conjugated to PEG gels through the thiol-ene mechanism, and that the cytokine can still signal to local cells when immobilized.

As further evidence of the biofunctionality of the BMP-2 modified thiol-ene gels, MSCs were encapsulated in enzymatically degradable formulations, with or without BMP-2. Further, the BMP-2 was presented as an entrapped, diffusible signal or as an immobilized signal that is only released upon cell-mediated gel degradation. In all experiments, the BMP-2 dose was 1000 ng/mL. Alkaline phosphatase activity, an early marker for osteogenesis, was measured in each of the different conditions. The immobilized SH-BMP-2 induced a 3.54 ± 0.71 fold increase in ALP activity relative to the control condition (Figure 7). The soluble BMP-2 had the highest relative ALP activity, but was only slightly higher than the immobilized dose with a fold increase of 4.72 ± 0.04 . In summary, BMP-2 was thiolated in a manner that retained critical aspects of the protein structure and bioactivity post-modification, and when immobilized into PEG hydrogel via thiol-ene conjugation, the local BMP-2 signaled to MSCs by increasing the ALP marker of osteogenic differentiation.

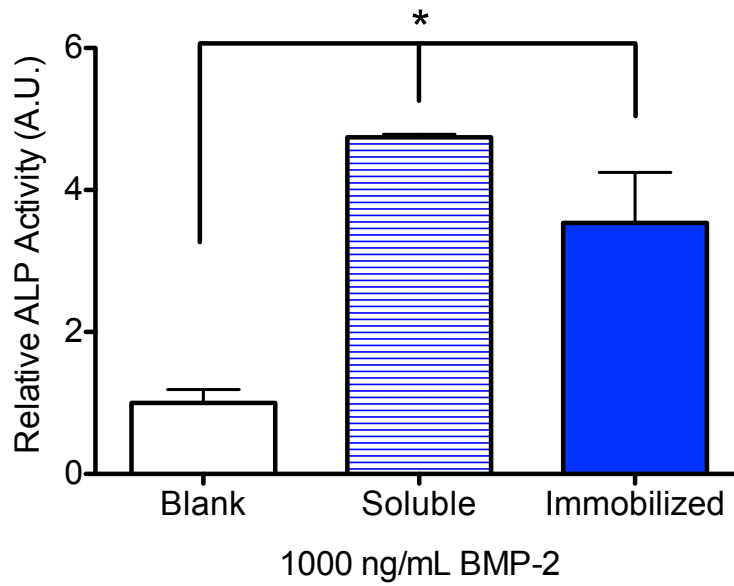


Figure 5.7 Covalently immobilized SH-BMP-2 retains bioactivity and directs MSC osteogenesis. MSC were encapsulated within thiol-ene hydrogels with 1) no BMP-2 (Blank), 2) 1000 ng/mL of soluble BMP-2 (Soluble) or 3) 1000 ng/mL of SH-BMP-2 immobilized to the hydrogel scaffold (Immobilized) delivered to the cells at the start of culture time. Alkaline phosphatase levels were measured after 3 days of culture and plotted relative to the blank control (1.00 ± 0.19). Soluble BMP-2 induced a relative ALP activity of 4.74 ± 0.04 , while immobilized BMP-2 still retained bioactivity with a relative ALP activity reading of 3.54 ± 0.71 . plotted: mean \pm S.D. * $p < 0.05$

5.3.7 Multifunctional thiol-ene hydrogels and the effect of combined protein presentation on bone regeneration

To investigate how immobilized proteins might simultaneously direct invasion (SH-SDF-1) and subsequently direct cell function of the colonized cells to increase mineralization (SH-BMP-2), hydrogels were introduced into critical sized rat calvarial defects. Hydrogels containing 1) entrapped SDF-1 (10 ng mL^{-1}), 2) immobilized SH-SDF-1 (10 ng mL^{-1}), 3) SH-BMP-2 (1000 ng mL^{-1}), and 4) co-delivery of immobilized SH-SDF-1 (10 ng mL^{-1}) and SH-BMP-2 (1000 ng mL^{-1}) were introduced at the time of surgery into the defect site and bone

regeneration was monitored over 4 weeks. At week 4, the animals were sacrificed and microCT scans were performed to measure mineralized bone formation in the defect regions. Figure 8A shows a top-down axial view of representative microCT scans for the four different conditions tested. The gray regions of the image are mineralized tissues that are above the optical density threshold of bone, where the red regions do not meet this threshold. The percent of closure of the original defect over the 4 weeks can be quantified from the microCT images and is presented in Figure 8B. Although not significant ($\alpha = 0.05$), the SH-BMP-2 condition showed the highest level of mineralized tissue in the original defect area. Contrary to our original hypothesis, the combination of both the SH-SDF-1 and SH-BMP-2 showed lower mineralization with only $21 \pm 20\%$ defect closure. Recent literature has begun to investigate the co-delivery of these two proteins in soluble form to bone defects. For example, work by Jin *et al.* utilized non-crosslinked collagen membrane to deliver soluble SDF-1 and BMP to critical-sized defects but did not observe an increase in bone formation when both proteins were delivered relative to simply BMP being delivered [46]. However, Hosagane *et al.* explored how soluble presentation of SDF-1 played a positive regulatory role *in vitro* on BMP-2 stimulation of osteogenesis in mesenchymal stem cells cultured on tissue culture polystyrene [52]. Complementary work has also highlighted the use of the β isoform of SDF-1 that has an increased vascular half-life due to four additional amino acids found on the C-terminus [53]. Herberg *et al.* delivered soluble SDF-1 β and BMP-2 entrapped within collagen sponges to critical sized rat calvarial defects and showed increased bone mineral density when 1 - 60 μg of SDF-1 β was co-delivered with 0.5 μg of BMP-2; however, this was only seen for conditions with doses of BMP-2 that were too low to induce bone formation on their own [54]. Although promising, this still underlines the need for supra-physiologic protein doses to direct only limited bone growth with soluble protein cues.

Collectively, these results motivate future studies that investigate the interplay between SDF-1 and BMP-2 in bone healing systems *in vivo*, and provide guidance to inform the design of important *in vitro* experiments that focus on dose and localized presentation of these proteins. Additionally, week 4 is an early time point to look at mineralized tissue formation, therefore future studies should be performed for longer time frames (e.g., 8 – 10 weeks) to allow more time for mineralization to occur to distinguish the long term effects of protein incorporation and delivery. It is hypothesized that more pronounced differences would occur between conditions at these longer time points and further reduce the variability within each condition.

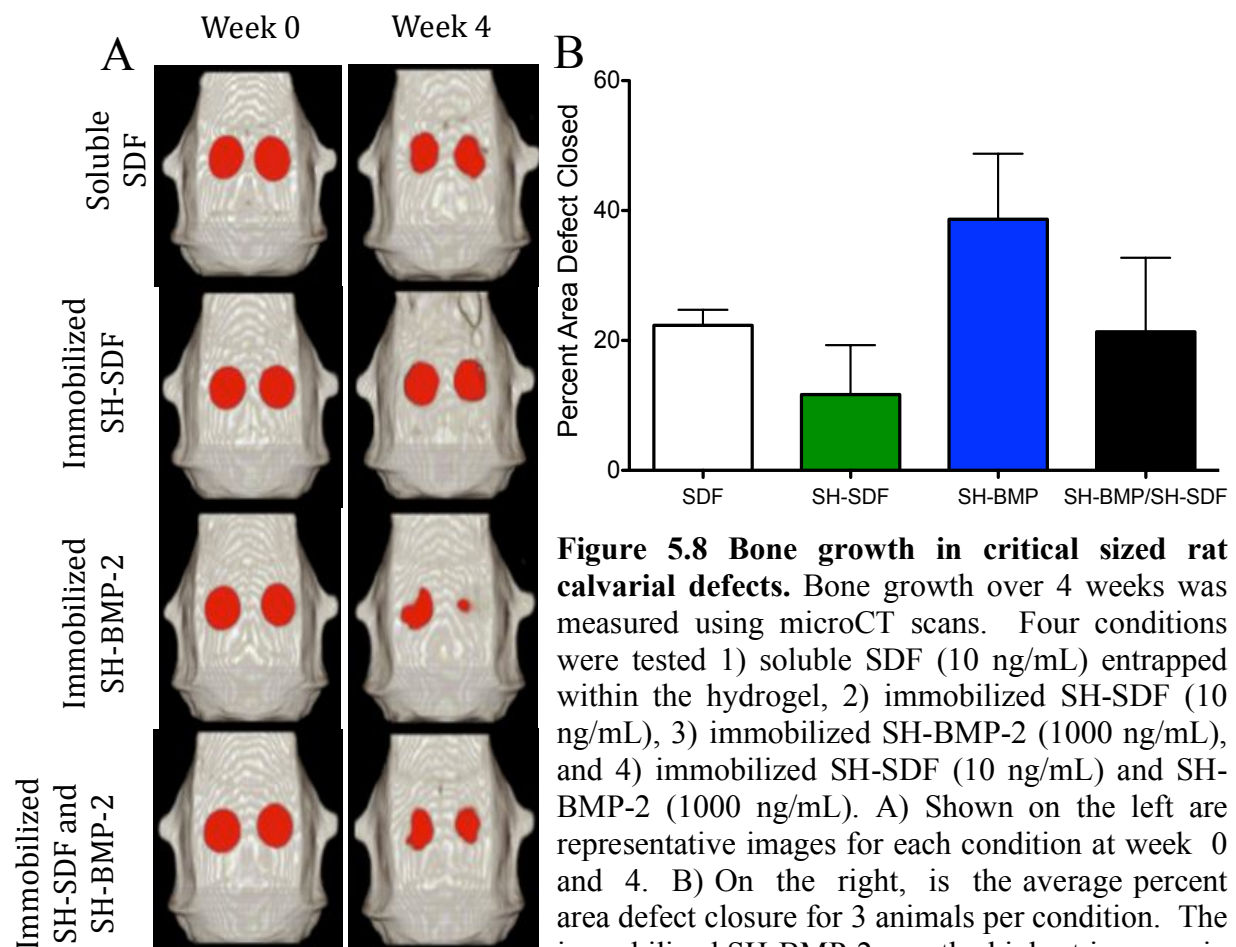


Figure 5.8 Bone growth in critical sized rat calvarial defects. Bone growth over 4 weeks was measured using microCT scans. Four conditions were tested 1) soluble SDF (10 ng/mL) entrapped within the hydrogel, 2) immobilized SH-SDF (10 ng/mL), 3) immobilized SH-BMP-2 (1000 ng/mL), and 4) immobilized SH-SDF (10 ng/mL) and SH-BMP-2 (1000 ng/mL). A) Shown on the left are representative images for each condition at week 0 and 4. B) On the right, is the average percent area defect closure for 3 animals per condition. The immobilized SH-BMP-2 saw the highest increase in bone fracture healing over the four-week period relative to the other conditions. mean \pm S.D.

5.4 Conclusions

Thiol-ene hydrogels provide a versatile platform to deliver immobilized biomolecules through bioconjugation to the network. Immobilization of biomolecules provides an effective delivery method of physiologically relevant concentrations of proteins in a localized manner. In this work, SDF-1 and BMP-2 were incorporated into thiol-ene hydrogels to study their effect on bone regeneration *in vivo* as SDF-1 is known to recruit cells to injury sites and BMP-2 is known to be a potent osteogenic cue for MSC. SH-SDF-1 was shown to be effectively modified with free-thiol moieties, retain structure and bioactivity *in vitro* and be effectively immobilized into the thiol-ene networks. Further, when introduced into a critical sized rat calvarial defect, the SH-SDF-1 appeared to increase cellular invasion into the network relative to simply delivering soluble SDF-1. This highlights the point that the contextual presentation of proteins plays a key role in the effectiveness of directing cell function.

BMP-2 was then chosen to direct mineralized tissue formation of the recruited and colonized cell populations found in the defect. It was also thiolated and found to retain both its structure and bioactivity *in vitro* through ELISA and a BMP-2 reporter cell line. Additionally, when immobilized into the hydrogel network SH-BMP-2 was found to upregulate alkaline phosphatase production in MSC, which is a key early marker of osteogenesis. However, limited mineralized tissue formation occurred when both SH-SDF-1 and SH-BMP-2 were immobilized into a hydrogel platform and introduced into the *in vivo* critical-sized defect model. Future investigations should elucidate the interplay between the localized concentration and co-delivery of SDF-1 and BMP-2 to aid in designing robust tissue engineering platforms for bone regeneration applications. This work outlines an effective method to immobilize key proteins to

direct cell function in a local and sustained manner, and to better engineer effective platforms to recruit and direct cell function in the complex *in vivo* environment.

5.5 Supplemental Information

5.5.1 Supplemental Materials and Methods

5.5.1.1 C2C12 Culture and BMP-2 Bioactivity Assay

The C2C12 BMP-2 reporter cell line was generously donated by the Rifkin laboratory and their development is described in the following reference [51]. Cells were thawed and plated in low-glucose Dulbecco's modified Eagle's medium, 10% fetal bovine serum (FBS), 50 U ml⁻¹ each of penicillin and streptomycin, and 1 µg ml⁻¹ Fungizone antimycotic until ~70% confluency. C2C12s were then encapsulated within the hydrogel through introduction into the macromer solution before photopolymerization (method discussed above) or seeded on TCPS. BMP-2 or SH-BMP-2 was introduced either in the culture medium in soluble form or immobilized within the hydrogel. Cells were cultured for 24 hours and then the medium was aspirated off replaced with 40 µL of Glo lysis buffer. For hydrogel experiments, gels were moved into a 1.7 mL tube, broken apart using a vibrating pestle, and then the 40 µL of Glo lysis buffer was introduced. The plates or tubes were placed on a shaker for 20 min at room temperature, and then 30 µL of the cell lysate was moved into a flat bottom, white plate. Luciferin (100 µL) was then added into each well and incubated for 3 min. Finally, a luminescence assay was conducted with a Synergy H1 microplate reader (Biotek).

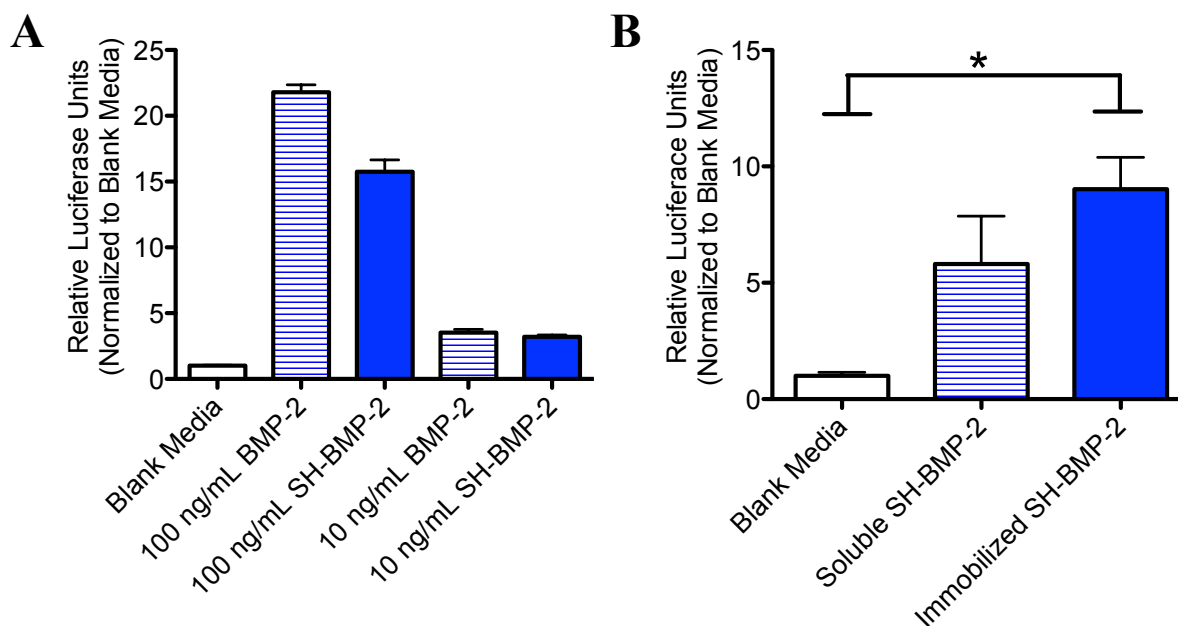


Figure 5.S1 SH-BMP-2 retains bioactivity. A) A C2C12 reporter cell line was dosed with two concentrations (100 ng mL^{-1} , 10 ng mL^{-1}) of BMP-2 and SH-BMP-2 on TCPS and luciferase production was normalized to the negative control. There was a slight decrease in luciferase production for the thiolated BMP-2 at 100 ng mL^{-1} , 21.8 ± 1.4 fold increase (BMP-2) vs. 15.8 ± 2.2 fold increase (SH-BMP-2); however, no decrease was seen at the lower concentration (10 ng mL^{-1}), 3.5 ± 0.6 (BMP-2) and 3.2 ± 0.3 (SH-BMP-2). This shows that SH-BMP-2 retains high levels of bioactivity. B) The C2C12s were then encapsulated within PEG hydrogels and treated with either soluble SH-BMP-2 or SH-BMP-2 to the network. After normalization to the negative control, the cells treated with the immobilized SH-BMP-2 had the highest levels of luciferase activity (9.0 ± 2.4 fold increase) relative to soluble delivery (5.8 ± 3.6 fold increase). Therefore, SH-BMP-2 retains bioactivity when immobilized to the PEG network. Mean \pm S.D. * $p < 0.05$

5.6 References

- [1] Tibbitt MW, Anseth KS. Hydrogels as extracellular matrix mimics for 3D cell culture. *Biotechnology and Bioengineering* 2009;103:655-63.
- [2] Discher DE, Mooney DJ, Zandstra PW. Growth Factors, Matrices, and Forces Combine and Control Stem Cells. *Science* 2009;324:1673-7.
- [3] Burdick JA, Murphy WL. Moving from static to dynamic complexity in hydrogel design. *Nature communications* 2012;3:1269.
- [4] Annabi N, Tamayol A, Uquillas JA, Akbari M, Bertassoni LE, Cha C, et al. 25th Anniversary Article: Rational Design and Applications of Hydrogels in Regenerative Medicine. *Adv Mater* 2014;26:85-124.
- [5] Azagarsamy MA, Anseth KS. Bioorthogonal Click Chemistry: An Indispensable Tool to Create Multifaceted Cell Culture Scaffolds. *ACS macro letters* 2013;2:5-9.
- [6] Hoyle CE, Bowman CN. Thiol-ene click chemistry. *Angewandte Chemie* 2010;49:1540-73.
- [7] Mariner PD, Wudel JM, Miller DE, Genova EE, Streubel SO, Anseth KS. Synthetic hydrogel scaffold is an effective vehicle for delivery of INFUSE (rhBMP2) to critical-sized calvaria bone defects in rats. *Journal of orthopaedic research : official publication of the Orthopaedic Research Society* 2013;31:401-6.
- [8] Kyburz KA, Anseth KS. Three-dimensional hMSC motility within peptide-functionalized PEG-based hydrogels of varying adhesivity and crosslinking density. *Acta biomaterialia* 2013;9:6381-92.
- [9] Schwartz MP, Fairbanks BD, Rogers RE, Rangarajan R, Zaman MH, Anseth KS. A synthetic strategy for mimicking the extracellular matrix provides new insight about tumor cell migration. *Integrative biology : quantitative biosciences from nano to macro* 2010;2:32-40.
- [10] Silva AKA, Richard C, Bessodes M, Scherman D, Merten OW. Growth Factor Delivery Approaches in Hydrogels. *Biomacromolecules* 2009;10:9-18.
- [11] Lee SH, Shin H. Matrices and scaffolds for delivery of bioactive molecules in bone and cartilage tissue engineering. *Adv Drug Deliver Rev* 2007;59:339-59.
- [12] Lin CC, Anseth KS. Controlling Affinity Binding with Peptide-Functionalized Poly(ethylene glycol) Hydrogels. *Adv Funct Mater* 2009;19:2325-31.
- [13] Lee SJ. Cytokine delivery and tissue engineering. *Yonsei medical journal* 2000;41:704-19.
- [14] Hoyle CE, Lowe AB, Bowman CN. Thiol-click chemistry: a multifaceted toolbox for small molecule and polymer synthesis. *Chemical Society reviews* 2010;39:1355-87.

- [15] Hume PS, He J, Haskins K, Anseth KS. Strategies to reduce dendritic cell activation through functional biomaterial design. *Biomaterials* 2012;33:3615-25.
- [16] McCall JD, Luoma JE, Anseth KS. Covalently tethered transforming growth factor beta in PEG hydrogels promotes chondrogenic differentiation of encapsulated human mesenchymal stem cells. *Drug delivery and translational research* 2012;2:305-12.
- [17] Mistry AS, Mikos AG. Tissue engineering strategies for bone regeneration. *Advances in biochemical engineering/biotechnology* 2005;94:1-22.
- [18] Caplan AI, Correa D. The MSC: an injury drugstore. *Cell Stem Cell* 2011;9:11-5.
- [19] Uccelli A, Moretta L, Pistoia V. Mesenchymal stem cells in health and disease. *Nature reviews Immunology* 2008;8:726-36.
- [20] Salem HK, Thiemermann C. Mesenchymal stromal cells: current understanding and clinical status. *Stem cells* 2010;28:585-96.
- [21] Ko IK, Lee SJ, Atala A, Yoo JJ. In situ tissue regeneration through host stem cell recruitment. *Experimental & molecular medicine* 2013;45:e57.
- [22] Karp JM, Teol GSL. Mesenchymal Stem Cell Homing: The Devil Is in the Details. *Cell Stem Cell* 2009;4:206-16.
- [23] Phinney DG, Prockop DJ. Concise review: mesenchymal stem/multipotent stromal cells: the state of transdifferentiation and modes of tissue repair--current views. *Stem cells* 2007;25:2896-902.
- [24] Yang C, Tibbitt MW, Basta L, Anseth KS. Mechanical memory and dosing influence stem cell fate. *Nature materials* 2014;13:645-52.
- [25] Gilbert PM, Havenstrite KL, Magnusson KE, Sacco A, Leonardi NA, Kraft P, et al. Substrate elasticity regulates skeletal muscle stem cell self-renewal in culture. *Science* 2010;329:1078-81.
- [26] Chen FM, Wu LA, Zhang M, Zhang R, Sun HH. Homing of endogenous stem/progenitor cells for in situ tissue regeneration: Promises, strategies, and translational perspectives. *Biomaterials* 2011;32:3189-209.
- [27] Vanden Berg-Foels WS. In situ tissue regeneration: chemoattractants for endogenous stem cell recruitment. *Tissue engineering Part B, Reviews* 2014;20:28-39.
- [28] Discher DE, Mooney DJ, Zandstra PW. Growth factors, matrices, and forces combine and control stem cells. *Science* 2009;324:1673-7.

- [29] Ji W, Yang F, Ma J, Bouma MJ, Boerman OC, Chen Z, et al. Incorporation of stromal cell-derived factor-1alpha in PCL/gelatin electrospun membranes for guided bone regeneration. *Biomaterials* 2013;34:735-45.
- [30] Tsiridis E, Upadhyay N, Giannoudis P. Molecular aspects of fracture healing: which are the important molecules? *Injury* 2007;38 Suppl 1:S11-25.
- [31] Kitaori T, Ito H, Schwarz EM, Tsutsumi R, Yoshitomi H, Oishi S, et al. Stromal cell-derived factor 1/CXCR4 signaling is critical for the recruitment of mesenchymal stem cells to the fracture site during skeletal repair in a mouse model. *Arthritis and rheumatism* 2009;60:813-23.
- [32] Ponte AL, Marais E, Gally N, Langonne A, Delorme B, Herault O, et al. The in vitro migration capacity of human bone marrow mesenchymal stem cells: comparison of chemokine and growth factor chemotactic activities. *Stem cells* 2007;25:1737-45.
- [33] Huang YC, Liu TJ. Mobilization of mesenchymal stem cells by stromal cell-derived factor-1 released from chitosan/tripolyphosphate/fucoidan nanoparticles. *Acta biomaterialia* 2012;8:1048-56.
- [34] He X, Ma J, Jabbari E. Migration of marrow stromal cells in response to sustained release of stromal-derived factor-1alpha from poly(lactide ethylene oxide fumarate) hydrogels. *International journal of pharmaceutics* 2010;390:107-16.
- [35] Thevenot PT, Nair AM, Shen J, Lotfi P, Ko CY, Tang L. The effect of incorporation of SDF-1alpha into PLGA scaffolds on stem cell recruitment and the inflammatory response. *Biomaterials* 2010;31:3997-4008.
- [36] Zlotnik A, Yoshie O. Chemokines: a new classification system and their role in immunity. *Immunity* 2000;12:121-7.
- [37] Ceradini DJ, Kulkarni AR, Callaghan MJ, Tepper OM, Bastidas N, Kleinman ME, et al. Progenitor cell trafficking is regulated by hypoxic gradients through HIF-1 induction of SDF-1. *Nature medicine* 2004;10:858-64.
- [38] Granero-Molto F, Weis JA, Miga MI, Landis B, Myers TJ, O'Rear L, et al. Regenerative effects of transplanted mesenchymal stem cells in fracture healing. *Stem cells* 2009;27:1887-98.
- [39] Purcell BP, Elser JA, Mu A, Margulies KB, Burdick JA. Synergistic effects of SDF-1alpha chemokine and hyaluronic acid release from degradable hydrogels on directing bone marrow derived cell homing to the myocardium. *Biomaterials* 2012;33:7849-57.
- [40] Urist MR. Bone: formation by autoinduction. *Science* 1965;150:893-9.
- [41] Seeherman H, Wozney JM. Delivery of bone morphogenetic proteins for orthopedic tissue regeneration. *Cytokine & growth factor reviews* 2005;16:329-45.

- [42] Yamamoto M, Takahashi Y, Tabata Y. Enhanced bone regeneration at a segmental bone defect by controlled release of bone morphogenetic protein-2 from a biodegradable hydrogel. *Tissue engineering* 2006;12:1305-11.
- [43] Osathanon T, Linnes ML, Rajachar RM, Ratner BD, Somerman MJ, Giachelli CM. Microporous nanofibrous fibrin-based scaffolds for bone tissue engineering. *Biomaterials* 2008;29:4091-9.
- [44] Saito N, Okada T, Horiuchi H, Ota H, Takahashi J, Murakami N, et al. Local bone formation by injection of recombinant human bone morphogenetic protein-2 contained in polymer carriers. *Bone* 2003;32:381-6.
- [45] Boyan BD, Lohmann CH, Somers A, Niederauer GG, Wozney JM, Dean DD, et al. Potential of porous poly-D,L-lactide-co-glycolide particles as a carrier for recombinant human bone morphogenetic protein-2 during osteoinduction in vivo. *Journal of biomedical materials research* 1999;46:51-9.
- [46] Jin Q, Giannobile WV. SDF-1 enhances wound healing of critical-sized calvarial defects beyond self-repair capacity. *PloS one* 2014;9:e97035.
- [47] Fairbanks BD, Schwartz MP, Bowman CN, Anseth KS. Photoinitiated polymerization of PEG-diacrylate with lithium phenyl-2,4,6-trimethylbenzoylphosphinate: polymerization rate and cytocompatibility. *Biomaterials* 2009;30:6702-7.
- [48] Sridhar BV, Doyle NR, Randolph MA, Anseth KS. Covalently tethered TGF-beta1 with encapsulated chondrocytes in a PEG hydrogel system enhances extracellular matrix production. *Journal of biomedical materials research Part A* 2014.
- [49] Teicher BA, Fricker SP. CXCL12 (SDF-1)/CXCR4 pathway in cancer. *Clinical cancer research : an official journal of the American Association for Cancer Research* 2010;16:2927-31.
- [50] Axelrad TW, Einhorn TA. Bone morphogenetic proteins in orthopaedic surgery. *Cytokine & growth factor reviews* 2009;20:481-8.
- [51] Zilberberg L, ten Dijke P, Sakai LY, Rifkin DB. A rapid and sensitive bioassay to measure bone morphogenetic protein activity. *BMC cell biology* 2007;8:41.
- [52] Hosogane N, Huang Z, Rawlins BA, Liu X, Boachie-Adjei O, Boskey AL, et al. Stromal derived factor-1 regulates bone morphogenetic protein 2-induced osteogenic differentiation of primary mesenchymal stem cells. *The international journal of biochemistry & cell biology* 2010;42:1132-41.
- [53] Herberg S, Fulzele S, Yang N, Shi X, Hess M, Periyasamy-Thandavan S, et al. Stromal cell-derived factor-1beta potentiates bone morphogenetic protein-2-stimulated osteoinduction of

genetically engineered bone marrow-derived mesenchymal stem cells in vitro. Tissue engineering Part A 2013;19:1-13.

[54] Herberg S, Susin C, Pelaez M, Howie RN, Moreno de Freitas R, Lee J, et al. Low-dose bone morphogenetic protein-2/stromal cell-derived factor-1beta cotherapy induces bone regeneration in critical-size rat calvarial defects. Tissue engineering Part A 2014;20:1444-53.

CHAPTER VI

PATTERNING MULTIPLE PROTEIN SIGNALS IN HYDROGELS UTILIZING BIOORTHOGONAL CLICK CHEMISTRIES

6.1 Introduction

Stem cells encounter a myriad of diverse and heterogeneous biochemical signals within their local microenvironment, and these extracellular signals direct many important functions (e.g., differentiation, migration, proliferation) [1, 2]. *In vivo*, many of these heterogeneous signals operate synergistically, and *in vitro* systems that allow one to study and understand these complex interactions would be beneficial. For example, elucidating specific and coordinated effects of protein signals on cells, especially in a context that is biomechanically relevant and spatially controlled in 3D, is a goal for the design of biomaterials scaffolds to promote tissue regeneration [3, 4]. However, fabrication of such material platforms necessitates versatile bioconjugation methods that are compatible with proteins, spatiotemporally controlled in 3D, and bioorthogonal. When conjugating proteins in 3D biomaterials systems, one often constrains chemical methods to those that are mild. For example, conjugation techniques that rely on radical chemistry must be careful of the reaction conditions, as radicals may damage the secondary structure of fragile proteins and render them bio-inactive [5, 6]. Further, 3D hydrogels systems often lead to long diffusion time scales for large proteins, so processes that use only a single step to conjugate multiple molecules are advantageous. Finally, when modifying cell-laden gels, the protein conjugation must often occur with a high degree of

specificity in a complex milieu of serum proteins.

Towards addressing some of these challenges, Pioneering work has demonstrated patterning of singular proteins in a defined manner [7, 8] or even multiple peptides [9]. For example, Deforest *et al.* used bioorthogonal chemistries to photoreversibly immobilize the extracellular matrix protein vitronectin within a cell-laden hydrogel. Mosiewicz *et al.* introduced a mild enzymatic conjugation approach that could spatially pattern a single protein and maintain bioactivity to direct cell migration [7]. Wylie *et al.* exploited physical binding interactions to achieve simultaneous immobilization of multiple proteins in distinct patterns [10]. However, there is a paucity of methods that are relevant for protein introduction, especially those that are simple to perform in 3D, specific in complex solutions (e.g., media), and allow spatiotemporal control — an aspect of the 4th dimension.

Building on this paradigm, we present a mild and simple chemical approach that uses multiple bio-click reactions to spatially define multiple protein cues simultaneously within a 3D hydrogel scaffold that is useful for cell culture. First, a photo-click reaction is used to covalently introduce multiple, pendant functional cues in a spatially controlled manner. In a second step, bioorthogonal click reactions are used to introduce proteins in the pre-patterned, templated regions to form high-throughput microarrays for 3D cell studies. We demonstrate application of these tools as a high throughput platform to study the cooperative effects of the osteogenic effector BMP-2 [11], chemokine SDF-1 [12, 13], and proliferative cue FGF-2 [14] over a broad experimental space on the expansion, differentiation, and migration of human mesenchymal stem cells (hMSCs). By precise control over spatial and dosing concentration, we aim to elucidate efficacious experimental conditions that can be translated into an *in vivo* bone regeneration model.

Specifically, a series of bioorthogonal click and light-based chemistries are utilized to pattern proteins simultaneously within an enzymatically degradable poly(ethylene glycol)-based hydrogel that was developed previously to culture hMSC with high viability and permit cell invasion and migration [15, 16]. Protein immobilization is achieved through two bioorthogonal click reactions: (i) copper-free, strain promoted azide alkyne cycloaddition (SPAAC) and (ii) inverse electron demand Diels-Alder reaction (IEDDA). Since these reactions are orthogonal to each other, it was envisaged that these reactions could be used to immobilize dual proteins simultaneously. A photoinitiated thiol-yne reaction is used to sequentially incorporate complementary moieties for each of the two bioorthogonal pairs (e.g., azide from SPAAC, tetrazine from IEDDA) in a spatiotemporal manner through the controlled illumination of gel regions with light [17, 18]. Additionally, the use of light enables user-control over the concentration of covalently functionalized molecules to the network thus tuning the total amount of protein immobilized in a given area. Finally, proteins tethered with a complimentary bioorthogonal pair (e.g., dibenzocyclooctyne (DBCO) from SPAAC, transcyclooctene (TCO) from IEDDA) are swelled into the hydrogel in cytocompatible media solutions and click with their complementary partner. This allows highly-defined spatial and dose patterning of proteins in mild, cytocompatible solutions to recapitulate key facets of the more complex organization and presentation of multiple cues within the *in vivo* cellular microenvironment.

As a demonstration of the method, we study the influence of multiple proteins on hMSC behavior *in vitro*. The ultimate goal is to elucidate important dosing and delivery regimes of proteins that might be used in concert to heal large bone defects. Here, we present BMP-2, SDF-1, and FGF-2 in a hydrogel system, and screen the effects of a broad range of concentrations and combinations on hMSC migration, proliferation, and differentiation. Experiments measure cell

invasion depth into the hydrogel system in real time, measure proliferation through EdU staining, and look at alkaline phosphatase staining to measure the differentiation of hMSC.

6.2 Materials and Methods

6.2.1 Gel Formulation and Synthesis

Azide-dithiol

To a solution of 5-azido pentanoic acid **1** (1.0 eq.) in DMF was added cystamine-hydrochloride (1.2 eq.) followed by triethylamine (2.0 eq.) and then the mixture was stirred for 10 mins. To the above mixture was added diisopropyl carbodiimide (DIC) (1.2 eq.) and dimethyl aminopyridine (DMAP) (0.2 eq.) at ice-bath temperature and the mixture was stirred at RT for 24 hrs. The reaction mixture was poured into water and extracted with ethyl acetate multiple times. The combined organic extracts were dried over sodium sulphate and the solvents were evaporated to concentration. The crude concentrate was then purified by silica gel column chromatography using ethyl acetate and hexane as mobile phase to obtain **1** as colorless powder (yield: 75%).

Tetrazine-dithiol

To a solution of tetrazine-PEG₁₂-carboxylic acid in DMF was added cystamine-hydrochloride (1.2 eq.) followed by triethylamine (2.0 eq.) and then the mixture was stirred for 10 mins. To the above mixture was added diisopropyl carbodiimide (DIC) (1.2 eq.) and dimethyl aminopyridine (DMAP) (0.2 eq.) at ice-bath temperature and the mixture was stirred at RT for 24 hrs. The above mixture was diluted with distilled water and dialyzed (using dialysis membrane with 500D M.wt cut-off) for 24 hrs replacing water 4 times to remove small

molecular reagents and unreacted starting material. The dialyzed solution was then lyophilized to obtain the disulphide containing tetrazine dimer (8 mg, yield: 65%).

Tetrazine-PEG-alkyne

To a solution of tetrazine-PEG₁₂-NHS ester (1.0 eq) in DMF was added NH₂PEG₄-alkyne (1.0 eq.) and the mixture was stirred at RT for 24 hrs. The above mixture was taken for hydrogel functionalization without any further purification.

Norbornene acid was conjugated to 4-arm PEG-hydroxyl (JenKem, USA) to yield 4-arm PEG-norbornene as previously described [15]. The peptide sequences KCGPQG↓IWGQCK and CRGDS were purchased from the American Peptide Company, reconstituted in deionized water, and frozen at -70°C until needed. Thiol-ene hydrogels were fabricated by combining 6 wt.% PEG-norbornene (3 mM, $f = 4$), a MMP-degradable peptide crosslinker (KCGPQG↓IWGQCK, 3.7 mM, $f = 2$) with an off-stoichiometric thiol to -ene ratio of 0.6-0.75, 1 mM CRGDS ($f = 1$), and 0.05% lithium phenyl-2,4,6-trimethylbenzoylphosphinate (LAP) [19]. The pre-polymerized solutions were photopolymerized using 365 nm light at 2 mW cm⁻² for 3 min (Figure 6.1A). Hydrogels were then swollen in PBS for 2 hrs, and then reacted with 200 μ L of 5 mM tetrazine-PEG-alkyne for 24 hours to modify the pendant un-reacted norbornenes present in the hydrogel (Figure 6.1B). After the reaction, the hydrogel is washed 3 times in PBS for 2 hours to remove any unreacted tetrazine-PEG₄-alkyne.

6.2.2 DLP patterning and quantification

Alkyne-functionalized hydrogels are photopatterned using dynamic light projection (DLP). First, hydrogels are swollen in a 200 μ L solution of either 5 mM azide-dithiol or 5 mM

tetrazine-dithiol, along with 5 mM TCEP and 0.05 wt% LAP in DI water for 2 hrs (Figure 6.1C). For cellular experiments 2 mM CRGDS is added to the patterning solution. The DLP is utilized with a 4x objective to shine 405 nm light in a 3.88 x 2.18 mm region with a pixel size of 4.5 μm and at specific exposure times defined by the grayscale value of an uploaded image created in illustrator. The total light exposure time is 40 s with an intensity of $\sim 40 \text{ mW cm}^{-2}$. After patterning, the gels are washed overnight in PBS with multiple solution changes. DBCO and TCO conjugated proteins are then swollen into the hydrogel in PBS or serum containing solutions and allowed to react for at least 4 hrs or overnight at 37°C. Finally, the gels are washed again in PBS for at least 4 hrs or overnight with multiple solution changes.

Rhodamine-labeled BSA (Sigma Aldrich) was purchased and functionalized with 35 molar equivalents of DBCO-NHS ester at 10 mg mL⁻¹ incubated on ice for 2 hrs. Similarly, fluorescein-labeled BSA (Sigma Aldrich) was labeled with TCO-NHS ester at 10 mg mL⁻¹ incubated on ice for 2 hrs. BMP-2 was functionalized with 35 molar eq. of DBCO-NHS ester at 1.5 mg mL⁻¹ incubated on ice for 2 hrs. The fluorescent BSA was swollen in as described above, and confocal images were taken of the patterns using an LSM 710 (Zeiss). Fluorescent intensity for the patterned regions was determined using the Zen Black (Zeiss) software. Fluorescent intensities were compared with known DBCO-BSA-rhodamine solutions swollen into similar hydrogels to determine patterned concentrations of immobilized proteins.

6.2.3 BMP-2 bioactivity assay

To ensure retention of DBCO-BMP-2 when immobilized into the network, alkaline phosphatase (ALP) staining was performed on seeded hMSC. Hydrogels were fabricated as discussed above, and 200 μL of 2 $\mu\text{g mL}^{-1}$ DBCO-BMP-2 in PBS is patterned into regions in the

hydrogels. Two conditions were created: with and without immobilized DBCO-BMP-2. hMSC were seeded at a concentration of 1×10^4 cells mL^{-1} and attached to regions where CRGDS was patterned. After 5 days of culture, hMSC were fixed in citrate buffered 60% acetone for 30 s. Following the manufacture protocol, ALP staining was performed using naphthol AS-MX phosphate and Fast Blue RR Salt based kit (85L1, Sigma-Aldrich). Brightfield images were taken of the two conditions to qualitatively compare ALP staining and activity for the two samples.

6.3 Results and Discussion

6.3.1 Bioorthogonal Reaction Scheme

Enzymatically degradable hydrogels were synthesized by reacting a 4-arm PEG-norbornene with the di-thiol peptide, KCGPQG ↓ IWGQCK, through a thiol-ene photopolymerization (Figure 6.1A). Next, the hydrogel was treated with tetrazine-PEG-alkyne to convert pendant norbornenes into alkyne moieties through inverse electron demand Diels-Alder (IEDDA). This enables photopatternability that is orthogonal to later reaction steps (Figure 6.1B). Then, sequential photoinitiated thiol-yne reactions were utilized to conjugate spatial patterns of pendant azides or pendant tetrazines (Figure 6.1C) and therefore permit subsequent bio-orthogonal conjugation of DBCO-labeled proteins (SPAAC) and TCO-labeled proteins (IEDDA) in a single step, respectively (Figure 6.1D). Dynamic light projection was exploited to control regions of illumination and the exposure time of light, which dictates the thiol-yne conjugation rate using the photoinitiator LAP. Once proteins were swollen into the hydrogel, these orthogonal bio-click moieties were covalently bound, and theoretically, the

reactions can occur even in the presence of cell-laden matrices with serum proteins and other cell-secreted proteins present.

With this outlined reaction scheme, critical control experiments were performed to determine the proper time scale for patterning, as well as the specificity of the bio-click reactions. Recently and somewhat unexpectedly, it was determined that the initial step of converting the pendant norbornene molecules within the hydrogel into alkynes was slower than anticipated. Methyl-tetrazine was chosen as the functional group as it known to be highly stable in serum conditions (>90% still present after 10 hrs in fetal bovine serum), and the second order reaction rate is $820 \text{ M}^{-1} \text{ s}^{-1}$ at 37°C [20]. However, protein patterning experiments were unsuccessful, so a small molecule study of methyl-tetrazine and norbornene in solution was performed by monitoring the decrease of the methyl-tetrazine absorbance at 515 nm. These results indicated that the half-life of the methyl-tetrazine with norbornene molecules was ~ 13 hrs. This slow rate is hypothesized to be the cause of the dramatically reduced patterning efficiency of the IEDDA pair, as the thiolated-tetrazine being patterned through thiol-yne photoconjugation was likely competing with unreacted norbornenes present in the hydrogel. Current studies are underway to explore other potential pathways to convert the norbornenes to alkynes, most promising of these is a non-methylated tetrazine. This molecules has been reported in the literature as having a second order reaction rate with norbornenes of $26,000 \text{ M}^{-1} \text{ s}^{-1}$ at 37°C [20]. Despite some of the synthetic issues, patterning has been achieved using the SPAAC patterning reaction scheme; however, it is difficult to rule out its occurrence through the thiol-ene photoconjugation route. The following sections document results to date, but these side reactions must be considered when interpreting them.

Figure 6.1 Spatial patterning of multiple proteins using bioorthogonal chemistry A) 4-arm PEG-norbornene and MMP-degradable di-thiol peptide react by thiol-ene photopolymerization in the presence of the photoinitiator LAP. B) To enable photopatterning of the bioorthogonal reaction pairs, treatment of tetrazine-PEG-azide converts pendant norbornene moieties within the network into pendant alkynes. C) Using thiol-yne photoconjugation, azide moieties and tetrazine moieties can be sequentially patterned using DLP to spatially control light exposure within the 3D hydrogel. D) After the complementary binding pair is spatially immobilized, treatment of DBCO-labeled proteins and TCO-labeled proteins enables distinct 3D spatial patterning of multiple protein signals.

6.3.2 User-tunable spatial and concentration patterning of proteins

Utilizing photoconjugation techniques allows for user-defined spatial and concentrations of protein immobilization within hydrogel networks, and when combined with dynamic light projection (DLP) allows for patterning over multiple cellularly relevant length scales. To quantify the control over spatial protein immobilization, a 3x10 array was designed (Figure 2a) where each column of 3 squares had an increasing gray-scale value of 10% from the left-most column (10%) to the right-most column (100%). This gray-scale results in increasing light exposure with an effective intensity of approximately 40 mW cm^{-2} in these regions, and 405 nm light was selected. In this example, thiolated-azide was immobilized through the photo-initiated thiol-yne reaction using this pattern, and then, DBCO-BSA-rhodamine was introduced for complementary reaction with the azide. Figure 2B shows confocal microscopy images of the patterns of the fluorescent protein. Image analysis was used to quantify the protein concentration by comparison to hydrogels equilibrated in solutions with known protein concentrations [21]. Immobilized DBCO-BSA-rhodamine concentration was plotted as a function of exposure time, and a linear increase in concentration was found with exposure time, up to 40 s with protein immobilization of $61.4 \pm 3.8 \text{ } \mu\text{g mL}^{-1}$ per second of 40 mW cm^{-2} light exposure. These results demonstrate that through precise control of light exposure, the

concentration and spatial patterning of proteins can be controlled within the PEG-based hydrogel systems.

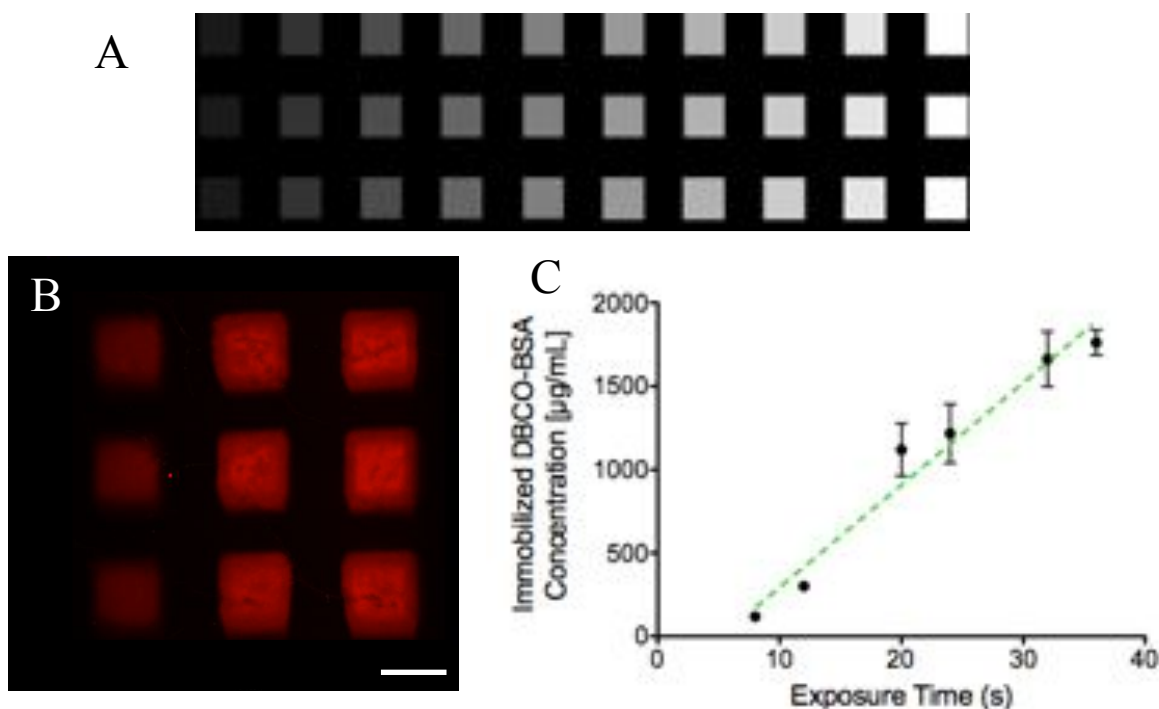


Figure 6.2 User-tuning of light dosage controls immobilized protein concentration. A) DLP was used to control the exposure time and regions of conjugation of the thiolated-azide. The pattern shown above creates a 3x10 array with increasing percentage (10%) of the 40 s light exposure time. B) Confocal microscopy was used to image and quantify protein immobilization. Shown here is a 10x image of the top view of the hydrogel of increasing light exposure from the left to right column of patterned squares of DBCO-BSA-rhodamine. Scale bar = 200 μm. C) Quantification of the level of fluorescence of each square in comparison to known standard samples allowed for the total immobilized protein to be quantified relative to exposure time. A linear increase in the amount of immobilized DBCO-BSA-rhodamine was measured over the 40 s exposure range.

6.3.3 Patterning of protein molecules within complex serum solutions

Cells are generally cultured in high concentration serum solutions, which are typically a complex milieu of ill-defined protein composition, to promote cell viability and function. Here, experiments were formed to test the specificity of the protein when serum is present and numerous other endogenous functionalities. Specifically, proteins were patterned by 405 nm

light for 40s with 75% effective intensity in the presence of 0%, 10%, and 100% fetal bovine serum solutions, and the resulting concentration of immobilized DBCO-BSA-rhodamine was quantified (Figure 3). Results are striking and show that the level of serum proteins in the patterning solution had no effect on the efficiency of the conjugation reaction. Additionally, the patterned protein showed high spatial fidelity in all three conditions mimicking the DLP pattern mask. Collectively, the SPAAC bio-click reaction provides a versatile technique to form protein-patterned hydrogels, allowing the introduction of exogenous proteins at controlled concentrations even in complex environments..

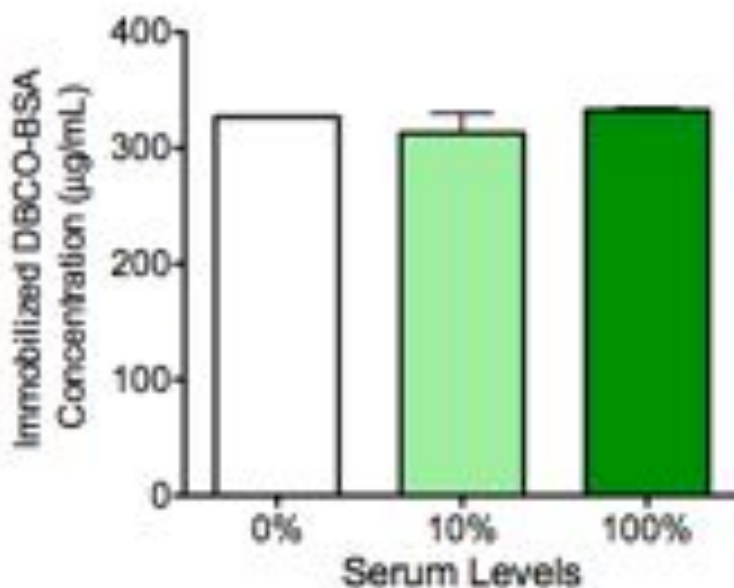


Figure 6.3 Patterning of proteins in the presence of complex serum solutions. Protein patterning was performed in gels equilibrated in 0%, 10% or 100% serum, and the concentration of gel-conjugated DBCO-BSA-rhodamine was quantified using fluorescence intensity. Patterning showed high fidelity in all three conditions without a reduction in immobilized protein.

6.3.4 Bioactivity of immobilized proteins

Beyond protein conjugation with spatial resolution, one must also ensure that the immobilized proteins retain their bioactivity and can signal to cells. To this end, BMP-2 was

modified with NHS-DBCO through reaction with primary amines present on the protein. The DBCO-BMP-2 was then immobilized within the network using the SPAAC patterning method, and CRGDS was patterned concurrently to promote hMSC viability and matrix interactions in the patterned regions. Hydrogels were patterned by exposure to 40s of 405 nm light with or without $2 \mu\text{g mL}^{-1}$ of DBCO-BMP-2, and hMSC were subsequently seeded on the gels. After 5 days, alkaline phosphatase activity was measured to detect if the immobilized DBCO-BMP-2 retained its bioactivity and could signal to hMSCs to induce osteogenesis. Figure 4 shows a bright field image of hMSCs fixed and stained for ALP activity (purple) in the presence (Fig. 4A) or absence (Fig 4B) of tethered BMP-2. ALP staining was much stronger in the presence of the DBCO-BMP-2, which is apparent from the much darker and robust purple staining of the hMSCs. This preliminary result demonstrates that immobilized proteins, specifically BMP-2, maintain some level of biological activity and ability to signal to hMSCs, such as influencing osteogenic differentiation.

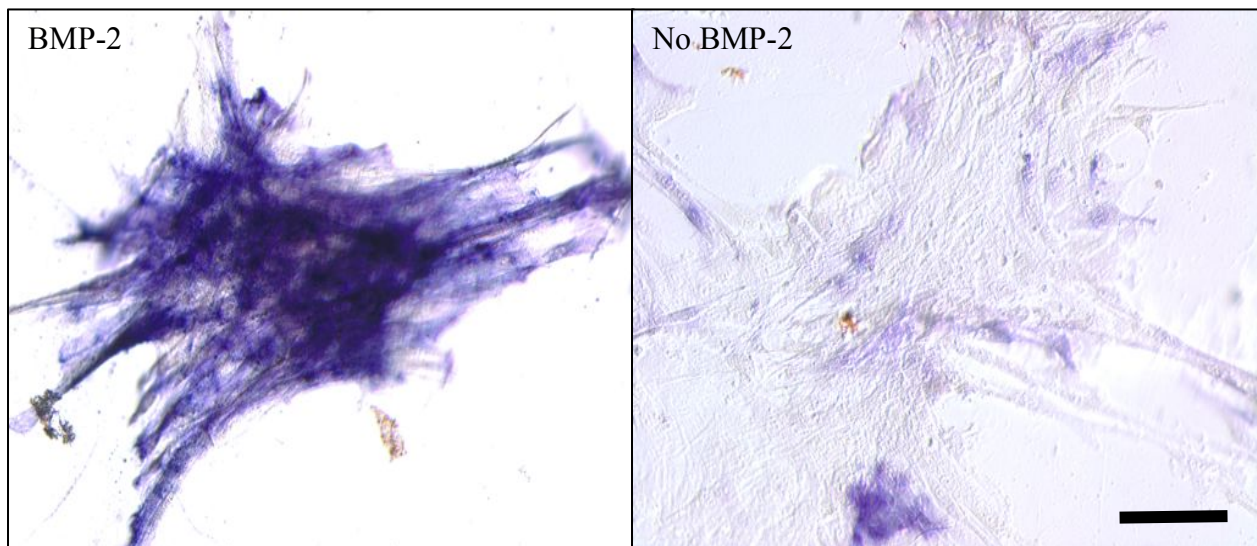


Figure 6.4 Immobilized DBCO-BMP-2 retains bioactivity in directing ALP expression in hMSC. DBCO-BMP-2 and CRGDS were patterned in specific regions of the hydrogel and hMSC were seeded on top of these regions and cultured for 5 days. hMSC were fixed and stained for ALP activity (purple) for the two conditions. Increased ALP activity was observed in

the presence of immobilized DBCO-BMP-2 relative to no BMP-2 present demonstrating that BMP-2 remains bioactive after modification and immobilization. Scale bar = 100 μm .

6.4 Current and Future Work

Ongoing work is investigating efficient reactions to modify pendant norbornenes with alkyne moieties. Once accomplished, patterning using the IEDDA click partner pathway (tetrazine and TCO) will be characterized in a similar manner as the SPAAC click partners (azide and DBCO) to demonstrate tunable control over protein immobilization in the presence of complex protein solutions as well as retention of protein bioactivity using this patterning technique. Then, protein patterning of two fluorescently labeled proteins using both bioorthogonal pathways will be performed to ensure they do not inhibit or reduce the fidelity of each other.

Our vision is to then use these patterning techniques to create arrays of multiple cues at increasing concentrations to rapidly screen through the singular and synergistic effects of BMP-2, SDF-1, and FGF-2 on 3D hMSC behavior (Figure 5). Individual protein arrays will be overlaid to measure the synergistic effects of two distinct protein combinations. For screening purposes, the effect of BMP-2 will be measured with ALP activity as discussed previously. SDF-1 is a potent chemokine to direct hMSC migration and invasion, and its effect will be quantified by the depth and number of hMSC invading into the hydrogel network. Finally, soluble FGF-2 is known to cause increased proliferation of hMSC in culture; therefore, hMSC proliferation will be measured by staining for 5-ethynyl-2'-deoxyuridine (EdU) to detect individual cell proliferation. Importantly, all of these metrics can be rapidly measured in spatially distinct regions using confocal microscopy and computational image analysis. This will elucidate regimes of interest for protein pairs that can be later explored through more in-depth analysis.

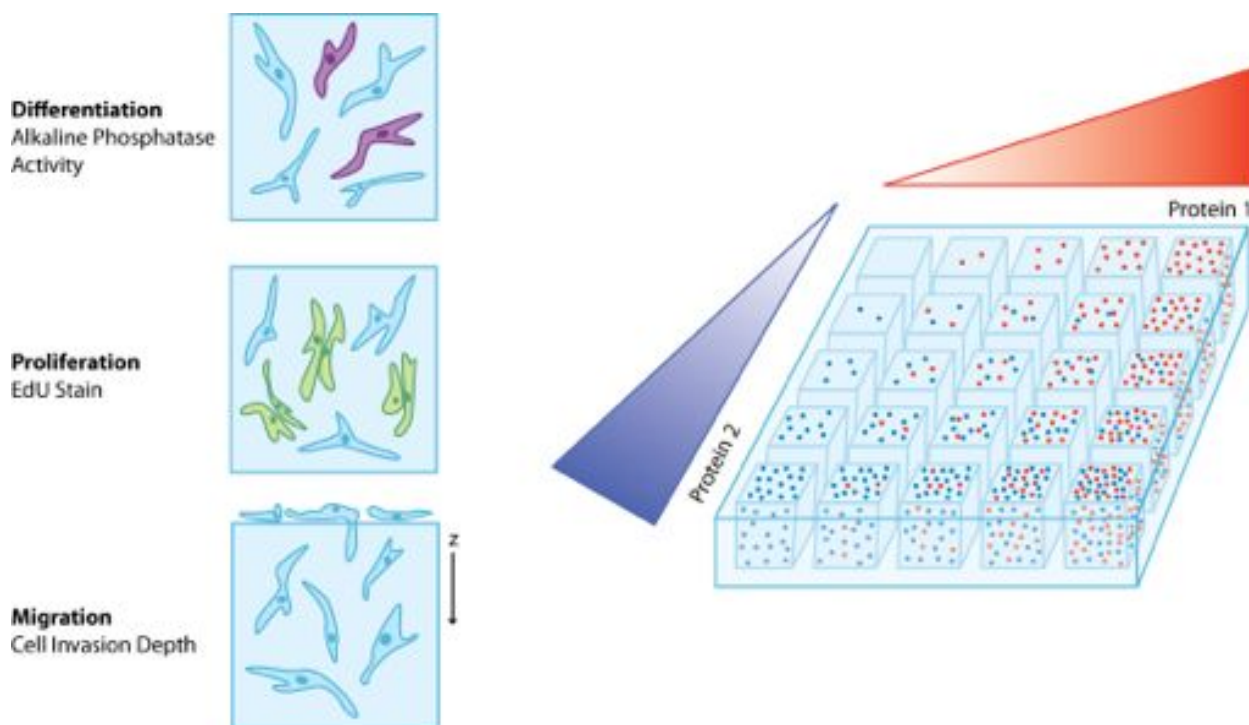


Figure 6.5 Screening multi-protein combinations on hMSC behavior Protein signals will be immobilized in highly-defined regions and concentrations to probe their singular and synergistic effects on hMSC behavior. A) The effect of BMP-2 will be measured through image analysis of ALP activity staining. Similarly, image analysis will be used to study the effect of FGF-2 by measuring EdU staining to determine proliferative cells. The depth of individual hMSC invasion into the hydrogel will be quantified by confocal imaging and image analysis. All of these analysis provide a rapid output that can be quantified computationally. B) Five-by-five arrays will be patterned three-dimensionally in peptide-functionalized hydrogels with an increasing concentration of Protein 1 in the x-axis and an increasing concentration of Protein 2 in the y-axis. This will provide 25 distinct microenvironments for hMSC culture. Additionally, using dynamic light projection multiple arrays can be patterned on a single hydrogel allowing for rapid analysis and increased statistical accuracy.

6.5 Conclusions

In sum, enzymatically degradable hydrogels have been patterned with full-length proteins using a series of bioorthogonal click reactions and light-mediated chemistries. It was found that the proposed patterning method provides an effective platform to create spatially distinct microenvironments with tunable protein concentrations for cell culture. Protein immobilization

was performed in complex protein solutions and found to retain high spatial and concentration fidelity. Further, proteins patterned with this method retain bioactivity to direct hMSC cell behavior. Specifically, immobilized DBCO-BMP-2 was shown to induce increased ALP activity with cultured hMSC, which is a key marker of hMSC osteogenesis. This novel and versatile patterning platform will be used for the rapid development of distinct cellular microenvironments to probe the effects of multiple signaling proteins in concert to elucidate important synergistic effects. The knowledge garnered from these studies will provide valuable engineering principles to better design future scaffolds for *in vivo* bone regeneration applications.

6.6 References

- [1] Burdick JA, Murphy WL. Moving from static to dynamic complexity in hydrogel design. *Nature communications* 2012;3:1269.
- [2] Discher DE, Mooney DJ, Zandstra PW. Growth factors, matrices, and forces combine and control stem cells. *Science* 2009;324:1673-7.
- [3] Richardson TP, Peters MC, Ennett AB, Mooney DJ. Polymeric system for dual growth factor delivery. *Nature biotechnology* 2001;19:1029-34.
- [4] Chen FM, Zhang M, Wu ZF. Toward delivery of multiple growth factors in tissue engineering. *Biomaterials* 2010;31:6279-308.
- [5] Hahn MS, Miller JS, West JL. Three-dimensional biochemical and biomechanical patterning of hydrogels for guiding cell behavior. *Advanced Materials* 2006;18:2679-+.
- [6] DeForest CA, Polizzotti BD, Anseth KS. Sequential click reactions for synthesizing and patterning three-dimensional cell microenvironments. *Nature materials* 2009;8:659-64.

- [7] Mosiewicz KA, Kolb L, van der Vlies AJ, Martino MM, Lienemann PS, Hubbell JA, et al. In situ cell manipulation through enzymatic hydrogel photopatterning. *Nature materials* 2013;12:1072-8.
- [8] DeForest CA, Tirrell DA. A photoreversible protein-patterning approach for guiding stem cell fate in three-dimensional gels. *Nature materials* 2015.
- [9] DeForest CA, Anseth KS. Cytocompatible click-based hydrogels with dynamically tunable properties through orthogonal photoconjugation and photocleavage reactions. *Nature Chemistry* 2011;3:925-31.
- [10] Wylie RG, Ahsan S, Aizawa Y, Maxwell KL, Morshead CM, Shoichet MS. Spatially controlled simultaneous patterning of multiple growth factors in three-dimensional hydrogels. *Nature materials* 2011;10:799-806.
- [11] Lo KWH, Ulery BD, Ashe KM, Laurencin CT. Studies of bone morphogenetic protein-based surgical repair. *Adv Drug Deliver Rev* 2012;64:1277-91.
- [12] Ji JF, He BP, Dheen ST, Tay SSW. Interactions of chemokines and chemokine receptors mediate the migration of mesenchymal stem cells to the impaired site in the brain after hypoglossal nerve injury. *Stem cells* 2004;22:415-27.
- [13] Kitaori T, Ito H, Schwarz EA, Tsutsumi R, Yoshitomi H, Oishi S, et al. Stromal Cell-Derived Factor 1/CXCR4 Signaling Is Critical for the Recruitment of Mesenchymal Stem Cells to the Fracture Site During Skeletal Repair in a Mouse Model. *Arthritis and rheumatism* 2009;60:813-23.
- [14] Eom YW, Oh JE, Lee JI, Baik SK, Rhee KJ, Shin HC, et al. The role of growth factors in maintenance of stemness in bone marrow-derived mesenchymal stem cells. *Biochemical and biophysical research communications* 2014;445:16-22.
- [15] Fairbanks BD, Schwartz MP, Halevi AE, Nuttelman CR, Bowman CN, Anseth KS. A Versatile Synthetic Extracellular Matrix Mimic via Thiol-Norbornene Photopolymerization. *Advanced Materials* 2009;21:5005-+.
- [16] Kyburz KA, Anseth KS. Three-dimensional hMSC motility within peptide-functionalized PEG-based hydrogels of varying adhesivity and crosslinking density. *Acta biomaterialia* 2013;9:6381-92.
- [17] Hoyle CE, Bowman CN. Thiol-ene click chemistry. *Angewandte Chemie* 2010;49:1540-73.
- [18] Hoyle CE, Lowe AB, Bowman CN. Thiol-click chemistry: a multifaceted toolbox for small molecule and polymer synthesis. *Chemical Society reviews* 2010;39:1355-87.

- [19] Fairbanks BD, Schwartz MP, Bowman CN, Anseth KS. Photoinitiated polymerization of PEG-diacrylate with lithium phenyl-2,4,6-trimethylbenzoylphosphinate: polymerization rate and cytocompatibility. *Biomaterials* 2009;30:6702-7.
- [20] Karver MR, Weissleder R, Hilderbrand SA. Synthesis and Evaluation of a Series of 1,2,4,5-Tetrazines for Bioorthogonal Conjugation. *Bioconjugate Chem* 2011;22:2263-70.
- [21] DeForest CA, Anseth KS. Photoreversible Patterning of Biomolecules within Click-Based Hydrogels. *Angew Chem Int Edit* 2012;51:1816-9.

CHAPTER VII

CONCLUSIONS AND RECOMMENDATIONS

The local *in vivo* microenvironment is a complex and dynamic structure that presents a myriad of biochemical and biophysical cues that direct cell behavior and is continuously remodeled over time through cell-mediated mechanisms [1, 2]. It plays a critical role in the complex bone healing cascade through dynamic structural changes and specific spatiotemporal presentation of biochemical cues that result in mesenchymal stem cell (MSC) infiltration and remodeling and further direct cell-matrix interactions that regulate MSC behavior [3, 4]. The focus of this thesis is to fabricate enzymatically-degradable PEG hydrogels functionalized with specific biomolecules (e.g. mimetic peptides, proteins) to permit MSC migration and further study the controlled presentation of chemokines and growth factors on *in vitro* MSC culture as well as bone regeneration *in vivo*. This work aims to elucidate how MSC interact and exchange information within their local microenvironment in user-defined synthetic hydrogels to engineer better extracellular matrix mimetic scaffolds that can serve as cell carrier or cell recruitment platforms for tissue engineering applications.

To this end, in Chapter III peptide-functionalized PEG hydrogels were fabricated to permit human MSC migration and the regulatory role of biochemical (e.g., adhesive ligands) and biophysical (e.g., network crosslinking density) cues on three-dimensional MSC migration was explored. Through thiol-ene photopolymerization the network crosslinking density (0.2 to 1.6 mM) and the adhesive ligand concentration (0.001 to 1 mM) was systematically varied within

the matrix metalloproteinase (MMP) degradable hydrogels in a user-tunable manner. Utilizing live-cell videomicroscopy and modeling individual cell mean square displacements using a Persistent Random Walk Model, it was found that hMSC migrated and spread at the highest rates in hydrogels with low crosslinking density and high adhesivity with speeds of $17.6 \pm 0.9 \mu\text{m/hr}$, persistence of $156.4 \pm 23.2 \text{ min}$, and mean free path of $47.6 \pm 8.8 \mu\text{m}$. High levels of cellular attachment and local interaction with the scaffold were further characterized by immunostaining the actin structures and $\beta 1$ integrin of encapsulated hMSC. Additionally, it was found that as adhesive ligand density increased over four orders of magnitude, hMSC migration speed also increased monotonically within the 3D hydrogels thus lacking the expected biphasic trend that has been observed for cell migration on 2D substrates.

For this work, cell adhesion sites were introduced into the otherwise bio-inert PEG backbone through the incorporation of the fibronectin peptide mimic, CRGDS, through network conjugation with the thiol-containing cysteine residue. The extracellular matrix *in vivo* is composed of a plethora of different cell adhesion sites; and more importantly, how strongly a cell binds to these various sites and with what specific integrin has major influence over downstream signaling cascades and subsequent behavior [5]. For example, an epithelial cell interacting with a substrate with $\alpha_v\beta_3$ integrin has drastically different cell morphology and migration than when interacting with a substrate with the $\alpha_5\beta_1$ integrin [6]. The thiol-ene peptide-functionalized hydrogels provide a versatile platform to introduce key binding sites that recapitulate relevant binding motifs that hMSC would closely interact with *in vivo* [7]. Future studies should explore the effect of incorporating different integrin binding sequences, for example: the CKRLDGS mimetic peptide that recapitulates fibrinogen present during the hematoma formation during a bone fracture and is bound by hMSC integrin $\alpha_v\beta_3$, the FYFDLR mimetic basement membrane

adhesion peptide that interacts with the $\alpha_1\beta_1$ and $\alpha_2\beta_1$ integrins, and the CKQAGDV peptide that mimics fibrinogen and is bound by $\alpha_5\beta_1$ [8]. The role of these integrins in 3D hMSC migration speed and persistence can be explored by using materials to dictate specific integrin-matrix interactions within enzymatically degradable hydrogels to engineer cell recruitment platforms that promote high levels of cell infiltration and colonization. Additionally, novel hypotheses could be tested as to how these integrin-initiated signaling cascades regulate other important hMSC behaviors, such as their differentiation capacity and the library of secreted molecules that play a pivotal role in governing the immune response and cell recruitment at bone fracture sites *in vivo* [9].

In Chapter IV, the dynamic hMSC remodeling of the enzymatically degradable hydrogels was characterized locally to better understand how hMSC remodel and re-engineer their microenvironments during 3D migration. Microrheological techniques were utilized to quantifiably characterize cell remodeling at different stages of 3D hMSC migration. Specifically, multiple particle tracking was performed by tracking the diffusion and displacement of 1 μm beads entrapped within the hydrogel scaffold proximal to migrating hMSC. Through rheological comparisons and particle image velocimetry, fingerprints of the local gel properties were created over relevant cellular length and time scales.

Two phases of hMSC migration were observed that yielded varying local gel properties: i) at early time points, hMSC were beginning to remodel local pericellular regions, spread, and migrate within the hydrogel, and ii) at later migratory time points, a subset of hMSC were highly motile within the hydrogel network. During the first phase of migration, the local gel properties were characterized using MPT and PIV methods to elucidate the role of cell-mediated degradation and the impact of cytoskeletal tension on the network, with areas farther from the

cell being rapidly degraded. This was attributed to the time scale of cell secreted MMP diffusion, which is thought to be much faster than the reaction time scale of network peptide cleavage (small Damköhler number). Interestingly, PIV measured persistent particle movement in this farther region, attributed to cytoskeletal tension and a broader gel structure on larger length scales than can be characterized by MPT. In the second phase of hMSC migration a subset of hMSC were observed to migrate within a viscoelastic fluid region, based on MPT measurements, within the hydrogel permitting high cell migratory speeds. Collectively, these microscopic gel remodeling events were the beginning of larger macroscopic cell-mediated remodeling of the matrix that resulted in irreversible tracks eroded throughout the hydrogel network. Overall, microrheological techniques provide unique insight into dynamic cell-matrix interactions, and these insights can be used to design smarter substrates that reciprocally interact with cells on relevant length and time scales.

This work focused on using microrheological techniques to measure cell-mediated degradation within enzymatically degradable scaffolds. For future experimental design, this method could easily be translated to investigate the degree of degradation in user-tunable photodegradable hydrogels for quantitative characterization of gel conditions around the gel-sol transition. For example, user-defined and created 3D tunnels could be formed with varying extents of degradation to measure the network crosslinking density threshold of 3D cell migration in photodegradable hydrogels, and through utilization of MPT techniques the local gel properties within the local cellular microenvironment could be quantified. The information garnered could help in designing hydrogels with complex 3D structures to direct cell and tissue organization or disease progression within an *in vitro* cell culture model.

In Chapter V, hydrogels that permitted high levels of isotropic hMSC migration were

functionalized with full-length proteins to direct hMSC behavior *in vitro* and study the effect of contextual presentation and local delivery of proteins in a bone healing model *in vivo*. Specifically, SDF-1 was effectively thiolated and immobilized within the hydrogel network at physiologically relevant concentrations. Thiolated SDF-1 was still found to retain its bioactivity by measuring the phosphorylation of the CXCR4 receptor found on hMSC. SH-SDF-1 was subsequently immobilized into a hydrogel scaffold that was introduced into a rat calvarial defect model, and through its local and sustained presentation was found to increase the level of cellularity and cell invasion into the defect site after 4 weeks relative to the delivery of entrapped, diffusible SDF-1. However, there was not an increase in mineralized bone tissue formation within the defects as measured by microCT scans, so BMP-2 was chosen to be co-delivered to the site as it is a potent osteogenic inducer of hMSC [10]. Therefore, BMP-2 was also thiolated and effectively immobilized into the hydrogel scaffold in user-defined concentrations. The SH-BMP-2 retained bioactivity when immobilized to the network and was found to induce high levels of ALP activity in encapsulated hMSC *in vitro*. Using the rat calvarial defect model the effect of the delivery of SH-BMP-2 and the co-delivery of SH-SDF-1 and SH-BMP-2 immobilized within hydrogel scaffolds on tissue mineralization was measured after 4 weeks using microCT scans. Interestingly, an increase in mineralization was observed when SH-BMP-2 was delivered alone, but co-delivery of the two proteins showed no increase in mineralized tissue formation. The difficulty with elucidating the role of specific proteins within the complex bone defect motivated the development of a screening platform to efficiently probe the effects of multiple proteins on hMSC behavior in highly defined cellular microenvironments.

In vivo, cells are presented with a myriad of proteins that direct cell function through synergistic mechanisms; however, it is impossible to tease these dose-dependent and pleiotropic

relationships out in the complex *in vivo* microenvironment. Therefore, Chapter VI highlights work to develop a high-throughput screening array to rapidly measure the synergistic effects of multiple proteins on hMSC behavior with a focus on relevant proteins that play an important role in directing hMSC function during the bone regeneration (e.g., BMP-2, SDF-1, FGF-2). Using a sequence of bioorthogonal and photochemical reactions, proteins can be immobilized into spatially defined regions into a hydrogel in complex solutions of endogenous functionalities. Specifically, protein immobilization is achieved through two bioorthogonal click reactions: i) copper-free, strain promoted azide alkyne cycloaddition (SPAAC) and ii) inverse electron demand Diels-Alder reaction (IEDDA). By spatially patterning one reaction partner from each reaction (e.g., azide from SPAAC, tetrazine from IEDDA) using photoinitiated thiol-yne chemistry and dynamic light projection (DLP), one can develop spatially defined regions of user-defined physiologic concentrations of two proteins to create 3D hydrogel array platforms to study cell behavior. Early work has shown that the SPAAC reaction is effective in patterning regions of user-defined concentrations within the enzymatically-degradable hydrogels. Additionally, this patterning technique was performed in the presence of serum proteins and found to retain high spatial and concentration fidelity despite the high density of excess biological functionalities. This method was also found to retain high levels of bioactivity of patterned proteins immobilized to the network as measured by the ALP expression of hMSC seeded onto patterns of immobilized BMP-2.

Ongoing and future work for this project is investigating efficient reactions to modify pendant norbornenes present during hydrogel formation into alkyne moieties. After this is achieved, the IEDDA patterning reaction will be characterized in a similar manner as the SPAAC patterning scheme, demonstrating tunable spatial patterning in the presence of a

complex protein solution and retention of bioactivity of the immobilized protein. Additional experiments will be performed to ensure the orthogonality of the two reactions when patterned in the same hydrogel. Our aim is to then use both of these patterning techniques to create arrays to screen the singular and synergistic effects of multiple proteins on hMSC behavior. Specifically, BMP-2, SDF-1, and FGF-2 will be chosen to understand their role in regulating hMSC differentiation, migration, or proliferation. Cell measurement outputs for each protein have been chosen based on their ability to be spatially and rapidly measured to swiftly screen through large dosing regimes of the proteins using confocal microscopy and computational image analysis. This versatile platform will be used to develop and screen through highly-defined cellular microenvironments to study the role multi-protein signals play on hMSC behavior. The knowledge discovered using this platform will aid in the design of more effective cell carrier and drug delivery platforms for *in vivo* bone regeneration applications.

In summary, this thesis investigated the role and presentation of biochemical and biophysical cues on 3D hMSC behavior (e.g., migration, matrix remodeling, differentiation, proliferation) using highly-defined thiol-ene PEG-based hydrogels *in vitro* and further investigated how these findings translated to the complex *in vivo* microenvironment in a calvarial bone defect model. Specific Aim I highlighted the characterization of hMSC migration within peptide-functionalized hydrogels while varying biochemical (e.g., adhesive ligand density) and biophysical (e.g., network crosslinking density) of the PEG hydrogel. In Specific Aim 2, microrheological techniques were utilized to quantifiably characterize the cell-mediated reengineering of the local gel mechanical properties during 3D hMSC migration providing new insight into cell-matrix interactions on relevant cellular length and time scales. In Specific Aim 3, full-length proteins (e.g., SDF-1, BMP-2) were covalently immobilized into a migration-

permissive hydrogel scaffold to direct hMSC behavior *in vitro* and study the effect of local and sustained protein delivery on cell invasion and mineralized tissue formation *in vivo* using a rat calvarial defect model. Finally, Specific Aim 4 highlights our ongoing work to develop a high-throughput screening tool to measure the synergistic effects of multiple proteins on hMSC behavior using a sequence of bioorthogonal and photochemical reactions to create highly defined and organized 3D cellular microenvironments. The methods presented in this thesis provide tools to more deeply characterize cell-matrix interaction and how cells interpret the presentation of local ECM cues that regulate their behavior. This thesis contributes novel insights into fundamental 3D hMSC behavior and how biomaterial design translates from *in vitro* to *in vivo* contexts to better engineer biomaterial niches that can serve as *in vitro* cell culture platforms and cell carrier or recruitment platforms for tissue regeneration applications.

7.1 References

- [1] Tibbitt MW, Anseth KS. Hydrogels as extracellular matrix mimics for 3D cell culture. *Biotechnology and Bioengineering* 2009;103:655-63.
- [2] Burdick JA, Murphy WL. Moving from static to dynamic complexity in hydrogel design. *Nature communications* 2012;3:1269.
- [3] Tsiridis E, Upadhyay N, Giannoudis P. Molecular aspects of fracture healing: which are the important molecules? *Injury* 2007;38 Suppl 1:S11-25.
- [4] Uccelli A, Moretta L, Pistoia V. Mesenchymal stem cells in health and disease. *Nature reviews Immunology* 2008;8:726-36.
- [5] Humphries JD, Byron A, Humphries MJ. Integrin ligands at a glance. *J Cell Sci* 2006;119:3901-3.
- [6] Truong H, Danen EHJ. Integrin switching modulates adhesion dynamics and cell migration. *Cell Adhes Migr* 2009;3:179-81.
- [7] Fairbanks BD, Schwartz MP, Halevi AE, Nuttelman CR, Bowman CN, Anseth KS. A Versatile Synthetic Extracellular Matrix Mimic via Thiol-Norbornene Photopolymerization. *Advanced Materials* 2009;21:5005-+.

[8] Ruoslahti E. RGD and other recognition sequences for integrins. Annual review of cell and developmental biology 1996;12:697-715.

[9] Caplan AI, Correa D. The MSC: an injury drugstore. Cell Stem Cell 2011;9:11-5.

[10] Seeherman H, Wozney JM. Delivery of bone morphogenetic proteins for orthopedic tissue regeneration. Cytokine & growth factor reviews 2005;16:329-45.

CHAPTER VIII

BIBLIOGRAPHY

CHAPTER I -

- [1] Watt FM, Huck WTS. Role of the extracellular matrix in regulating stem cell fate. *Nat Rev Mol Cell Bio* 2013;14:467-73.
- [2] Lu PF, Weaver VM, Werb Z. The extracellular matrix: A dynamic niche in cancer progression. *J Cell Biol* 2012;196:395-406.
- [3] Moroni F, Mirabella T. Decellularized matrices for cardiovascular tissue engineering. *American journal of stem cells* 2014;3:1-20.
- [4] Faulk DM, Johnson SA, Zhang L, Badylak SF. Role of the extracellular matrix in whole organ engineering. *Journal of cellular physiology* 2014;229:984-9.
- [5] Ott HC, Matthiesen TS, Goh SK, Black LD, Kren SM, Netoff TI, et al. Perfusion-decellularized matrix: using nature's platform to engineer a bioartificial heart. *Nature medicine* 2008;14:213-21.
- [6] Karp G. *Cell and molecular biology : concepts and experiments*. 3rd ed. New York: J. Wiley; 2002.
- [7] Hubbell JA. Biomaterials in Tissue Engineering. *Bio-Technol* 1995;13:565-76.
- [8] Humphries MJ. The Molecular-Basis and Specificity of Integrin Ligand Interactions. *J Cell Sci* 1990;97:585-92.
- [9] Annabi N, Tamayol A, Uquillas JA, Akbari M, Bertassoni LE, Cha C, et al. 25th Anniversary Article: Rational Design and Applications of Hydrogels in Regenerative Medicine. *Adv Mater* 2014;26:85-124.
- [10] Kharkar PM, Kiick KL, Kloxin AM. Designing degradable hydrogels for orthogonal control of cell microenvironments. *Chemical Society reviews* 2013;42:7335-72.
- [11] Azagarsamy MA, Anseth KS. Bioorthogonal Click Chemistry: An Indispensable Tool to Create Multifaceted Cell Culture Scaffolds. *ACS macro letters* 2013;2:5-9.
- [12] Hoyle CE, Bowman CN. Thiol-ene click chemistry. *Angewandte Chemie* 2010;49:1540-73.

- [13] Codelli JA, Baskin JM, Agard NJ, Bertozzi CR. Second-generation difluorinated cyclooctynes for copper-free click chemistry. *Journal of the American Chemical Society* 2008;130:11486-93.
- [14] Hudalla GA, Eng TS, Murphy WL. An approach to modulate degradation and mesenchymal stem cell behavior in poly(ethylene glycol) networks. *Biomacromolecules* 2008;9:842-9.
- [15] Hern DL, Hubbell JA. Incorporation of adhesion peptides into nonadhesive hydrogels useful for tissue resurfacing. *J Biomed Mater Res* 1998;39:266-76.
- [16] DeLong SA, Moon JJ, West JL. Covalently immobilized gradients of bFGF on hydrogel scaffolds for directed cell migration. *Biomaterials* 2005;26:3227-34.
- [17] DeForest CA, Anseth KS. Cytocompatible click-based hydrogels with dynamically tunable properties through orthogonal photoconjugation and photocleavage reactions. *Nature Chemistry* 2011;3:925-31.
- [18] Wylie RG, Ahsan S, Aizawa Y, Maxwell KL, Morshead CM, Shoichet MS. Spatially controlled simultaneous patterning of multiple growth factors in three-dimensional hydrogels. *Nature materials* 2011;10:799-806.
- [19] DeForest CA, Polizzotti BD, Anseth KS. Sequential click reactions for synthesizing and patterning three-dimensional cell microenvironments. *Nature materials* 2009;8:659-64.
- [20] Fairbanks BD, Schwartz MP, Halevi AE, Nuttelman CR, Bowman CN, Anseth KS. A Versatile Synthetic Extracellular Matrix Mimic via Thiol-Norbornene Photopolymerization. *Adv Mater* 2009;21:5005-+.
- [21] Lutolf MP, Lauer-Fields JL, Schmoekel HG, Metters AT, Weber FE, Fields GB, et al. Synthetic matrix metalloproteinase-sensitive hydrogels for the conduction of tissue regeneration: engineering cell-invasion characteristics. *Proceedings of the National Academy of Sciences of the United States of America* 2003;100:5413-8.
- [22] DeForest CA, Sims EA, Anseth KS. Peptide-Functionalized Click Hydrogels with Independently Tunable Mechanics and Chemical Functionality for 3D Cell Culture. *Chem Mater* 2010;22:4783-90.
- [23] DeForest CA, Anseth KS. Photoreversible Patterning of Biomolecules within Click-Based Hydrogels. *Angew Chem Int Edit* 2012;51:1816-9.
- [24] Engler AJ, Sen S, Sweeney HL, Discher DE. Matrix elasticity directs stem cell lineage specification. *Cell* 2006;126:677-89.
- [25] Yang C, Tibbitt MW, Basta L, Anseth KS. Mechanical memory and dosing influence stem cell fate. *Nature materials* 2014.
- [26] Wang H, Tibbitt MW, Langer SJ, Leinwand LA, Anseth KS. Hydrogels preserve native phenotypes of valvular fibroblasts through an elasticity-regulated PI3K/AKT pathway.

Proceedings of the National Academy of Sciences of the United States of America 2013;110:19336-41.

[27] Gilbert PM, Havenstrite KL, Magnusson KE, Sacco A, Leonardi NA, Kraft P, et al. Substrate elasticity regulates skeletal muscle stem cell self-renewal in culture. *Science* 2010;329:1078-81.

[28] Jabbari E. Bioconjugation of hydrogels for tissue engineering. *Current opinion in biotechnology* 2011;22:655-60.

[29] Perlin L, MacNeil S, Rimmer S. Production and performance of biomaterials containing RGD peptides. *Soft matter* 2008;4:2331-49.

[30] Brennan AB, Kirschner CM, Society for Biomaterials. Bio-inspired materials for biomedical engineering.

[31] Gould ST, Darling NJ, Anseth KS. Small peptide functionalized thiol-ene hydrogels as culture substrates for understanding valvular interstitial cell activation and de novo tissue deposition. *Acta biomaterialia* 2012;8:3201-9.

[32] Bian L, Guvendiren M, Mauck RL, Burdick JA. Hydrogels that mimic developmentally relevant matrix and N-cadherin interactions enhance MSC chondrogenesis. *Proceedings of the National Academy of Sciences of the United States of America* 2013;110:10117-22.

[33] MacArthur JW, Jr., Purcell BP, Shudo Y, Cohen JE, Fairman A, Trubelja A, et al. Sustained release of engineered stromal cell-derived factor 1-alpha from injectable hydrogels effectively recruits endothelial progenitor cells and preserves ventricular function after myocardial infarction. *Circulation* 2013;128:S79-86.

[34] Hiesinger W, Frederick JR, Atluri P, McCormick RC, Marotta N, Muenzer JR, et al. Spliced stromal cell-derived factor-1 alpha analog stimulates endothelial progenitor cell migration and improves cardiac function in a dose-dependent manner after myocardial infarction. *J Thorac Cardiovasc Sur* 2010;140:1174-80.

[35] Madl CM, Mehta M, Duda GN, Heilshorn SC, Mooney DJ. Presentation of BMP-2 mimicking peptides in 3D hydrogels directs cell fate commitment in osteoblasts and mesenchymal stem cells. *Biomacromolecules* 2014;15:445-55.

[36] Liang YK, Kiick KL. Heparin-functionalized polymeric biomaterials in tissue engineering and drug delivery applications. *Acta biomaterialia* 2014;10:1588-600.

[37] Rabenstein DL. Heparin and heparan sulfate: structure and function. *Natural product reports* 2002;19:312-31.

[38] Purcell BP, Lobb D, Charati MB, Dorsey SM, Wade RJ, Zellars KN, et al. Injectable and bioresponsive hydrogels for on-demand matrix metalloproteinase inhibition. *Nature materials* 2014;13:653-61.

- [39] Mosiewicz KA, Kolb L, van der Vlies AJ, Martino MM, Lienemann PS, Hubbell JA, et al. In situ cell manipulation through enzymatic hydrogel photopatterning. *Nature materials* 2013;12:1072-8.
- [40] Leight JL, Wozniak MA, Chen S, Lynch ML, Chen CS. Matrix rigidity regulates a switch between TGF-beta1-induced apoptosis and epithelial-mesenchymal transition. *Molecular biology of the cell* 2012;23:781-91.
- [41] Cosgrove BD, Gilbert PM, Porpiglia E, Mourkioti F, Lee SP, Corbel SY, et al. Rejuvenation of the muscle stem cell population restores strength to injured aged muscles. *Nature medicine* 2014;20:255-64.
- [42] Dingal PC, Discher DE. Combining insoluble and soluble factors to steer stem cell fate. *Nature materials* 2014;13:532-7.
- [43] Patterson J, Hubbell JA. Enhanced proteolytic degradation of molecularly engineered PEG hydrogels in response to MMP-1 and MMP-2. *Biomaterials* 2010;31:7836-45.
- [44] Tibbitt MW, Kloxin AM, Dyamenahalli KU, Anseth KS. Controlled two-photon photodegradation of PEG hydrogels to study and manipulate subcellular interactions on soft materials. *Soft matter* 2010;6:5100-8.
- [45] Kloxin AM, Lewis KJ, DeForest CA, Seedorf G, Tibbitt MW, Balasubramaniam V, et al. Responsive culture platform to examine the influence of microenvironmental geometry on cell function in 3D. *Integrative biology : quantitative biosciences from nano to macro* 2012;4:1540-9.
- [46] Kyburz KA, Anseth KS. Three-dimensional hMSC motility within peptide-functionalized PEG-based hydrogels of varying adhesivity and crosslinking density. *Acta biomaterialia* 2013;9:6381-92.
- [47] Khetan S, Guvendiren M, Legant WR, Cohen DM, Chen CS, Burdick JA. Degradation-mediated cellular traction directs stem cell fate in covalently crosslinked three-dimensional hydrogels. *Nature materials* 2013;12:458-65.
- [48] Leight JL, Alge DL, Maier AJ, Anseth KS. Direct measurement of matrix metalloproteinase activity in 3D cellular microenvironments using a fluorogenic peptide substrate. *Biomaterials* 2013;34:7344-52.
- [49] Lee SH, Moon JJ, Miller JS, West JL. Poly(ethylene glycol) hydrogels conjugated with a collagenase-sensitive fluorogenic substrate to visualize collagenase activity during three-dimensional cell migration. *Biomaterials* 2007;28:3163-70.
- [50] Packard BZ, Artym VV, Komoriya A, Yamada KM. Direct visualization of protease activity on cells migrating in three-dimensions. *Matrix Biol* 2009;28:3-10.
- [51] Schultz KM, Anseth KS. Monitoring degradation of matrix metalloproteinases-cleavable PEG hydrogels via multiple particle tracking microrheology. *Soft matter* 2013;9:1570-9.

[52] Schultz KM, Furst EM. Microrheology of biomaterial hydrogelators. *Soft matter* 2012;8:6198-205.

[53] Tan JL, Tien J, Pirone DM, Gray DS, Bhadriraju K, Chen CS. Cells lying on a bed of microneedles: An approach to isolate mechanical force. *Proceedings of the National Academy of Sciences of the United States of America* 2003;100:1484-9.

[54] Legant WR, Miller JS, Blakely BL, Cohen DM, Genin GM, Chen CS. Measurement of mechanical tractions exerted by cells in three-dimensional matrices. *Nat Methods* 2010;7:969-U113.

CHAPTER II –

[1] Uccelli A, Moretta L, Pistoia V. Mesenchymal stem cells in health and disease. *Nature reviews Immunology* 2008;8:726-36.

[2] Caplan AI, Correa D. The MSC: an injury drugstore. *Cell Stem Cell* 2011;9:11-5.

[3] Karp JM, Teol GSL. Mesenchymal Stem Cell Homing: The Devil Is in the Details. *Cell Stem Cell* 2009;4:206-16.

[4] Mistry AS, Mikos AG. Tissue engineering strategies for bone regeneration. *Advances in biochemical engineering/biotechnology* 2005;94:1-22.

[5] Mariner PD, Wudel JM, Miller DE, Genova EE, Streubel SO, Anseth KS. Synthetic hydrogel scaffold is an effective vehicle for delivery of INFUSE (rhBMP2) to critical-sized calvaria bone defects in rats. *Journal of orthopaedic research : official publication of the Orthopaedic Research Society* 2013;31:401-6.

[6] Tibbitt MW, Anseth KS. Hydrogels as extracellular matrix mimics for 3D cell culture. *Biotechnology and Bioengineering* 2009;103:655-63.

[7] Friedl P, Wolf K. Plasticity of cell migration: a multiscale tuning model. *J Cell Biol* 2010;188:11-9.

[8] Kim H-D, Peyton SR. Bio-inspired materials for parsing matrix physicochemical control of cell migration: a review. *Integrative biology: quantitative biosciences from nano to macro* 2012;4:37-52.

[9] Hoyle CE, Bowman CN. Thiol-ene click chemistry. *Angewandte Chemie* 2010;49:1540-73.

CHAPTER III –

[1] Uccelli A, Moretta L, Pistoia V. Mesenchymal stem cells in health and disease. *Nature Reviews Immunology* 2008;8:726-36.

- [2] Salem HK, Thiernemann C. Mesenchymal Stromal Cells: Current Understanding and Clinical Status. *Stem Cells* 2010;28:585-96.
- [3] Discher DE, Mooney DJ, Zandstra PW. Growth Factors, Matrices, and Forces Combine and Control Stem Cells. *Science* 2009;324:1673-7.
- [4] Chen F-M, Wu L-A, Zhang M, Zhang R, Sun H-H. Homing of endogenous stem/progenitor cells for in situ tissue regeneration: Promises, strategies, and translational perspectives. *Biomaterials* 2011;32:3189-209.
- [5] Friedl P, Wolf K. Plasticity of cell migration: a multiscale tuning model. *J Cell Biol* 2010;188:11-9.
- [6] Lutolf MP, Gilbert PM, Blau HM. Designing materials to direct stem-cell fate. *Nature* 2009;462:433-41.
- [7] Kim H-D, Peyton SR. Bio-inspired materials for parsing matrix physicochemical control of cell migration: A Review. *Integrative Biology* 2012;4:37-52.
- [8] Doyle AD, Wang FW, Matsumoto K, Yamada KM. One-dimensional topography underlies three-dimensional fibrillar cell migration. *J Cell Biol* 2009;184:481-90.
- [9] Peyton SR, Kalcioğlu ZI, Cohen JC, Runkle AP, Van Vliet KJ, Lauffenburger DA, et al. Marrow-derived stem cell motility in 3D synthetic scaffold is governed by geometry along with adhesivity and stiffness. *Biotechnology and Bioengineering* 2011;108:1181-93.
- [10] Peyton SR, Putnam AJ. Extracellular matrix rigidity governs smooth muscle cell motility in a biphasic fashion. *J Cell Physiol* 2005;204:198-209.
- [11] Palecek SP, Loftus JC, Ginsberg MH, Lauffenburger DA, Horwitz AF. Integrin-ligand binding properties govern cell migration speed through cell-substratum adhesiveness. *Nature* 1997;385:537-40.
- [12] Purcell BP, Elser JA, Mu A, Margulies KB, Burdick JA. Synergistic effects of SDF-1 α chemokine and hyaluronic acid release from degradable hydrogels on directing bone marrow derived cell homing to the myocardium. *Biomaterials* 2012;33:7849-57.
- [13] Pelham RJ, Jr., Wang YI. Cell locomotion and focal adhesions are regulated by substrate flexibility. *Proc Natl Acad Sci USA* 1997;94:13661-5.
- [14] Lo C-M, Wang H-B, Dembo M, Wang Y-I. Cell Movement Is Guided by the Rigidity of the Substrate. *Biophysical Journal* 2000;79:144-52.
- [15] Engler A, Bacakova L, Newman C, Hategan A, Griffin M, Discher D. Substrate Compliance versus Ligand Density in Cell on Gel Responses. *Biophysical Journal* 2004;86:617-28.

- [16] Maheshwari G, Brown G, Lauffenburger DA, Wells A, Griffith LG. Cell adhesion and motility depend on nanoscale RGD clustering. *J Cell Sci* 2000;113:1677-86.
- [17] Grinnell F, Petroll WM. Cell Motility and Mechanics in Three-Dimensional Collagen Matrices. *Annual Review of Cell and Developmental Biology* 2010;26:335-61.
- [18] Zaman MH, Trapani LM, Sieminski AL, MacKellar D, Gong H, Kamm RD, et al. Migration of tumor cells in 3D matrices is governed by matrix stiffness along with cell-matrix adhesion and proteolysis. *PNAS* 2006;103:10889-94.
- [19] Ehrbar M, Sala A, Lienemann P, Ranga A, Mosiewicz K, Bittermann A, et al. Elucidating the Role of Matrix Stiffness in 3D Cell Migration and Remodeling. *Biophysical Journal* 2011;100:284-93.
- [20] Lei Y, Gojgini S, Lam J, Segura T. The spreading, migration and proliferation of mouse mesenchymal stem cells cultured inside hyaluronic acid hydrogels. *Biomaterials* 2011;32:39-47.
- [21] Raeber GP, Lutolf MP, Hubbell JA. Molecularly Engineered PEG Hydrogels: A Novel Model System for Proteolytically Mediated Cell Migration. *Biophysical Journal* 2005;89:1374-88.
- [22] Raeber GP, Lutolf MP, Hubbell JA. Mechanisms of 3-D migration and matrix remodeling of fibroblasts within artificial ECMs. *Acta Biomaterialia* 2007;3:615-29.
- [23] Zhang YH, Zhao CQ, Jiang LS, Dai LY. Substrate stiffness regulates apoptosis and the mRNA expression of extracellular matrix regulatory genes in the rat annular cells. *Matrix Biology* 2011;30:135-44.
- [24] Hanjaya-Putra D, Yee J, Ceci D, Truitt R, Yee D, Gerecht S. Vascular endothelial growth factor and substrate mechanics regulate in vitro tubulogenesis of endothelial progenitor cells. *Journal of Cellular and Molecular Medicine* 2010;14:2436-47.
- [25] Gould ST, Darling NJ, Anseth KS. Small peptide functionalized thiol-ene hydrogels as culture substrates for understanding valvular interstitial cell activation and de novo tissue deposition. *Acta Biomaterialia* 2012;8:3201-9.
- [26] Gaudet C, Marganski WA, Kim S, Brown CT, Gunderia V, Dembo M, et al. Influence of type I collagen surface density on fibroblast spreading, motility, and contractility. *Biophysical Journal* 2003;85:3329-35.
- [27] Schwartz MP, Fairbanks BD, Rogers RE, Rangarajan R, Zaman MH, Anseth KS. A synthetic strategy for mimicking the extracellular matrix provides new insight about tumor cell migration. *Integrative Biology* 2010;2:32-40.

- [28] Fairbanks BD, Schwartz MP, Halevi AE, Nuttelman CR, Bowman CN, Anseth KS. A Versatile Synthetic Extracellular Matrix Mimic via Thiol-Norbornene Photopolymerization. *Advanced Materials* 2009;21:5005-10.
- [29] Nagase H, Fields GB. Human matrix metalloproteinase specificity studies using collagen sequence-based synthetic peptides. *Biopolymers* 1996;40:399-416.
- [30] Patterson J, Hubbell JA. Enhanced proteolytic degradation of molecularly engineered PEG hydrogels in response to MMP-1 and MMP-2. *Biomaterials* 2010;31:7836-45.
- [31] Ho IAW, Chan KYW, Ng W-H, Guo CM, Hui KM, Cheang P, et al. Matrix metalloproteinase 1 is necessary for the migration of human bone marrow-derived mesenchymal stem cells toward human glioma. *Stem Cells* 2009;27:1366-75.
- [32] Halfon S, Abramov N, Grinblat B, Ginis I. Markers distinguishing mesenchymal stem cells from fibroblasts are downregulated with passaging. *Stem Cells Dev* 2011;20:53-66.
- [33] Parikka V, Väänänen A, Risteli J, Salo T, Sorsa T, Väänänen HK, et al. Human mesenchymal stem cell derived osteoblasts degrade organic bone matrix in vitro by matrix metalloproteinases. *Matrix Biol* 2005;24:438-47.
- [34] Djouad F, Delorme B, Maurice M, Bony C, Apparailly F, Louis-Pence P, et al. Microenvironmental changes during differentiation of mesenchymal stem cells towards chondrocytes. *Arthritis Res Ther* 2007;9.
- [35] Fairbanks BD, Schwartz MP, Bowman CN, Anseth KS. Photoinitiated polymerization of PEG-diacrylate with lithium phenyl-2,4,6-trimethylbenzoylphosphinate: polymerization rate and cytocompatibility. *Biomaterials* 2009;30:6702-7.
- [36] Dickinson RB, Tranquillo RT. Optimal estimation of cell movement indices from the statistical analysis of cell tracking data. *AIChE Journal* 1993;39:1995-2010.
- [37] Engler AJ, Sen S, Sweeney HL, Discher DE. Matrix elasticity directs stem cell lineage specification. *Cell* 2006;126:677-89.
- [38] Rubinstein M, Colby RH. *Polymer Physics*. 9 ed. New York: Oxford University Press Inc.; 2003.
- [39] Sakai T, Matsunaga T, Yamamoto Y, Ito C, Yoshida R, Suzuki S, et al. Design and fabrication of a high-strength hydrogel with ideally homogeneous network structure from tetrahedron-like macromonomers. *Macromolecules* 2008;41:5379-84.
- [40] Malkoch M, Vestberg R, Gupta N, Mespouille L, Dubois P, Mason AF, et al. Synthesis of well-defined hydrogel networks using Click chemistry. *Chemical Communications* 2006:2774-6.

- [41] Yang T, Long H, Malkoch M, Gamstedt EK, Berglund L, Hult A. Characterization of Well-Defined Poly(ethylene glycol) Hydrogels Prepared by Thiol-ene Chemistry. *Journal of Polymer Science Part a-Polymer Chemistry* 2011;49:4044-54.
- [42] Humphries JD, Byron A, Humphries MJ. Integrin ligands at a glance. *J Cell Sci* 2006;119:3901-3.
- [43] Hakkinen KM, Harunaga JS, Doyle AD, Yamada KM. Direct comparisons of the morphology, migration, cell adhesions, and actin cytoskeleton of fibroblasts in four different three-dimensional extracellular matrices. *Tissue Eng Part A* 2011;17:713-24.
- [44] Wu S, Wells A, Griffith LG, Lauffenburger DA. Controlling multipotent stromal cell migration by integrating “course-graining” materials and “fine-tuning” small molecules via decision tree signal-response modeling. *Biomaterials* 2011;32:7524-31.
- [45] DeForest CA, Anseth KS. Photoreversible Patterning of Biomolecules within Click-Based Hydrogels. *Angewandte Chemie International Edition* 2012;51:1816-9.

CHAPTER IV –

- [1] Slaughter BV, Khurshid SS, Fisher OZ, Khademhosseini A, Peppas NA. Hydrogels in regenerative medicine. *Advanced Materials* 2009;21:3307-3329.
- [2] Hubbell JA. Biomaterials in tissue engineering. *Nature Biotechnology* 1995;13:565-576.
- [3] Peppas NA, Langer R. New challenges in biomaterials. *Science* 1994;263:1715-1720.
- [4] Kloxin AM, Kloxin CJ, Bowman CN, Anseth KS. Mechanical properties of cellularly responsive hydrogels and their experimental determination. *Advanced Materials* 2010;22:3484-3494.
- [5] Hern DL, Hubbell JA. Incorporation of adhesion peptides into nonadhesive hydrogels useful for tissue resurfacing. *Journal of Biomedical Material Research Part A* 1998;39:266-276.
- [6] DeLong SA, Moon JJ, and West JL. Covalently immobilized gradients of bfgf on hydrogel scaffolds for directed cell migration. *Biomaterials* 2005;26:3227-3234.
- [7] Lutolf MP, Lauer-Fields JL, Schoekel HG, Metters AT, Weber FE, Fields GB, Hubbell JA. Synthetic matrix metalloproteinase-sensitive hydrogels for the conduction of tissue regeneration: engineering cell-invasion characteristics. *Proceedings of the National Academy of Science* 2003;100:5413-5418.
- [8] Patterson J, Hubbell JA. Enhanced proteolytic degradation of molecularly engineered peg hydrogels in response to mmp-1 and mmp-2. *Biomaterials* 2010;31:7836-7845.

- [9] Lin CC, Boyer PD, Aimetti AA, Anseth KS. Regulating mcp-1 diffusion in affinity hydrogels for enhancing immuno-isolation. *Journal of Controlled Release* 2010;142:384-391.
- [10] Discher DE, Jamney P, Wang Y. Tissue cells feel and respond to the stiffness of their substrate. *Science* 2005;310:1139-1143.
- [11] Engler AJ, Sen S, Sweeney HL, Discher DE. Matrix elasticity directs stem cell lineage specification. *Cell* 2006;126:677-689.
- [12] Schwartz MP, Fairbanks BD, Rogers RE, Rangarajan R, Zaman MH, Anseth KS. A synthetic strategy for mimicking the extracellular matrix provides insight about tumor cell migration. *Integrative Biology* 2010;2:32-40.
- [13] Anderson SB, Lin CC, Kuntzler DV, Anseth KS. The performance of human mesenchymal stem cells encapsulated in cell-degradable polymer peptide hydrogels. *Biomaterials*, 32:3564-3574, 2011.
- [14] Kyburz KA, Anseth KS. Three-dimensional hmsc motility within peptide-functionalized peg-based hydrogels of varying adhesivity and crosslinking density. *Acta Biomaterialia* 2013;9:6381-6392.
- [15] Tan JL, Tien J, Pirone DM, Gray DS, Bhadriraju K, Chen CS. Cells lying on a bed of microneedles: An approach to isolate mechanical force. *Proceedings of the National Academy of Science* 2003;100:1484-1489.
- [16] Tambe DT, Hardin CC, Angelini TE, Rajendran K, Park CY, Serra-Picamal X, Zhou EH, Zaman MH, Butler JP, Weitz DA, Fredberg JJ, Treppe X. Collective cell guidance by cooperative intercellular forces. *Nature Materials* 2011;10:469-475.
- [17] Legant WR, Miller JS, Blakely BL, Cohen DM, Genin GM, Chen CS. Measurement of mechanical tractions exerted by cells in three-dimensional matrices. *Nature Methods* 2010;7:969-973.
- [18] Guvendiren M, Burdick JA. Engineering synthetic hydrogel microenvironments to instruct stem cells. *Current Opinion in Biotechnology* 2013;24:841-846.
- [19] Bloom RJ, George JP, Celedon A, Sun SX, Wirtz D. Mapping local matrix remodeling induced by a migrating tumor cell using three-dimensional multiple-particle tracking. *Biophysical Journal* 2008;95:4077-4088.
- [20] Crocker JC, Grier DG. Methods of digital video microscopy for colloidal studies. *Journal of Colloid Interface Science* 1996;179:298-310.
- [21] Mason TG, Ganesan K, van Zanten JH, Wirtz D, Kuo SC. Particle tracking microrheology of complex fluids. *Physical Review Letters* 1997;79:3282-3285.

- [22] Crocker JC, Weeks ER. Particle tracking using idl. <http://www.physics.emory.edu/~weeks/idl/index.html>, 2011.
- [23] Savin T, Doyle PS. Static and dynamic errors in particle tracking microrheology. *Biophysical Journal* 2005;88:623-638.
- [24] Schultz KM, Anseth KS. Monitoring degradation of matrix metalloproteinases- cleavable peg hydrogels via multiple particle tracking microrheology. *Soft Matter* 2013;9:1570-1579.
- [25] Schultz KM, Baldwin AD, Kiick KL, Furst EM. Capturing the comprehensive modulus profile and reverse percolation transition of a degrading hydrogel. *Macro Letters* 2012;1:706-708.
- [26] Adolf D, Martin JE. Time-cure superposition during crosslinking. *Macromolecules* 1990;23:3700-3704.
- [27] Winter HH, Chambon F. Analysis of linear viscoelasticity of a crosslinking polymer at the gel point. *Journal of Rheology* 1986;30:367-382.
- [28] Aimetti AA, Machen AJ, Anseth KS. Poly(ethylene glycol) hydrogels formed by thiol-ene photopolymerization for enzyme-responsive protein delivery. *Biomaterials* 2009;30:6048-6054.
- [29] Fairbanks BD, Schwartz MP, Halevi AE, Nuttelman CR, Bowman CN, Anseth KS. A versatile synthetic extracellular matrix mimic via thiol-norbornene photopolymerization. *Adv. Mater* 2009;21:3114-3121.
- [30] Raeber GP, Lutolf MP, Hubbell JA. Molecularly engineered peg hydrogels: a novel model system for proteolytically mediated cell migration. *Biophysical Journal* 2005;89:1374-1388.
- [31] Kienberger F, Pastushenko VP, Kada G, Gruber HJ, Riener C, Schindler H, Hinterdorfer P. Static and dynamical properties of single poly (ethylene glycol) molecules investigated by force spectroscopy. *Single Molecules* 2000;1:123-128.
- [32] Miller JS, Shen CJ, Legant WR, Baranski JD, Blakely BL, Chen CS. Bioactive hydrogels made from step-growth derived peg-peptide macromers. *Biomaterials* 2010;31:3736-3743.
- [33] Weber LM, Lopez CG, Anseth KS. Effects of peg hydrogel crosslinking density on protein diffusion and encapsulated islet survival and function. *Journal of Biomedical Material Research Part A* 2009;90A:720-729.
- [34] Fairbanks BD, Schwartz MP, Bowman CN, Anseth KS. Photoinitiated polymerization of peg-diacrylate with lithium phenyl-2,4,6-trimethylbenzoylphosphine: polymerization rate and cytocompatibility. *Biomaterials* 2009;30:6702-6707.
- [35] Nuttelman CR, Tripodi MC, Anseth KS. Synthetic hydrogel niches that promote hmsc

viability. Matrix Biology 2005;24:208-218.

[36] Tseng Q. Piv (particle image velocimetry) | imagej plugin. <https://sites.google.com/site/qingzongtseng/piv>, 2014.

CHAPTER V –

[1] Tibbitt MW, Anseth KS. Hydrogels as extracellular matrix mimics for 3D cell culture. Biotechnology and Bioengineering 2009;103:655-63.

[2] Discher DE, Mooney DJ, Zandstra PW. Growth Factors, Matrices, and Forces Combine and Control Stem Cells. Science 2009;324:1673-7.

[3] Burdick JA, Murphy WL. Moving from static to dynamic complexity in hydrogel design. Nature communications 2012;3:1269.

[4] Annabi N, Tamayol A, Uquillas JA, Akbari M, Bertassoni LE, Cha C, et al. 25th Anniversary Article: Rational Design and Applications of Hydrogels in Regenerative Medicine. Adv Mater 2014;26:85-124.

[5] Azagarsamy MA, Anseth KS. Bioorthogonal Click Chemistry: An Indispensable Tool to Create Multifaceted Cell Culture Scaffolds. ACS macro letters 2013;2:5-9.

[6] Hoyle CE, Bowman CN. Thiol-ene click chemistry. Angewandte Chemie 2010;49:1540-73.

[7] Mariner PD, Wudel JM, Miller DE, Genova EE, Streubel SO, Anseth KS. Synthetic hydrogel scaffold is an effective vehicle for delivery of INFUSE (rhBMP2) to critical-sized calvaria bone defects in rats. Journal of orthopaedic research : official publication of the Orthopaedic Research Society 2013;31:401-6.

[8] Kyburz KA, Anseth KS. Three-dimensional hMSC motility within peptide-functionalized PEG-based hydrogels of varying adhesivity and crosslinking density. Acta biomaterialia 2013;9:6381-92.

[9] Schwartz MP, Fairbanks BD, Rogers RE, Rangarajan R, Zaman MH, Anseth KS. A synthetic strategy for mimicking the extracellular matrix provides new insight about tumor cell migration. Integrative biology : quantitative biosciences from nano to macro 2010;2:32-40.

[10] Silva AKA, Richard C, Bessodes M, Scherman D, Merten OW. Growth Factor Delivery Approaches in Hydrogels. Biomacromolecules 2009;10:9-18.

[11] Lee SH, Shin H. Matrices and scaffolds for delivery of bioactive molecules in bone and cartilage tissue engineering. Adv Drug Deliver Rev 2007;59:339-59.

- [12] Lin CC, Anseth KS. Controlling Affinity Binding with Peptide-Functionalized Poly(ethylene glycol) Hydrogels. *Adv Funct Mater* 2009;19:2325-31.
- [13] Lee SJ. Cytokine delivery and tissue engineering. *Yonsei medical journal* 2000;41:704-19.
- [14] Hoyle CE, Lowe AB, Bowman CN. Thiol-click chemistry: a multifaceted toolbox for small molecule and polymer synthesis. *Chemical Society reviews* 2010;39:1355-87.
- [15] Hume PS, He J, Haskins K, Anseth KS. Strategies to reduce dendritic cell activation through functional biomaterial design. *Biomaterials* 2012;33:3615-25.
- [16] McCall JD, Luoma JE, Anseth KS. Covalently tethered transforming growth factor beta in PEG hydrogels promotes chondrogenic differentiation of encapsulated human mesenchymal stem cells. *Drug delivery and translational research* 2012;2:305-12.
- [17] Mistry AS, Mikos AG. Tissue engineering strategies for bone regeneration. *Advances in biochemical engineering/biotechnology* 2005;94:1-22.
- [18] Caplan AI, Correa D. The MSC: an injury drugstore. *Cell Stem Cell* 2011;9:11-5.
- [19] Uccelli A, Moretta L, Pistoia V. Mesenchymal stem cells in health and disease. *Nature reviews Immunology* 2008;8:726-36.
- [20] Salem HK, Thiemermann C. Mesenchymal stromal cells: current understanding and clinical status. *Stem cells* 2010;28:585-96.
- [21] Ko IK, Lee SJ, Atala A, Yoo JJ. In situ tissue regeneration through host stem cell recruitment. *Experimental & molecular medicine* 2013;45:e57.
- [22] Karp JM, Teol GSL. Mesenchymal Stem Cell Homing: The Devil Is in the Details. *Cell Stem Cell* 2009;4:206-16.
- [23] Phinney DG, Prockop DJ. Concise review: mesenchymal stem/multipotent stromal cells: the state of transdifferentiation and modes of tissue repair--current views. *Stem cells* 2007;25:2896-902.
- [24] Yang C, Tibbitt MW, Basta L, Anseth KS. Mechanical memory and dosing influence stem cell fate. *Nature materials* 2014;13:645-52.
- [25] Gilbert PM, Havenstrite KL, Magnusson KE, Sacco A, Leonardi NA, Kraft P, et al. Substrate elasticity regulates skeletal muscle stem cell self-renewal in culture. *Science* 2010;329:1078-81.
- [26] Chen FM, Wu LA, Zhang M, Zhang R, Sun HH. Homing of endogenous stem/progenitor cells for in situ tissue regeneration: Promises, strategies, and translational perspectives. *Biomaterials* 2011;32:3189-209.

- [27] Vanden Berg-Foels WS. In situ tissue regeneration: chemoattractants for endogenous stem cell recruitment. *Tissue engineering Part B, Reviews* 2014;20:28-39.
- [28] Discher DE, Mooney DJ, Zandstra PW. Growth factors, matrices, and forces combine and control stem cells. *Science* 2009;324:1673-7.
- [29] Ji W, Yang F, Ma J, Bouma MJ, Boerman OC, Chen Z, et al. Incorporation of stromal cell-derived factor-1alpha in PCL/gelatin electrospun membranes for guided bone regeneration. *Biomaterials* 2013;34:735-45.
- [30] Tsiridis E, Upadhyay N, Giannoudis P. Molecular aspects of fracture healing: which are the important molecules? *Injury* 2007;38 Suppl 1:S11-25.
- [31] Kitaori T, Ito H, Schwarz EM, Tsutsumi R, Yoshitomi H, Oishi S, et al. Stromal cell-derived factor 1/CXCR4 signaling is critical for the recruitment of mesenchymal stem cells to the fracture site during skeletal repair in a mouse model. *Arthritis and rheumatism* 2009;60:813-23.
- [32] Ponte AL, Marais E, Gally N, Langonne A, Delorme B, Herault O, et al. The in vitro migration capacity of human bone marrow mesenchymal stem cells: comparison of chemokine and growth factor chemotactic activities. *Stem cells* 2007;25:1737-45.
- [33] Huang YC, Liu TJ. Mobilization of mesenchymal stem cells by stromal cell-derived factor-1 released from chitosan/tripolyphosphate/fucoidan nanoparticles. *Acta biomaterialia* 2012;8:1048-56.
- [34] He X, Ma J, Jabbari E. Migration of marrow stromal cells in response to sustained release of stromal-derived factor-1alpha from poly(lactide ethylene oxide fumarate) hydrogels. *International journal of pharmaceutics* 2010;390:107-16.
- [35] Thevenot PT, Nair AM, Shen J, Lotfi P, Ko CY, Tang L. The effect of incorporation of SDF-1alpha into PLGA scaffolds on stem cell recruitment and the inflammatory response. *Biomaterials* 2010;31:3997-4008.
- [36] Zlotnik A, Yoshie O. Chemokines: a new classification system and their role in immunity. *Immunity* 2000;12:121-7.
- [37] Ceradini DJ, Kulkarni AR, Callaghan MJ, Tepper OM, Bastidas N, Kleinman ME, et al. Progenitor cell trafficking is regulated by hypoxic gradients through HIF-1 induction of SDF-1. *Nature medicine* 2004;10:858-64.
- [38] Granero-Molto F, Weis JA, Miga MI, Landis B, Myers TJ, O'Rear L, et al. Regenerative effects of transplanted mesenchymal stem cells in fracture healing. *Stem cells* 2009;27:1887-98.

- [39] Purcell BP, Elser JA, Mu A, Margulies KB, Burdick JA. Synergistic effects of SDF-1 α chemokine and hyaluronic acid release from degradable hydrogels on directing bone marrow derived cell homing to the myocardium. *Biomaterials* 2012;33:7849-57.
- [40] Urist MR. Bone: formation by autoinduction. *Science* 1965;150:893-9.
- [41] Seeherman H, Wozney JM. Delivery of bone morphogenetic proteins for orthopedic tissue regeneration. *Cytokine & growth factor reviews* 2005;16:329-45.
- [42] Yamamoto M, Takahashi Y, Tabata Y. Enhanced bone regeneration at a segmental bone defect by controlled release of bone morphogenetic protein-2 from a biodegradable hydrogel. *Tissue engineering* 2006;12:1305-11.
- [43] Osathanon T, Linnes ML, Rajachar RM, Ratner BD, Somerman MJ, Giachelli CM. Microporous nanofibrous fibrin-based scaffolds for bone tissue engineering. *Biomaterials* 2008;29:4091-9.
- [44] Saito N, Okada T, Horiuchi H, Ota H, Takahashi J, Murakami N, et al. Local bone formation by injection of recombinant human bone morphogenetic protein-2 contained in polymer carriers. *Bone* 2003;32:381-6.
- [45] Boyan BD, Lohmann CH, Somers A, Niederauer GG, Wozney JM, Dean DD, et al. Potential of porous poly-D,L-lactide-co-glycolide particles as a carrier for recombinant human bone morphogenetic protein-2 during osteoinduction in vivo. *Journal of biomedical materials research* 1999;46:51-9.
- [46] Jin Q, Giannobile WV. SDF-1 enhances wound healing of critical-sized calvarial defects beyond self-repair capacity. *PloS one* 2014;9:e97035.
- [47] Fairbanks BD, Schwartz MP, Bowman CN, Anseth KS. Photoinitiated polymerization of PEG-diacrylate with lithium phenyl-2,4,6-trimethylbenzoylphosphinate: polymerization rate and cytocompatibility. *Biomaterials* 2009;30:6702-7.
- [48] Sridhar BV, Doyle NR, Randolph MA, Anseth KS. Covalently tethered TGF-beta1 with encapsulated chondrocytes in a PEG hydrogel system enhances extracellular matrix production. *Journal of biomedical materials research Part A* 2014.
- [49] Teicher BA, Fricker SP. CXCL12 (SDF-1)/CXCR4 pathway in cancer. *Clinical cancer research : an official journal of the American Association for Cancer Research* 2010;16:2927-31.
- [50] Axelrad TW, Einhorn TA. Bone morphogenetic proteins in orthopaedic surgery. *Cytokine & growth factor reviews* 2009;20:481-8.
- [51] Zilberberg L, ten Dijke P, Sakai LY, Rifkin DB. A rapid and sensitive bioassay to measure bone morphogenetic protein activity. *BMC cell biology* 2007;8:41.

[52] Hosogane N, Huang Z, Rawlins BA, Liu X, Boachie-Adjei O, Boskey AL, et al. Stromal derived factor-1 regulates bone morphogenetic protein 2-induced osteogenic differentiation of primary mesenchymal stem cells. *The international journal of biochemistry & cell biology* 2010;42:1132-41.

[53] Herberg S, Fulzele S, Yang N, Shi X, Hess M, Periyasamy-Thandavan S, et al. Stromal cell-derived factor-1 β potentiates bone morphogenetic protein-2-stimulated osteoinduction of genetically engineered bone marrow-derived mesenchymal stem cells in vitro. *Tissue engineering Part A* 2013;19:1-13.

[54] Herberg S, Susin C, Pelaez M, Howie RN, Moreno de Freitas R, Lee J, et al. Low-dose bone morphogenetic protein-2/stromal cell-derived factor-1 β cotherapy induces bone regeneration in critical-size rat calvarial defects. *Tissue engineering Part A* 2014;20:1444-53.

CHAPTER VI –

[1] Burdick JA, Murphy WL. Moving from static to dynamic complexity in hydrogel design. *Nature communications* 2012;3:1269.

[2] Discher DE, Mooney DJ, Zandstra PW. Growth factors, matrices, and forces combine and control stem cells. *Science* 2009;324:1673-7.

[3] Richardson TP, Peters MC, Ennett AB, Mooney DJ. Polymeric system for dual growth factor delivery. *Nature biotechnology* 2001;19:1029-34.

[4] Chen FM, Zhang M, Wu ZF. Toward delivery of multiple growth factors in tissue engineering. *Biomaterials* 2010;31:6279-308.

[5] Hahn MS, Miller JS, West JL. Three-dimensional biochemical and biomechanical patterning of hydrogels for guiding cell behavior. *Advanced Materials* 2006;18:2679-+.

[6] DeForest CA, Polizzotti BD, Anseth KS. Sequential click reactions for synthesizing and patterning three-dimensional cell microenvironments. *Nature materials* 2009;8:659-64.

[7] Mosiewicz KA, Kolb L, van der Vlies AJ, Martino MM, Lienemann PS, Hubbell JA, et al. In situ cell manipulation through enzymatic hydrogel photopatterning. *Nature materials* 2013;12:1072-8.

[8] DeForest CA, Tirrell DA. A photoreversible protein-patterning approach for guiding stem cell fate in three-dimensional gels. *Nature materials* 2015.

[9] DeForest CA, Anseth KS. Cytocompatible click-based hydrogels with dynamically tunable properties through orthogonal photoconjugation and photocleavage reactions. *Nature Chemistry* 2011;3:925-31.

- [10] Wylie RG, Ahsan S, Aizawa Y, Maxwell KL, Morshead CM, Shoichet MS. Spatially controlled simultaneous patterning of multiple growth factors in three-dimensional hydrogels. *Nature materials* 2011;10:799-806.
- [11] Lo KWH, Ulery BD, Ashe KM, Laurencin CT. Studies of bone morphogenetic protein-based surgical repair. *Adv Drug Deliver Rev* 2012;64:1277-91.
- [12] Ji JF, He BP, Dheen ST, Tay SSW. Interactions of chemokines and chemokine receptors mediate the migration of mesenchymal stem cells to the impaired site in the brain after hypoglossal nerve injury. *Stem cells* 2004;22:415-27.
- [13] Kitaori T, Ito H, Schwarz EA, Tsutsumi R, Yoshitomi H, Oishi S, et al. Stromal Cell-Derived Factor 1/CXCR4 Signaling Is Critical for the Recruitment of Mesenchymal Stem Cells to the Fracture Site During Skeletal Repair in a Mouse Model. *Arthritis and rheumatism* 2009;60:813-23.
- [14] Eom YW, Oh JE, Lee JI, Baik SK, Rhee KJ, Shin HC, et al. The role of growth factors in maintenance of stemness in bone marrow-derived mesenchymal stem cells. *Biochemical and biophysical research communications* 2014;445:16-22.
- [15] Fairbanks BD, Schwartz MP, Halevi AE, Nuttelman CR, Bowman CN, Anseth KS. A Versatile Synthetic Extracellular Matrix Mimic via Thiol-Norbornene Photopolymerization. *Advanced Materials* 2009;21:5005-+.
- [16] Kyburz KA, Anseth KS. Three-dimensional hMSC motility within peptide-functionalized PEG-based hydrogels of varying adhesivity and crosslinking density. *Acta biomaterialia* 2013;9:6381-92.
- [17] Hoyle CE, Bowman CN. Thiol-ene click chemistry. *Angewandte Chemie* 2010;49:1540-73.
- [18] Hoyle CE, Lowe AB, Bowman CN. Thiol-click chemistry: a multifaceted toolbox for small molecule and polymer synthesis. *Chemical Society reviews* 2010;39:1355-87.
- [19] Fairbanks BD, Schwartz MP, Bowman CN, Anseth KS. Photoinitiated polymerization of PEG-diacrylate with lithium phenyl-2,4,6-trimethylbenzoylphosphinate: polymerization rate and cytocompatibility. *Biomaterials* 2009;30:6702-7.
- [20] Karver MR, Weissleder R, Hilderbrand SA. Synthesis and Evaluation of a Series of 1,2,4,5-Tetrazines for Bioorthogonal Conjugation. *Bioconjugate Chem* 2011;22:2263-70.
- [21] DeForest CA, Anseth KS. Photoreversible Patterning of Biomolecules within Click-Based Hydrogels. *Angew Chem Int Edit* 2012;51:1816-9.

CHAPTER VII

- [1] Tibbitt MW, Anseth KS. Hydrogels as extracellular matrix mimics for 3D cell culture. *Biotechnology and Bioengineering* 2009;103:655-63.
- [2] Burdick JA, Murphy WL. Moving from static to dynamic complexity in hydrogel design. *Nature communications* 2012;3:1269.
- [3] Tsiridis E, Upadhyay N, Giannoudis P. Molecular aspects of fracture healing: which are the important molecules? *Injury* 2007;38 Suppl 1:S11-25.
- [4] Uccelli A, Moretta L, Pistoia V. Mesenchymal stem cells in health and disease. *Nature reviews Immunology* 2008;8:726-36.
- [5] Humphries JD, Byron A, Humphries MJ. Integrin ligands at a glance. *J Cell Sci* 2006;119:3901-3.
- [6] Truong H, Danen EHJ. Integrin switching modulates adhesion dynamics and cell migration. *Cell Adhes Migr* 2009;3:179-81.
- [7] Fairbanks BD, Schwartz MP, Halevi AE, Nuttelman CR, Bowman CN, Anseth KS. A Versatile Synthetic Extracellular Matrix Mimic via Thiol-Norbornene Photopolymerization. *Advanced Materials* 2009;21:5005-+.
- [8] Ruoslahti E. RGD and other recognition sequences for integrins. *Annual review of cell and developmental biology* 1996;12:697-715.
- [9] Caplan AI, Correa D. The MSC: an injury drugstore. *Cell Stem Cell* 2011;9:11-5.
- [10] Seeherman H, Wozney JM. Delivery of bone morphogenetic proteins for orthopedic tissue regeneration. *Cytokine & growth factor reviews* 2005;16:329-45.